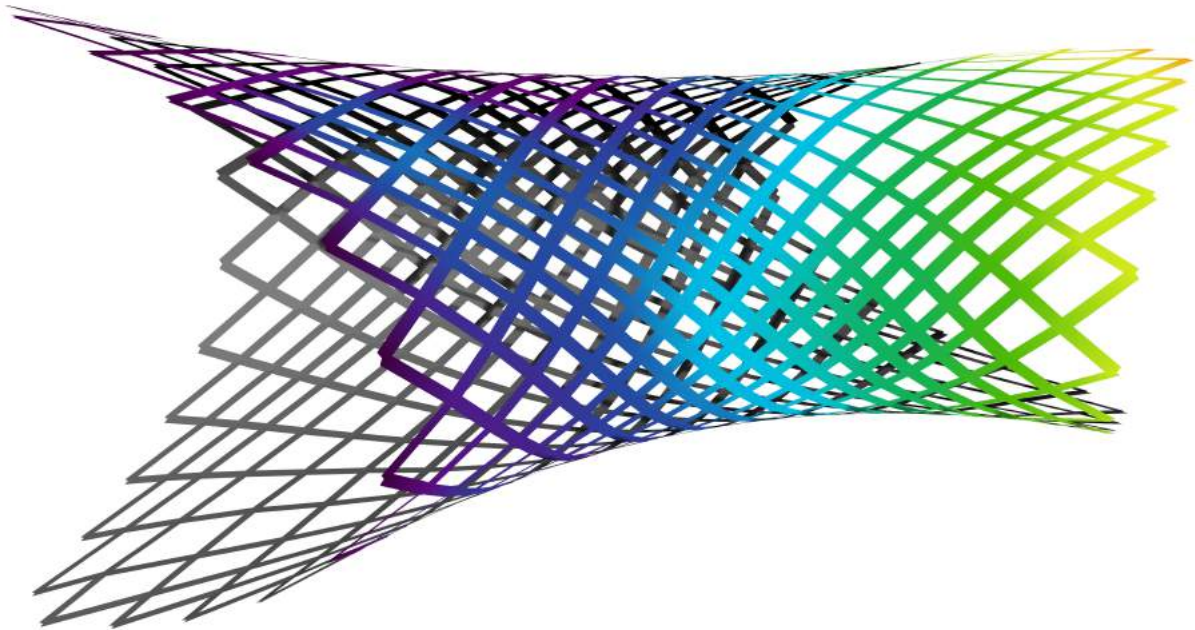




CHALMERS
UNIVERSITY OF TECHNOLOGY



Parametric modelling and FE analysis of architectural FRP modules

Establishment of a computational design and analysis
approach for preliminary design

Master's thesis in Structural Engineering and Building Technology

HANNA ISABELLA NÄRHI

Parametric modelling and FE analysis of architectural FRP modules

Establishment of a computational design and analysis approach for preliminary design

HANNA ISABELLA NÄRHI



CHALMERS
UNIVERSITY OF TECHNOLOGY

Department of Industrial and Materials Science
Division of Material and Computational Mechanics
CHALMERS UNIVERSITY OF TECHNOLOGY
Gothenburg, Sweden 2018

Parametric modelling and FE analysis of architectural FRP modules
Establishment of a computational design and analysis approach for preliminary design
HANNA ISABELLA NÄRHI

© HANNA ISABELLA NÄRHI, 2018.

Supervisor:

Dr.-Ing. Thiemo Fildhuth, Knippers Helbig GmbH, Stuttgart

Examiner:

Dr. Mats Ander, Department of Industrial and Materials Science, Chalmers, Gothenburg

Department of Industrial and Materials Science
Division of Material and Computational Mechanics
Chalmers University of Technology
SE-412 96 Gothenburg
Telephone +46 31 772 1000

Cover: Displacement plot for FRP module with beam elements, modelled parametrically in Rhinoceros 3D, Grasshopper and SOFiSTiK. The displacements have been imported into Rhinoceros 3D and Grasshopper, from SOFiSTiK, using parametric tools developed for this study.

Typeset in L^AT_EX
Gothenburg, Sweden 2018

Parametric modelling and FE analysis of architectural FRP modules
Establishment of a computational design and analysis approach for preliminary design
HANNA ISABELLA NÄRHI
Department of Industrial and Materials Science
Division of Material and Computational Mechanics
Chalmers University of Technology

Abstract

Despite low weight and high strength and stiffness, Fibre Reinforced Polymers, FRP, are seldom used in building construction. This could be due to complexity in dimensioning and manufacturing, as well as lack of building design codes and standards for FRP. The University of Stuttgart has developed an analysis and manufacturing method for FRP in architectural contexts. This is the basis for a research project at Knippers Helbig GmbH, where a new type of FRP module is developed for upcoming building projects. The analysis method developed at The university of Stuttgart is however not applicable for this FRP module, and demands are also stricter since the modules will be used in building design.

In this master's thesis a new analysis method is developed. For analysis SOFiSTiK was required, which imposed limitations, thus simplifications were necessary. The module material is mainly uni-directional, with mechanically coupled node zones. Due to the thickness of the module cross sections, it was assumed that coupling effects could be neglected and that the material behaviour will be transversely isotropic. It was also assumed that beam elements could be used in analysis due to mainly uni-axial load transfer.

To verify the assumptions, case studies were carried out in MATLAB and SOFiSTiK with Classical Lamination Theory as a basis. Two parametric FE models were created using SOFiSTiK QUAD and beam elements. The results were compared using parametric tools developed for this study. There was a correspondence between the results obtained in the MATLAB and SOFiSTiK analyses, as well as between the QUAD and beam models, except for in the case of torsion and shear where internal stresses were within a similar range, but displacements were not. Here it was concluded that verification by mechanical tests are required.

The models were applied to variations of a full scale module, with similar results. The performance of the beam models were significantly better, and it was concluded that the QUAD model could not be used in large scale models due to long computational times. Due to similarities in internal stresses and forces the beam model should be safe-sided and accurate enough for preliminary design, assuming that the models can be verified against mechanical tests.

Keywords: FRP, CFRP, carbon fibre, FEA, parametric design, structural design, structural analysis, computational mechanics, finite element method, architecture

Parametrisk modellering och analys av arkitektoniska FRP moduler
Etablering av modellerings- och analysmetod för preliminär dimensionering
HANNA ISABELLA NÄRHI
Institutionen för Industri- och materialvetenskap
Avdelningen för Material- och beräkningsmekanik
Chalmers University of Technology

Sammanfattning

Trots låg vikt och hög hållfasthet och styvhet är fiberkompositer, FRP, sällan använda inom byggnadskonstruktion. En anledning kan vara på grund av komplexitet i dimensionering och tillverkning, samt att byggnadsnormer och standarder saknas för FRP. Institutionerna ITKE och ICD vid Stuttgarts Universitet har utvecklat en analys- och tillverkningsmetod för FRP i arkitektoniska kontexter. Detta ligger till grund för ett utvecklingsprojekt på konstruktörsfirman Knippers Helbig GmbH, där en ny typ av FRP-modul utvecklas för kommande byggnadsprojekt. Analysmetoden som utvecklats vid Stuttgarts Universitet är inte tillämpbar för den studerade FRP-modulen, och kraven är strängare eftersom modulerna ska användas i byggnadsdesign.

En ny analysmetod utvecklas i detta examensarbete. För strukturanalys krävdes SOFiSTiK, vilket medförde begränsningar, förenklingar var därför nödvändiga. Modulmaterialet är främst "uni-directional" (enkel-riktat), "mekaniskt kopplade" nodzoner. På grund av modultvärsnittens tjocklek antogs dessa effekter försumbara och materialbeteendet transversellt isotropiskt. Det antogs också att balkelement kan användas i strukturanalys eftersom lastöverföringen är främst enaxlig.

För att verifiera antagandena utfördes studier i MATLAB och SOFiSTiK med Klassisk Laminatteori som teoretisk bas. Två parametriska modeller med SOFiSTiK QUAD- och balkelement utvecklades. Resultaten jämfördes med hjälp av parametriska verktyg utvecklade för den här studien. Resultaten från MATLAB och SOFiSTiK överensstämde, och även QUAD- och balkmodellerna med undantag för fallen med skjuvning och vridning, där spänningarna överensstämde, men deformationer gjorde inte det. Här drogs slutsatsen att kalibrering mot fysiska tester är nödvändiga för verifiering av resultaten.

De parametriska modellerna tillämpades på variationer av en fullskalig modul. Det observerades att balkmodellen presterade avsevärt bättre, och att QUAD-modellen därför inte är tillämpbar i storskaliga modeller på grund av för långa beräkningstider. Balkmodellen ansågs vara konservativ och tillräckligt korrekt för preliminär dimensionering, eftersom snittkrafter och spänningar stämde överens, förutsatt att metoden kan verifieras mot fysiska tester.

Nyckelord: FRP, CFRP, kolfiber, FEA, parametrisk design, konstruktion, strukturanalys, beräkningsmekanik, finitea elementmetoden, arkitektur

TABLE OF CONTENTS

Abstract	v
Sammanfattning	vi
Nomenclature	ix
Terminology	xii
Preface	
1 Background	1
1.1 FRP in architectural and structural applications	2
1.2 New type of architectural FRP modules	6
2 Problem statement	9
2.1 Parametric design and FE analysis approach	10
2.2 Limitations and excluded topics	11
2.3 Hypotheses	13
3 Methods	15
3.1 Methods	16
3.2 Report outline	18
3.3 Case studies	20
4 Preconditions	23
4.1 FRP module definitions and parameters	24
4.2 Parametric 3D modelling and structural analysis tools	29
5 Theoretical background	33
5.1 Fibre reinforced plastic composites	34
5.2 Mechanical properties of FRP laminae	38
5.3 Constitutive equations for FRP laminates	40
5.4 Mechanical coupling in FRP laminates	45
5.5 Equivalent material parameters for Fully Orthotropic Laminates	48
6 Material parameters for structural analysis	51
6.1 Analysis of FRP composites	53
6.2 Mechanical response of FRP laminae	55
6.3 Mechanical response of FRP laminates	58
6.4 Equivalent material parameters	64

7	Material parameters for FE analysis	69
7.1	Parametric QUAD and beam models for verification of material parameters	71
7.2	Adaptations of material parameters for FE analysis	73
7.3	Verification of material parameters for QUAD elements	77
7.4	Materials and cross sections for beam elements	88
8	Development of a parametric design and analysis approach	97
8.1	Preliminary evaluation of detailed parametric models	99
8.2	Comparison and evaluation of QUAD and beam models	102
9	Verification of the proposed parametric design and analysis approach	107
9.1	Verification and calibration approaches	109
10	Application of the proposed parametric design and analysis approach	111
10.1	Evaluation of FE models for full scale FRP module	113
10.2	Comparison between QUAD and beam models	117
11	Discussion	121
11.1	Establishment of design and analysis approach	123
11.2	Evaluation of assumptions and results	125
12	Conclusion and recommendations	129
12.1	Concluding remarks	130
12.2	Suggestions for future research	131

References

List of Figures

List of Tables

Appendices

A Explanations and definitions

B Programs and parametric tools

Nomenclature

Roman upper case letters

A	Extensional stiffness matrix
A	Beam cross section area
A_{ij}	Components of the A matrix
A_y	Shear deformation area in the y -direction
B	Coupling stiffness matrix
B_{ij}	Components of the B matrix
D	Bending stiffness matrix
D_{ij}	Components of the D matrix
E_f	Longitudinal modulus of fibre phase
E_L	Longitudinal modulus of a composite
E_m	Longitudinal modulus of matrix phase
E_T	Transverse modulus of a composite
G_{LT}	Shear modulus of a composite
I_y	Area moment of inertia
I_z	Area moment of inertia
L	Plate length
M	Moment vector
M	Plate moment
M_T	Beam torsional moment
M_y	Beam bending moment
M_z	Beam bending moment
N	Force vector
N	Plate normal force
N_x	Beam normal force
P_L	Load carried by composite
P_{fL}	Load carried by fibres
P_{mL}	Load carried by matrix
Q	Lamina stiffness matrix
\bar{Q}	Lamina stiffness matrix in reference coordinate system
Q_{ij}	Components of the Q matrix
R	Radius of plate curvature
S	Lamina compliance matrix
T	Transformation matrix
T_1	Transformation matrix
T_2	Transformation matrix

V_f	Fibre volume fraction
V_m	Matrix volume fraction
W_T	Torsional constant for beam cross sections

Roman lower case letters

k	Lamina number in laminate
n	Number of laminae in a laminate
h_k	Bottom position of a lamina in a laminate
t	Laminate thickness
t_k	Lamina thickness
u	Displacement in the x -direction
u_0	Mid-plane displacement in the x -direction
v	Displacement in the y -direction
v_0	Mid-plane displacement in the y -direction
v_c	Composite volume
v_f	Fibre volume
v_m	Matrix volume
w_0	Mid-plane displacement in the z -direction

Greek upper case letters

Δ	Difference operator
----------	---------------------

Greek lower case letters

α_L	Longitudinal thermal expansion coefficient
α_T	Transverse thermal expansion coefficient
ϵ	Strain vector
ε	Strain
ϵ^0	Plate mid plane strain
ε_c	Composite strain
ε_f	Fibre strain
ε_m	Matrix strain
η	Parameter for estimation of composite transverse and shear stiffness
γ	Shear strain
κ	Curvature
κ	Curvature
ν	Poisson's ratio
ϕ_x	Shear angle in x direction

ϕ_y	Shear angle in y direction
ψ	Third Euler angle
σ	Stress vector
σ	Normal stress
σ_x	Beam normal stress
τ	Shear stress
τ_{\max}	Maximum beam shear stress
τ_T	Torsional shear stress in beam
τ_{xy}	Maximum beam shear stress in the xy plane
θ	Orientation of lamina
φ_x	Slope of laminate mid-plane in x -direction
φ_y	Slope of laminate mid-plane in y -direction
ξ	Parameter for estimation of composite transverse and shear stiffness

Miscellaneous symbols

∂	Partial derivative
------------	--------------------

Terminology

Acronyms

CAD	Computer Aided Design
CFRP	Carbon Fibre Reinforced Polymer
CLT	Classical Laminate Theory
FEA	Finite Element Analysis
FOL	Fully Orthotropic Laminate
FRP	Fibre Reinforced Polymer
GFRP	Glass Fibre Reinforced Polymer
LOC	Laminate Orientation Code
OOP	Object Oriented Programming
ROM	Rule of Mixtures
SAR	Structural Area
SLN	Structural Line
SPT	Structural Point

Terms

angle-ply laminate	pg. 46
balanced laminate	pg. 46
CADINP	pg. 31
Classical Lamination Theory	pg. 41
cross-ply laminate	pg. 46
C#	pg. 30
fibre bundle	pg. 24
fibre mesh	pg. 24
Fully Orthotropic Laminate	pg. 48
generally orthotropic lamina	pg. 38
lamina	pg. 38
laminate	pg. 40
Laminate Orientation Code	pg. 40
layup	pg. 40
longitudinal direction	pg. 34
matrix	pg. 34
mechanical coupling	pg. 45
mesh angle	pg. 26
mesh density	pg. 26
mesh segment	pg. 26

node zone	pg. 26
parametric modelling	pg. 29
ply	pg. 38
QUAD	pg. 31
reinforcement	pg. 34
specially orthotropic lamina	pg. 38
structural area	pg. 31
structural line	pg. 31
structural point	pg. 31
symmetric laminate	pg. 46
transverse direction	pg. 34
transversely isotropic	pg. 34
uni-directional	pg. 34
uni-directional laminate	pg. 46
uni-directional zone	pg. 26
volume fraction	pg. 35

Preface

This master's thesis is the conclusion of my studies at the Architecture and Engineering program at Chalmers University of Technology in Gothenburg. During my studies I have developed an interest for computational and parametric design, structural analysis and lightweight structures. I have deepened my knowledge in these topics for the past two years in Stuttgart Germany where I have done internships related to architecture and structural engineering, and also conducted this master's thesis work.

The master's thesis has been carried out at the engineering firm Knippers Helbig GmbH, in Stuttgart, under the supervision of Dr.-Ing. Thiemo Fildhuth. The examiner and supervisor at Chalmers, in Gothenburg, has been Dr. Mats Ander, at the Department of Industrial Materials Science. I extend my gratitude to both Thiemo Fildhuth and Mats Ander who have offered invaluable guidance and feedback throughout this thesis work.

I would like to also give my thanks to persons and organisations who have been helpful during the work on this thesis. First I would like to thank the German-Swedish Chamber of Commerce, for granting me a travel scholarship from Emil Possehl's scholarship fund, for conducting my master thesis within the technical field in Germany. And a thank you to my opponents, Marina Mossberg and Samuel Eliasson.

My colleagues and the management at Knippers Helbig in Stuttgart are also thanked. I would like to thank my colleague Amin Li, who has offered help and guidance on many occasions during this work, and our office manager in Stuttgart, Matthias Oppe, for giving me the opportunity to conduct my thesis at the office. And a big thank you to all my colleagues who have been helpful and offered moral support, or who have just been great company during our lunch and coffee breaks.

And finally, to the two people who have always been a great support and have helped me keep on track to reach my goal, my mom Pirjo Närhi and sister Saga Tinnevik - ett stort och ödmjukt tack.

*Jag har världen framför mina fötter
Jag vill ut i den
Släpp mig fri*

*Jag har världen framför mina fötter
Vad håller mig fast?
Bara tankens kraft*

*Jag har världen framför mina fötter
Jag känner det släppa
Tvekans grepp*

*Jag har världen framför mina fötter
Jag väntar ett ögonblick till
Sen är den min*

1

BACKGROUND

1.1 FRP in architectural and structural applications

Despite their high strength, low weight and high stiffness, **Fibre Reinforced Polymers, FRP**, are not often used in building construction [1], even though FRP have been on the topic in the building industries since the 1950's, and is widely used in for instance the automotive and aerospace industries [2], see Figure 1.1. This could be because of the complexity in the dimensioning methods and manufacturing techniques which are not directly transferable to an architectural context, as well as the lack of established design codes and standards for the use of these types of materials in buildings [2].



Figure 1.1: Nearly half of the air frame of the Boeing 787 consists of carbon fibre reinforced plastics and other composites [3].
From [4]. Reproduced with permission, CC-BY-SA 3.0 [5].

1.1.1 FRP in structural applications

In the building industry there is a lack of comprehensive and widespread knowledge of the mechanical behaviours of FRP, which is necessary for a successful implementation [2]. The anisotropic nature of FRP composites requires accurate modelling and analysis techniques through **Finite Element Analysis, FEA**. In the building industry FEA is common practice, but the lack of knowledge and proper analysis strategies for FRP materials often results in over simplified models.

Currently there exists no EN Eurocode which provide design rules for FRP material in building design [6]. Despite this, several structures, where FRP has been used as a structural material, have been realised in Europe. There is a growing interest for these materials, with several research projects related to modelling and testing of analysis models and prototype testing. Several international journals also exist which are dedicated to the topic of FRP materials in building contexts. Thus there is a current demand for standardised guidelines as well as accurate modelling and analysis methods.

Based on these developments and the practical experience gained, there exists now enough knowledge to establish a foundation for a new European guidelines. A set of pre-normative guidelines has been published [6] as a step in this process, *Prospect for New Guidance in the Design of FRP*. After an evaluation process of these the *CEN Technical Committee 250 (CEN/T250)*, will determine if these can be converted into EN Eurocodes [7].



Figure 1.2: Examples of existing structures in Europe where FRP composites have been used as structural materials.

(a) The pedestrian bridge at Kolding, Denmark, is made from 100% pultruded GFRP profiles [6].

©Luigi Ascione. From [6]. Reproduced with permission.

(b) More than 80% of this Solar Charging station, SUDI™, in Joué les Tours, France, is made from composites [6].

©Luigi Ascione. From [6]. Reproduced with permission.

1.1.2 FRP in architectural applications

Some of the benefits of FRP composites, such as low weight and the possibility to mould the material into a large variety of shapes can be a functional and aesthetic advantage for architects and designers [1]. Complex shapes can be achieved using FRP composites, and used as for instance facade panels where great materials savings can be done in the supporting structure compared to if traditional materials are used, see Figure 1.3.

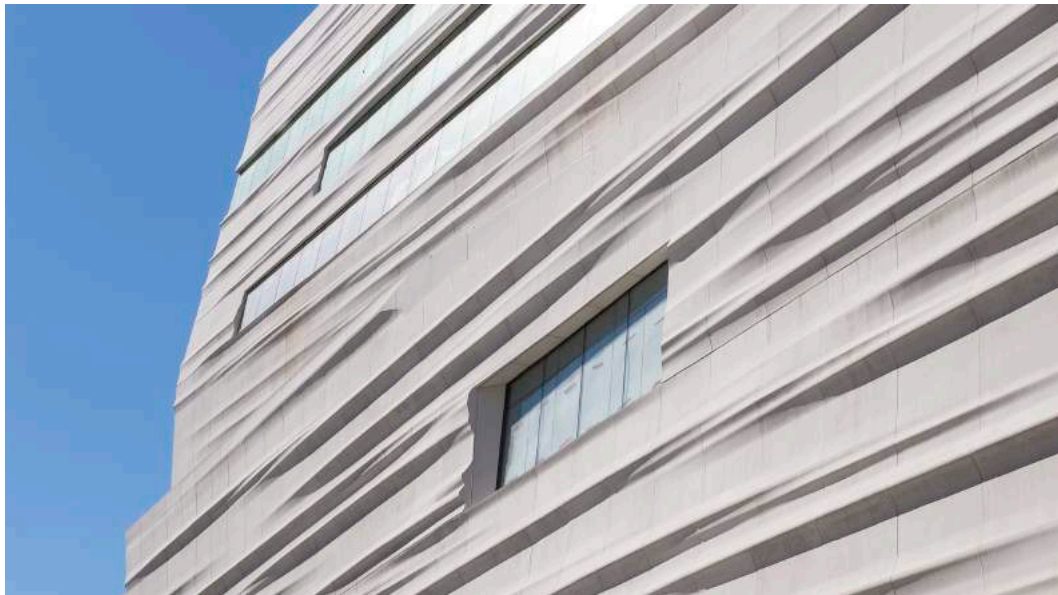


Figure 1.3: SFMOMA façade of Snøhetta expansion; photo: ©Henrik Kam, courtesy SFMOMA. Reproduced with permission. From [8].

More than 700 unique FRP panels make up the facade of the San Francisco Museum of Modern Art, SFMOMA [9]. It was estimated that 453.6 tonnes of additional steel would have been required in the supporting structure if the facade had been constructed using glass-reinforced concrete instead [1].

1.1.3 Architectural and structural collaboration

The computational and 3D modelling methods available today have made it possible to design and analyse geometrically and structurally complex buildings. The automotive and aerospace industries have successfully adopted these tools and methods, and developed dedicated fabrication methods and simulation strategies [2]. These methods however, are rarely suitable for architectural or structural contexts, as these require shaping moulds and are based on serialised production of many similar parts, which is rarely the case in architecture where each building is unique [10].

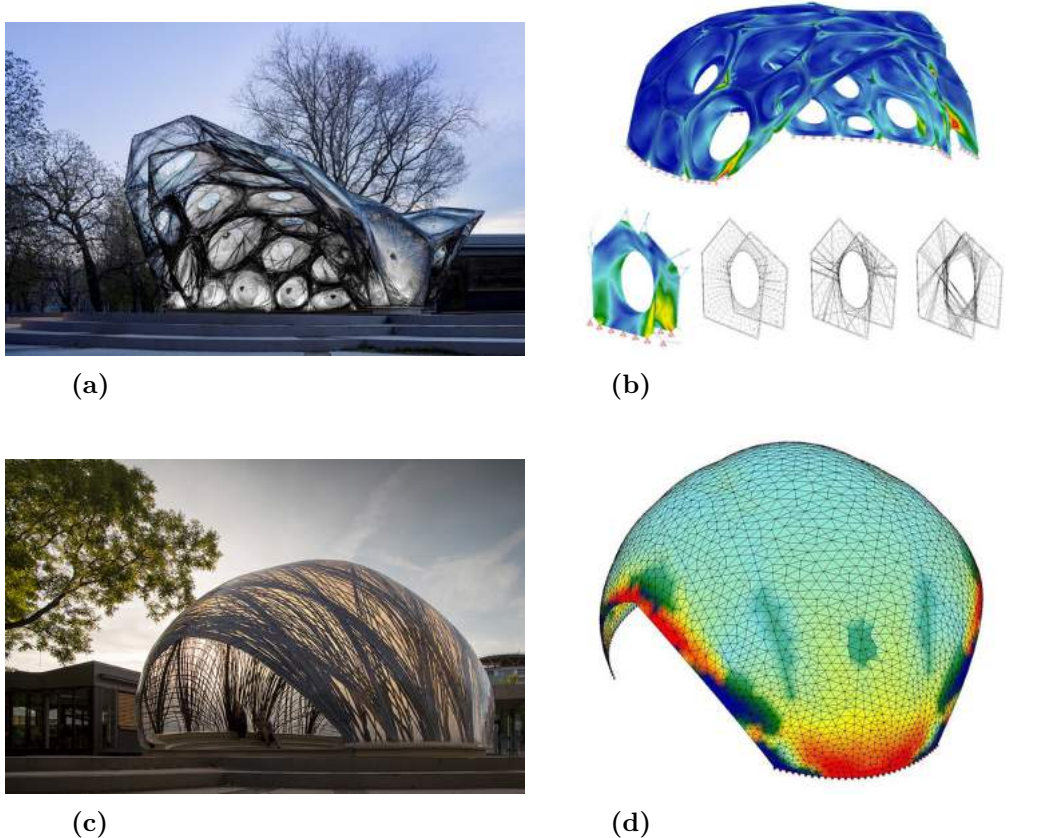


Figure 1.4: ICD/ITKE Research pavilions photos and development process.

- (a) Photograph of research pavilion 2013-2014.
From ITKE [11]. Reproduced with permission.
- (b) Analysis model for research pavilion 2013-2014.
From ITKE [12]. Reproduced with permission.
- (c) Photograph of research pavilion 2014-2015.
From ITKE [13]. Reproduced with permission.
- (d) Analysis model for research pavilion 2014-2015.
From ITKE[14]. Reproduced with permission.

Through a series of pavilion designs, a new core-less, free-winding robotic manufacturing method for **glass and carbon FRP** composites, **GFRP/CFRP**, has been developed at the *Institute of Building Structures and Structural Design (ITKE)* and *Institute for Computational Design and Construction (ICD)* at the University of Stuttgart, see Figure 1.4 [10]. Pavilions have historically driven technological development in architecture since they are temporary and don't have to conform to the standard building codes.

The manufacturing method which has been developed by the ITKE and ICD is a robotic winding method, see Figure 1.5. Thin FRP rovings are wound in a dense pattern with multiple fibre directions forming a shell-like structure. This eliminates the need of moulds, and allow for expressive free form shapes [15].

The load transfer in these modules is closely linked to the fibre directions, but also the geometry of the structure. These multiple directions which give rise to a multi-axial stress state, as well as the coupling between geometry and structural models, require new methods of analysis to be developed [2]. Parametric tools, which are becoming common practice in architecture, made it possible to develop a context specific method of analysis for these pavilions, where the fibre orientations could be optimised through an iterative analysis process using parametric design and analysis tools.



Figure 1.5: Thin FRP rovings are wound freely in the air by robots.
From ITKE [16]. Reproduced with permission.

1.2 New type of architectural FRP modules

The Stuttgart University research pavilions are the basis for a research and development project at Knippers Helbig GmbH, Stuttgart, where the goal is to establish a design and analysis method which can be applied in upcoming projects, for a new type of FRP module which is currently being developed, see Figure 1.6.

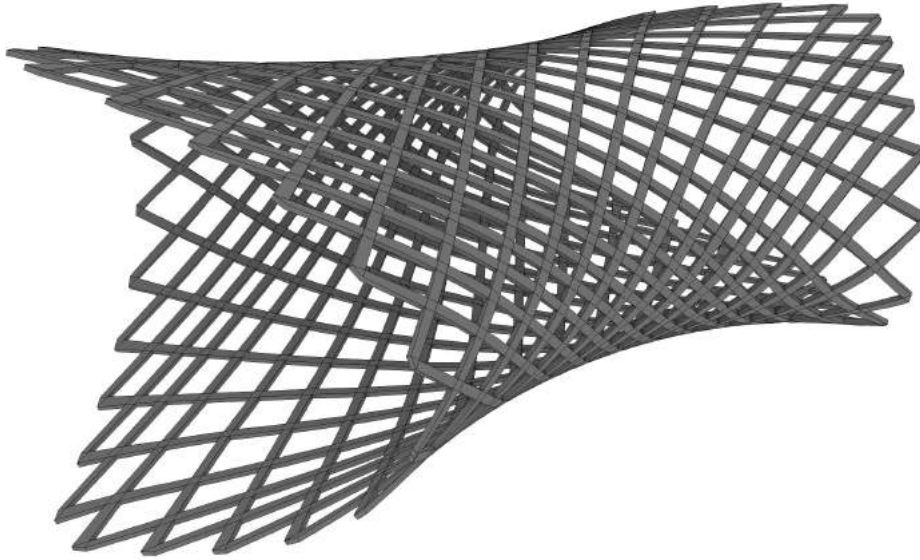


Figure 1.6: Principal geometry, topology and layout of uni-directional fibre bundles of the proposed FRP module.

This FRP module differs from the research pavilions in the way that the fibre mesh is perforated and the fibres are organised such that they form distinct fibre bundles with quite large cross sections, which provide uni-axial load paths. The structural behaviour of this module differs thus from the pavilion designs, in which the fibres were distributed in multiple directions where they formed a shell like structure, whereas in this module the load transfer is more beam-like and uni-axial. The geometry and fibre bundles layout of this FRP module have been decided through an architectural design process rather than by structural optimisation. This poses a new challenge as the analysis method used for the research pavilions no longer can be applied.

The large fibre bundle cross sections form two distinctive zones in the module - zones of uni-directional beam like sections with uni-axial load transfer, and node zones where the fibre bundles overlap with multi-directional load transfer, further there will be a discontinuity zone due to a distinct change in geometry and stiffness, see Figure 1.7.

The manufacturing method of these modules will affect the geometry of the node, which in turn will affect the structural behaviour of the module. The manufacturing method of these modules have not been determined in this stage, however it is fairly certain there will be layers of fibres stacked sequentially, with alternating orientations as in Figure 1.8. Two methods can be employed here, the first where the fibre layers are continuous as in Figures 1.8a to 1.8c forming a distinct undulating node, or as in Figures 1.8d to 1.8f where the layers are discontinuous and thus the node will remain flat.



Figure 1.7: Discontinuity of the node zones.

- (A) Uni-directional zone with uni-axial load transfer.
- (B) Discontinuity region due to change of geometry and stiffness.
- (C) Node zone with multi-axial load transfer.

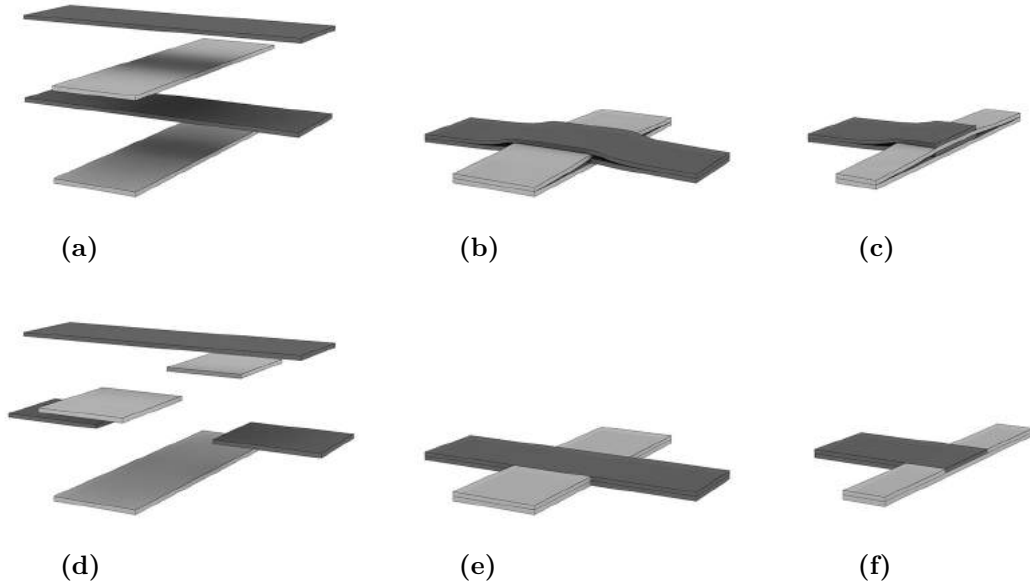


Figure 1.8: Principal geometry and fibre layout of different types of nodes.

- (a) Continuous FRP layers with different orientations at the node zones of the FRP module.
- (b) Undulating geometry at the node zone due to overlapping FRP layers.
- (c) Section view of undulating node.
- (d) Discontinuous FRP layers with different orientations at the node zones.
- (e) Flat geometry at node due to discontinuous FRP layers.
- (f) Section view of flat node.

2

PROBLEM STATEMENT

2.1 Parametric design and FE analysis approach

The goal of the master's thesis work at Knippers Helbig GmbH, is to use these modules in upcoming projects, and as such the requirements of these modules are much stricter than for the research pavilions. Several aspects must be considered such as applicability in practice, manufacturing, compliance and safety. The lack of standards and norms also puts high demands on the accuracy of analysis, and mechanical testing is required.

The FRP modules are planned to be used in large scale projects where multiple of these modules are assembled to form a large structure. This structure will be analysed using conventional structural engineering software where the possibilities to analyse anisotropic materials are limited. This means that the analysis method must be simplified with regard to material formulations, number of elements and geometry, while at the same time efficiently provide accurate results which can be used for dimensioning in preliminary design.

2.1.1 Aim and scope

The aim is to establish a simplified, reliable and accurate parametric design and analysis approach for preliminary design of the FRP modules described in Section 1.2. The established design method should be applicable to varying geometries and mesh densities and must therefore be parametric. The proposed design and analysis approach should fulfil a number of requirements which are listed below.

Global and detailed analysis context

The design approach should be applicable to a structural engineering context - meaning, it should be possible to include and analyse the FRP modules in a large scale structural model, a *global structural model*. Typically this kind of model would include a large number of structural elements and several load combinations. The design approach should also be applicable to small scale models for detailed design.

Conservative approach

There are many uncertainties regarding this type of FRP module and the establish design and analysis method should therefore generate results on the safe side.

Applicability of results

It should also be possible to extract the results, namely deflections and displacements as well as internal forces and stresses, from such a global model in an easy manner and use these for detailed design.

Parametric design approach

Due to the many uncertainties the method should be fully parametric so it is possible to make geometrical and structural adjustments, and apply the method to a variety of geometries and meshes.

Verification

Mechanical tests will be conducted on physical prototypes and the design approach should also be established such that verification against test data can be done in a straight forward manner.

2.2 Limitations and excluded topics

A number of limitations are imposed on the study and are presented below. Additionally some topics have been excluded and are also presented below.

Geometry and topology limitations

The study will be limited to one type of geometry and topology, but considerations will be made so that the method can be applied to varying geometries and topologies.

Computational limitations

There are computational limitations with regard to processing power, computational time as well as softwares. The analysis should therefore be simplified with regard to number of FE elements to reduce computational times. The main softwares which will be used are SOFiSTiK, MATLAB, Rhinoceros 3D and Grasshopper.

Structural analysis limitations

The structural analysis is required to be performed in SOFiSTiK. This is partly because it is the main software used for structural analysis at Knippers Helbig GmbH, and also due to the fact that the established method should be applicable in a civil engineering context, using large scale global models which must comply with building standards and design codes, for this purpose SOFiSTiK is well suited. Additionally SOFiSTiK provide built in interfaces with multiple CAD softwares and has its own native scripting language which is quite useful for parametric design and analysis.

The structural analysis which is basis for establishment of simplified material formulations will be limited to in-plane mechanical behaviour, and the assumptions of the Euler-Bernoulli beam theory and the Kirchhoff-Love plate theory will be used. In SOFiSTiK the analysis will be conducted using Timoshenko beam theory and Mindlin-Reissner plate theory, since these are default settings for structural analysis. There will however be no consideration or adaptations of stiffness or material formulations with regard to shear deformation, plate thickness or out-of-plane stiffness.

Material formulations

The possibilities to analyse anisotropic and layered materials in SOFiSTiK exist, but are complicated and limited. Therefore it is preferred to use either isotropic or orthotropic, as well as non-layered material for analysis in SOFiSTiK. Thus the material formulations used in structural analysis should be limited to orthotropic or transversely isotropic materials.

Discontinuity zones

Discontinuities, especially at the FRP module boundary edges as well as the node discontinuity zones, presented in Figure 1.7 will not be regarded. In this study only one the flat node type will be regarded.

Structural form finding and optimisation of topology mesh

There will be no structural optimisation or form finding of the geometry or topology, nor will there be any optimisation with regard to dimensions. Preliminary dimensions will be used as well as a predetermined geometry and topology.

Residual stresses and imperfections

Residual stresses and imperfections which may arise due to manufacturing will not be regarded in the study.

2. PROBLEM STATEMENT

Interlaminar stresses

Effects of interlaminar stresses which occur between the layers of FRP lamina will not be considered here.

Fatigue and failure

Fatigue and failure mechanics will not be regarded in the study.

Non-linearity and instability

Instability and third order effects due to geometric discontinuity zones or imperfections will not be studied.

2.3 Hypotheses

Throughout the work a number of assumptions and hypotheses are made and are verified or discarded. These are presented below.

Transverse isotropy

A simplified orthotropic material behaviour can be assumed for this type of FRP module, and in zones where fibres overlap, the material can be assumed to be transversely isotropic.

Uni-axial load transfer

It is assumed that the load transfer in the FRP modules is mainly uni-axial and that analysis using beam theory will be sufficient.

Verification and calibration

It is assumed that the material parameters and design and analysis method can be calibrated and verified against mechanical tests.

Applicability of results

The results from a simplified global analysis can be used in a detailed design situation.

3

METHODS

3.1 Methods

The principal methodology and work flow can be seen in Figure 3.1. The methodology can be categorised into five parts which are briefly described below.

Problem formulation

The problem is formulated and a number of requirements and limitations are stated. The geometry and boundary conditions for the analysis is defined, and initial material parameters are summarised.

Theoretical material studies

A literature study in FRP mechanics and Classical Laminate Theory forms the basis of finding suitable constitutive equations for FRP laminates. The result of these studies is the basis for a number of assumptions of simplifications that can be made for the constitutive equations for specific types of FRP Laminates. A number of studies are conducted to evaluate these assumptions, and to derive material parameters which can be used in a simplified analysis situation.

The derived material parameters are used in FE analysis to create equivalent materials which can be applied to shell and beam elements, and the material parameters are adjusted and verified against the theory and assumptions.

Development of parametric analysis approach

A parametric design and analysis approach is developed for the specific topology studied, using SOFiSTiK QUAD (shell) and beam elements.

A number of case studies are conducted for different setups, and strain and stress results of the different models are compared and evaluated. The parametric FE model should also be calibrated against mechanical tests.

Evaluation of parametric analysis approach

The parametric FE analysis and design approach is applied to a full scale free form FRP module, using both SOFiSTiK QUAD and beam elements. The results are compared and evaluated.

Recommendation of parametric analysis approach

Finally a summary of the results is made and the results are evaluated. The parametric FE and analysis approach is also evaluated, and a recommendation is made and suggestions for future work is given.

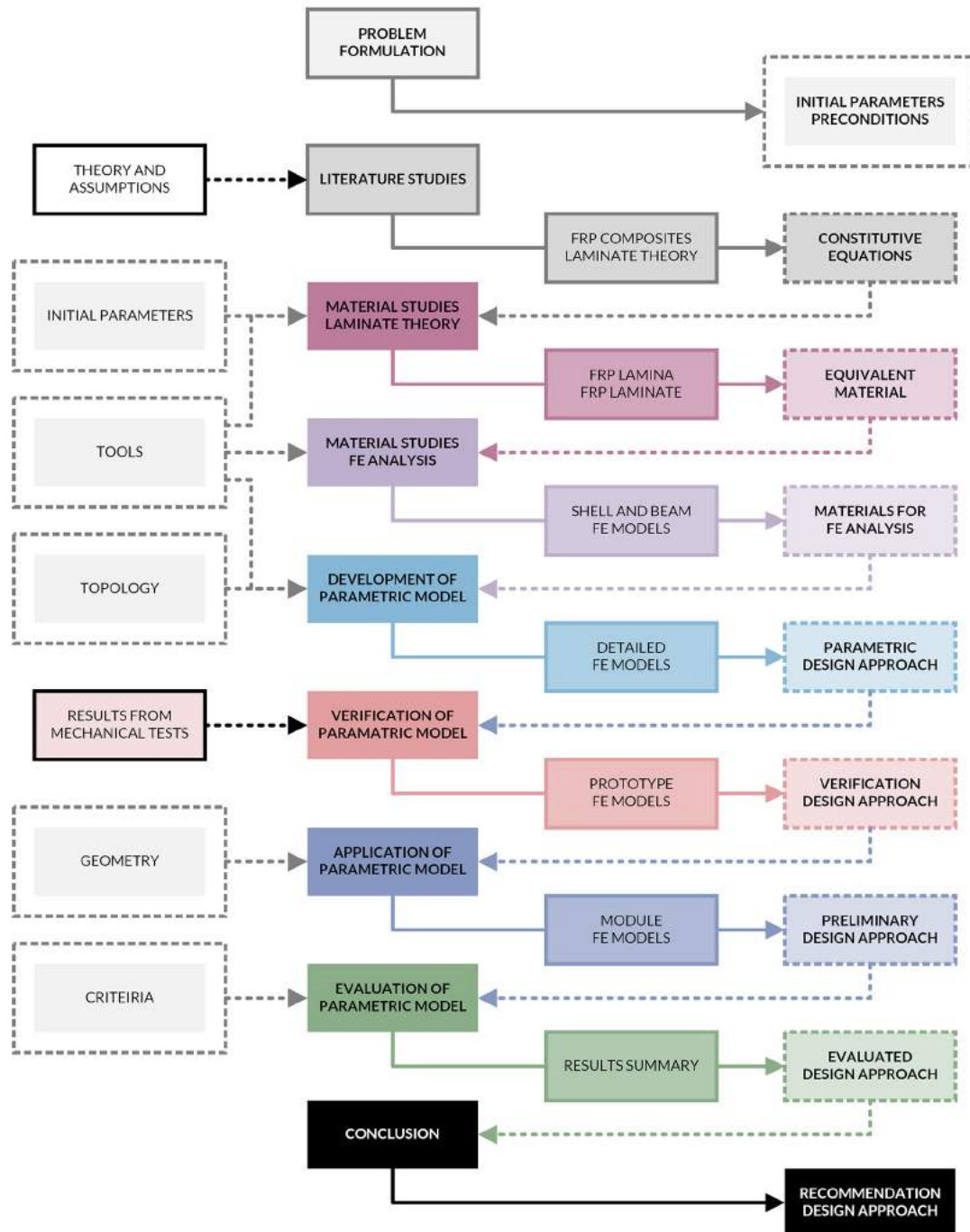


Figure 3.1: Flowchart describing the method and report outline.

3.2 Report outline

The report outline can be seen in Figure 3.2 and can be used as a reading guide to the report. The report is structured chronologically and in six major parts which are described below.

Introduction

The problem is introduced in Chapter 1 - *Background* and defined further in Chapter 2 - *Problem statement*.

Methodology and outline of work

The methodology is introduced here in Chapter 3 - *Methods*, where the methods chosen, principal work flow and report outline are explained. Following this, the geometry, topology and initial material parameters for the FRP module, as well as the tools used are presented in Chapter 4 - *Preconditions*.

Theoretical background

Following this a theoretical background to FRP mechanics and Classical Laminate Theory, which is essential for understanding the following chapters, is given in Chapter 5 - *Theoretical background*. Here it is assumed that the reader is already familiar with strength of materials, structural mechanics as well as the Finite Element Method.

Case studies

The theoretical background is the basis for a number of assumptions. In Chapter 6 - *Material parameters for structural analysis* these assumptions are presented, and evaluated using analytical analysis. Following this, equivalent material parameters which can be used in FE analysis are derived.

In Chapter 7 - *Material parameters for FE analysis* the derived material parameters are adjusted and applied in FE analysis, using shell and beam elements. The results of the analysis are evaluated against analytical results. Material formulations and cross sections are established in SOFiSTiK for use in parametric analysis models.

In Chapter 8 - *Development of a parametric design and analysis approach* a parametric design and analysis approach is developed for small FE models using shell and beam elements. The models are evaluated and compared. Following this in Chapter 9 - *Verification of the proposed parametric design and analysis approach* methods for calibration of the FE models are presented before finally applying the parametric analysis and design approach to a full scale free form FRP module in Chapter 10 - *Application of the proposed parametric design and analysis approach*.

Evaluation and recommendation

The results of the case studies and the proposed parametric design and analysis approach are evaluated in Chapter 11 - *Discussion*, and finally a recommendation is made and suggestions for future work are given in Chapter 12 - *Conclusion and recommendations*.

References, explanations and appendices

The final part of the report contains appendices describing the parametric studies in greater detail, summaries of input parameters and results, as well as references and list of figures and tables.

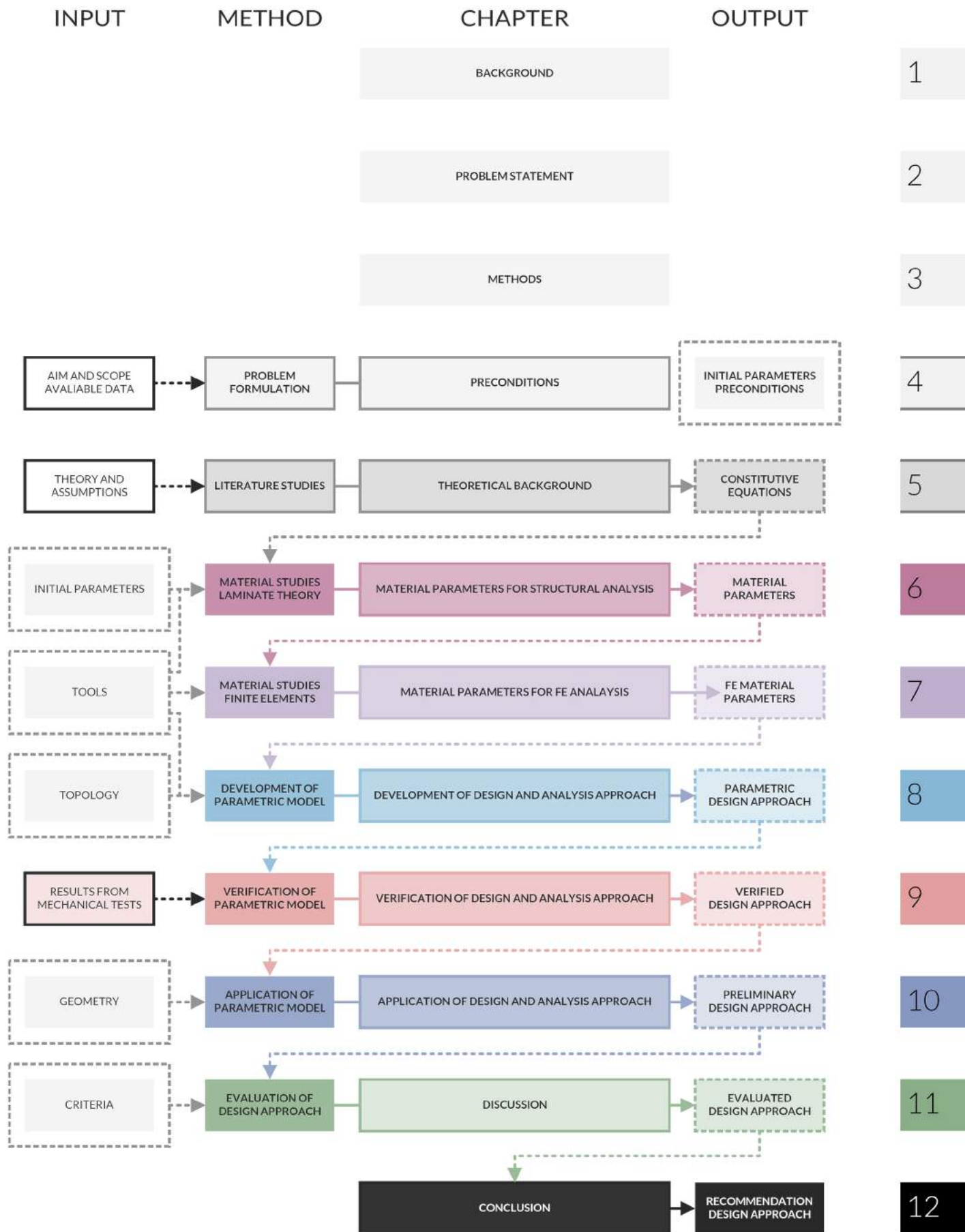


Figure 3.2: Flowchart describing the method and report outline.

3.3 Case studies

A number of case studies were conducted to verify the assumptions made and to establish a parametric analysis and design approach. The case studies are briefly described below. Further descriptions and results are presented in Chapters 6 to 10.

Material parameters for structural analysis

It was assumed that thick laminates with symmetric and balanced layups, and alternating lamina orientations, will behave like fully orthotropic laminates. To verify this assumption three case studies were conducted.

Mechanical response of FRP laminae

Material studies are carried out on FRP laminae with varying orientations and fibre volume fractions to evaluate which laminae are most critical with regard to mechanical coupling.

Mechanical response of FRP laminates

Symmetric and balanced laminates are studied to evaluate which orientations are most critical with regard to mechanical coupling in these specific laminate types. For the most critical orientations it is evaluated how mechanical coupling is affected when the number of laminae increases in order to evaluate if mechanical coupling can be neglected.

Equivalent material parameters

Assuming that the laminates are fully orthotropic efficient engineering constants were derived and used to construct equivalent transversely isotropic laminates. A study was conducted to compare and evaluate the mechanical response of the symmetric, balanced and equivalent laminates.

Material parameters for FE analysis

The engineering constants which were derived were used to define nine transversely isotropic materials for analysis in SOFiSTiK, and these materials were compared against the analysis performed in MATLAB for the same materials.

Adaptations of material parameters for FE analysis

Adaptations of the engineering constants were necessary in order to be able to use the material in analyse in SOFiSTiK.

Verification of material parameters for QUAD elements

A case study was conducted in SOFiSTiK using the adapted material parameters for QUAD elements. The same case study was conducted in MATLAB and the results of the studies were compared and evaluated.

Adaptations of parameters for beam elements

A case study was conducted in SOFiSTiK comparing the mechanical response in SOFiSTiK QUAD and beam elements, with the adapted materials, and adaptations were made to the beam cross sections. The displacements and internal forces and stresses were compared and evaluated for the QUAD models and the beam models with adapted cross sections.

Development of a parametric design and analysis approach

Three parametric models were developed in Grasshopper for structural analysis of the FRP module. The three models were compared and evaluated.

Preliminary evaluation of detailed parametric models

The three models were developed and analysed in SOFiSTiK. The QUAD model was assumed to be the most accurate as this model was the only one to take into account the uni-directional as well as node zones. The other models were compared, using different parametric setups, against the QUAD model and disregarded if the results were not corresponding.

Comparison and evaluation of QUAD and beam models

A case study was conducted for the evaluated QUAD and beam models, for different geometrical setups and all materials and cross sections. The results were evaluated and compared.

Verification of the proposed parametric design and analysis approach

The assumptions made in previous chapters should be verified against mechanical tests, and the parametric model should be adjusted and calibrated if possible. Within this scope mechanical testing has not been possible. This is however necessary in order to verify the model.

Verification and calibration approaches

Suggestions for verification and calibration approaches are given, and a summary of assumptions and aspects of the parametric design and analysis approach which should be considered is given.

Application of the proposed parametric design and analysis approach

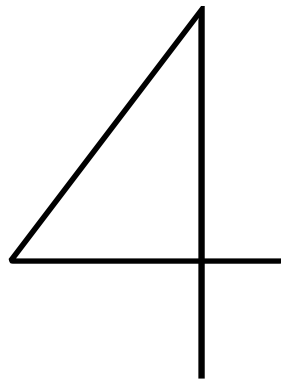
The parametric models were applied to variations of a full scale FRP module, where meshing and computation time, as well as deflections and internal forces and stresses were compared.

Evaluation of FE models for full scale FRP module

The meshing and computation times were compared and evaluated for three different types of mesh densities.

Comparison between QUAD and beam models

Case studies were conducted for three mesh densities comparing the mechanical response for compression and tension, bending and torsion for the QUAD and beam models. The results were compared and evaluated.



PRECONDITIONS

4.1 FRP module definitions and parameters

In this chapter the geometry, topology and initial parameters for the FRP module is explained. The parametric design and analysis approach which is developed in this study will be applied to the module shown here, but the proposed design and analysis method can be applied to any geometry with the the same geometrical and topological principals which are explained in this chapter.

4.1.1 Geometry and topology

The FRP module can be divided into four geometrical elements, the start edge (Figure 4.1a), the end edge (Figure 4.1b), the center lines of the **fibre bundles** in the one direction (Figure 4.1c) and the fibre bundle curves in the other direction (Figure 4.1d). The final topology pattern will be referred to as the **mesh**, or **fibre mesh**, in the following text. The topology for this module has been defined as in Figure 4.1 and 4.2, and the definitions and terminology is explained below.

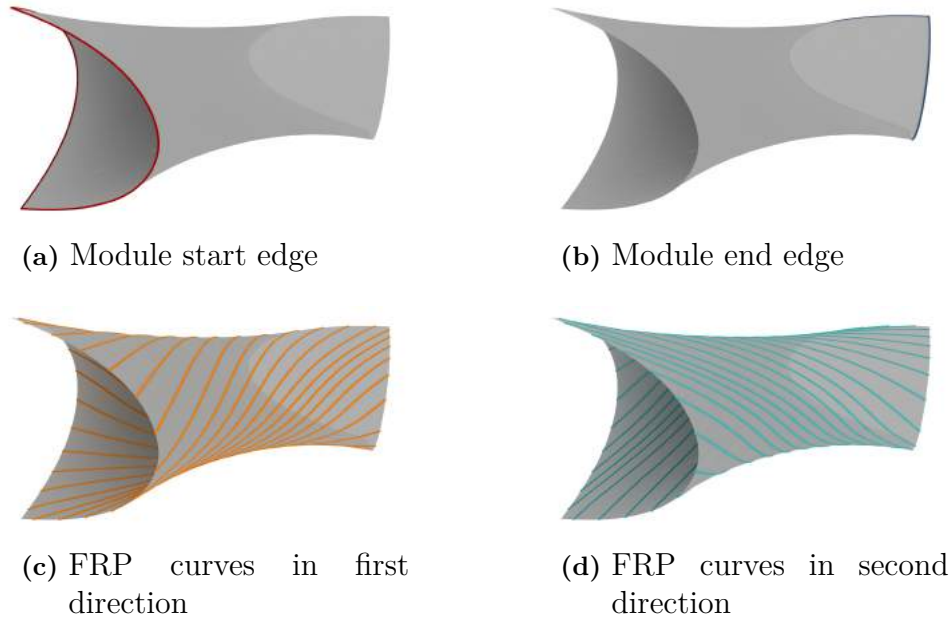


Figure 4.1: The geometrical elements of the FRP module.

Topology definition

Split edge curves

The edge curves, or module boundaries, are not planar, and because of this the edges are first split at the kinks into two edge curve segments, see Figure 4.2a.

Subdivide start curve

The first edge of the curve segments is subdivided into segments of equal lengths. The intersection of two of these segments are shown in Figure 4.2b.

Subdivide end curve

The end edge curves are also split and marked with points as the start curve, see Figure 4.2c.

Geodesic curve

A geodesic line is drawn between a point on the start curve and a point on the edge curve. This is repeated for all points along the module boundaries, see Figure 4.2d.

Apply rotation

Next the points are moved in a rotating fashion, in opposite directions on the two edges, so that the curve is now extended on the surface as in Figure 4.2e. This is repeated for all the geodesic curves and points on the module edges and surface.

Reverse rotation

Finally the rotation is reversed in order to create curves which are oriented in the opposite direction as, see Figure 4.2f.

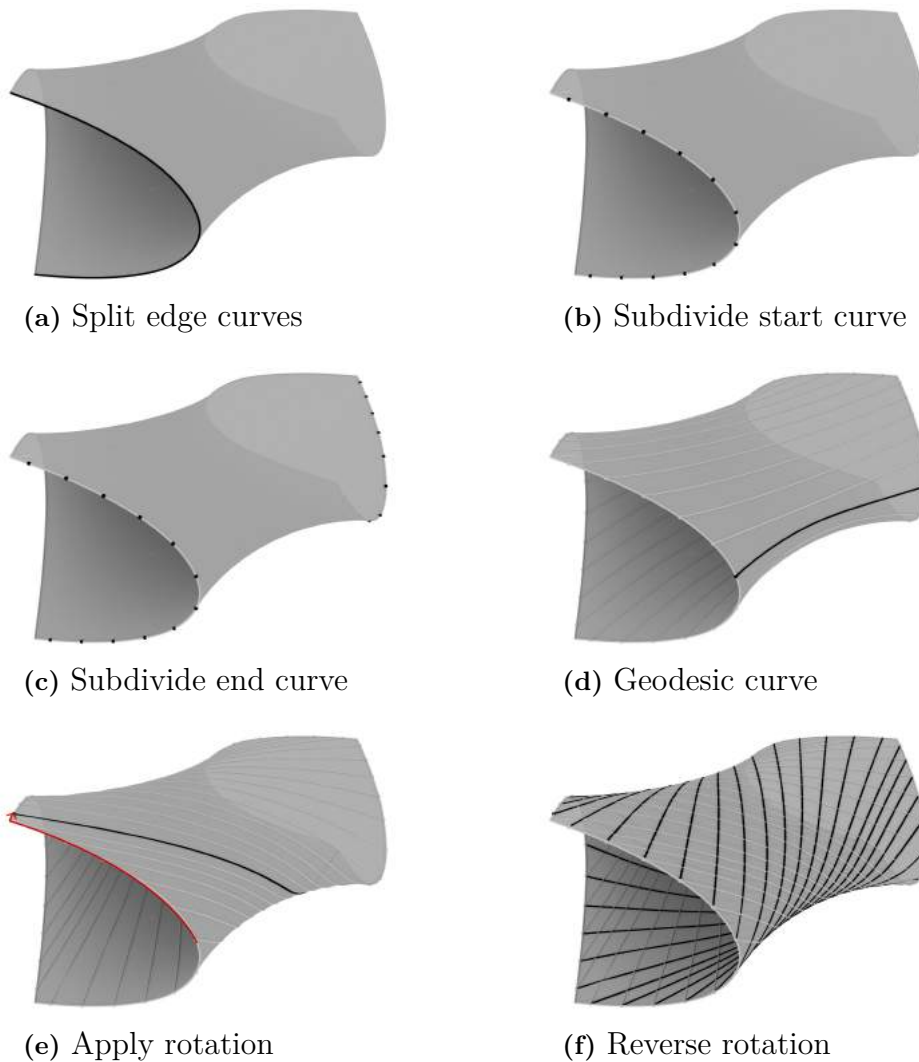


Figure 4.2: The topology of the FRP module is defined in these six steps.

4. PRECONDITIONS

Topology terminology

Mesh segment

In Figure 4.3a a **mesh segment** of the topology is shown.

Uni-directional zone

In Figure 4.3b a **uni-directional** element is shown. These zones consists of only uni-directional fibre bundles.

Node zone

In Figure 4.3c a **node zone** is shown. These zones consists of overlapping fibre bundles as previously explained in Chapter 1, Section 1.2.

Mesh angle

The angle, θ , at the intersection of two uni-directional elements is called **mesh angle**.

Mesh density

The number of points on the edge determines the **mesh density**, in Figure 4.4 three mesh densities are shown.

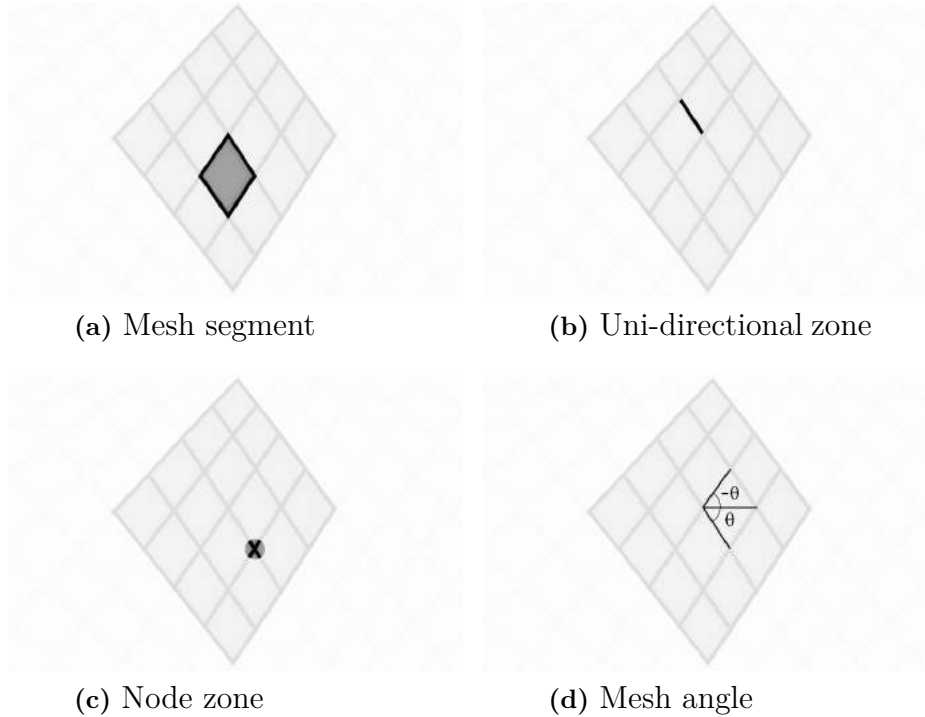


Figure 4.3: Terminology for the FRP module topology.

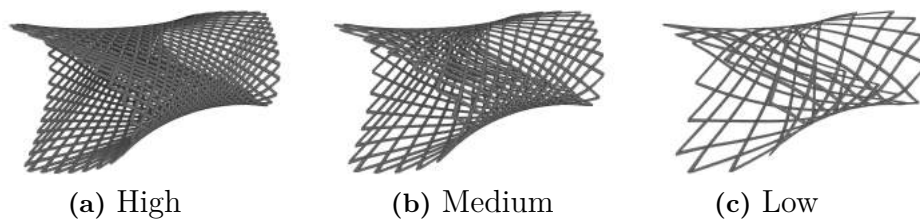


Figure 4.4: Different mesh densities of the FRP module.

4.1.2 Coordinate system and directions

In Figure 4.5 the coordinate system which is used as reference coordinate system for the FRP module is shown, the axes are denoted by x , y and z . In Figure 4.6 the reference coordinate systems which are used as local reference coordinates for the uni-directional and node zones respectively. The axes for the uni-directional zones are denoted by L , T and T' , and the axes for the node zones are denoted by 1, 2 and 3.

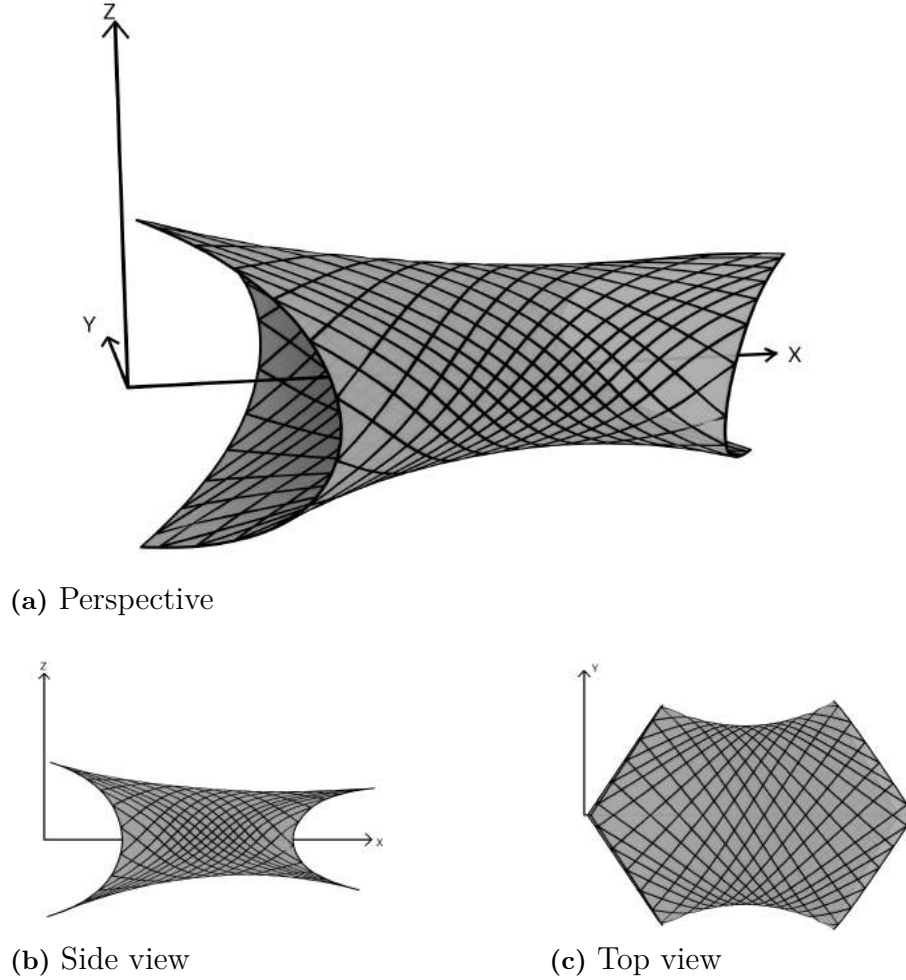


Figure 4.5: Reference coordinate system for the FRP module

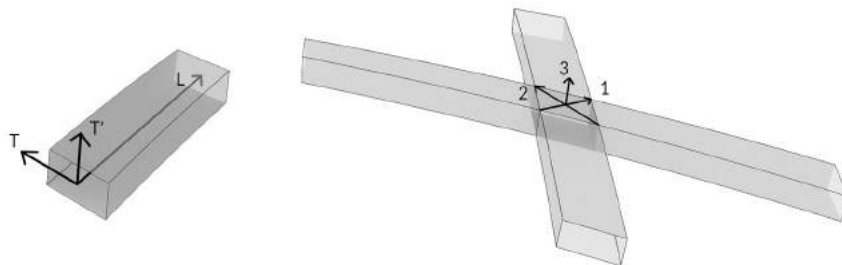


Figure 4.6: Local reference coordinate systems for the uni-directional elements (left) and the node zones (right). The orientation of the coordinate axes has been chosen based on the conventions used Classical Laminate Theory, see Chapter 5 - *Theoretical background*

4.1.3 Cross sections

The cross sections which are used can be seen in Table 4.1. A rectangular cross section is used for the fibre bundle cross sections in analysis. A description of fibre layups used in this study is given in Appendix A.1.1. The CFRP material parameters are explained in Section 4.1.4 below, and further in Chapters 6 and 7. In FE analysis a solid steel cross sections is used as a boundary element for the FRP module, see Chapter 10. The self weights of the materials have been omitted in analysis.

Table 4.1: Cross section parameters.

Cross section	Material	Width [mm]	Height [mm]
Fibre bundle	CFRP	20	10
Module edge	S355	45	45

4.1.4 Initial material parameters

The initial material parameters which are used in analysis can be seen in Tables 4.2 and 4.3 and have been based on data sheet [17][18] and literature values [19, pg. 26,40][20][6]. The shear moduli in the tables below have been calculated from Equation 4.1 [21, pg. 22]. The shear modulus for fibres is typically in a smaller range (27-50 GPa [6]), however this has small influence on the overall strength as the shear strength of the FRP composite is to a large extent determined by the matrix, see Chapter 5, Section 5.1.2. Characteristic values which will be used in design should be determined through mechanical tests according to EN1990 [6], however the initial parameters below provide a sufficient initial guesses, until material parameters can be determined through tests.

$$G = \frac{E}{2(1 + \nu)} \quad [\text{GPa}] \quad (4.1)$$

Table 4.2: Material properties of fibres

Material property	Variable	Value	Unit
Elastic longitudinal modulus	E_{fL}	238	GPa
Shear modulus	G_f	91.538	GPa
Poisson's ratio	ν_f	0.3	—
Thermal expansion coefficient	α_f	-0.4	$10^{-6}/^{\circ}\text{C}$
Fibre volume fraction	V_f	0.52	—

Table 4.3: Material properties of matrix.

Material property	Variable	Value	Unit
Elastic longitudinal modulus	E_{mL}	3.1	GPa
Shear modulus	G_m	1.174	GPa
Poisson's ratio	ν_m	0.32	—
Thermal expansion coefficient	α_m	50	$10^{-6}/^{\circ}\text{C}$
Matrix volume fraction	V_m	$1 - V_f$	—

4.2 Parametric 3D modelling and structural analysis tools

Computational tools make it possible to generate complex geometries and systems, and designers and architects often use digital models to describe and visualise ideas. One drawback of many of digital 3D modelling and structural analysis tools available is the lack of interactivity in design, it can often be difficult to make changes to one aspect of a model without making substantial changes to other parts [22]. **parametric modelling** tools have made it possible to use parameters to create interactive models in which the designer can change a few parameters and the entire model will update. Parametric design has been described by Wasson Jabi as ‘*A process based on algorithmic thinking that enables the expression of parameters and rules that, together, define, encode and clarify the relationship between design intent and design response.*’ [23][22]

4.2.1 Parametric modelling with Rhinoceros 3D and Grasshopper

Rhinoceros®, sometimes abbreviated as Rhino, is a 3D modelling tool and **Computer Aided Design, CAD**, tool developed by Robert McNeel & Associates [24]. As of version 6, this software includes parametric capabilities with the built in plugin Grasshopper®, which was previously a stand alone plugin for Rhino. Grasshopper is a graphical algorithm editor which is closely integrated with the Rhino interface, and can be used without extensive knowledge about programming [25]. It is also possible to extend the capabilities in both Rhino and Grasshopper, by installing third party plugins, or by programming using the built in or external programming editors.

It is possible to directly export geometry for structural analysis using the interface between SOFiSTiK and Rhinoceros 3D, provided by SOFiSTiK [26]. This interface is not parametric and it can thus be tedious to set the structural properties for large or complex models. Structural properties are stored in the 3D geometry objects as attributes, therefore it can be practical to use the scripting and programming, or external plugins, to automate the process of applying these attributes. For this study a combination of plugins from external sources, grasshopper scripts, and custom made plugins were used to create parametric models and to establish a parametric design and analysis method for the studied FRP module type. Some terms which are related to 3D modelling, which will be used in the following text can be found in Appendix A.2.

4.2.1.1 Parametric 3D models

A large number of case studies were conducted and several parametric models were created to simplify and automate the process, a description of these models can be found in Chapters 7 to 10.

4.2.1.2 Grasshopper tools for evaluation of results

In order to evaluate and compare the results in a straight forward and consistent manner a number of tools were developed in Grasshopper for this specific study. These tools were used to import displacements and internal stress and force results from SOFiSTiK into Rhino in order to calculate strains and curvatures and well as generate models showing displacements and stresses, both as deformed meshes and with colour gradients. These tools are described in Appendix B.2.

4. PRECONDITIONS

4.2.1.3 Grasshopper plugins

The external plugins which were used in this study are listed and briefly described below.

Human

The plugin Human is a plugin which extends Grasshopper's capability of creating and referencing geometry, and handling the Rhino document [27]. In this study this plugin was used to write *object attributes* (see Appendix A.2) containing structural information to geometrical objects in Rhino.

Weaverbird

Weaverbird is a topological mesh editor plugin for Grasshopper [28]. In this study this plugin was used to rebuild free form surfaces NURBS surfaces into polygonised meshes. Typically a polygonised mesh is less inaccurate than a NURBS surface, but in the cases where precision has been of less importance this plugin has been used to reduce computation times. See Appendix A.2 for a brief explanation of NURBS and polygon meshes.

TT toolbox

TT Toolbox is a plugin developed by Thornton Tomasetti and features a range of tools which can be used in Grasshopper [29]. In this study this plugin has been used to read data from Excel spreadsheets into Grasshopper.

Lunchbox

Lunchbox is another plugin for Grasshopper which contains several tools for use in Rhino and Grasshopper [30]. This plugin has been used to automate the *baking* (see Appendix A.2), or generation, of geometry from Grasshopper to Rhino.

ColorMesh

The plugin ColorMesh is a plugin which can be used to colour meshes to for instance visualise data [31]. This plugin has been used to visualise and compare structural analysis results from SOFiSTiK which have been imported into Grasshopper.

4.2.2 Object oriented programming with C#

To automate the creation of structural attributes for geometrical objects a number of components were programmed using the **Object Oriented Programming language, OOP, C#** (pronounced C-sharp), which is developed by Microsoft®[32]. The plugins were written using the built in C# editor in Grasshopper, and were compiled using Visual Studio 2015 [33] using templates for compilation provided by McNeel [34]. Some terms which are related to OOP, which will be used in the following text can be found in Appendix A.2.

4.2.2.1 Grasshopper components to extend SOFiSTiK interface

The interface provided between Rhinoceros and SOFiSTiK is not parametric, therefore three components were written using C# in order to automate this process. These components create structural information which can be written as attributes to geometrical objects in Rhino. These components are described in Appendix B.2.

4.2.3 Structural analysis in SOFiSTiK

SOFiSTiK is a FE analysis software for building and infrastructure projects [35]. One of the benefits with SOFiSTiK is that it has a built-in interface with several BIM and CAD softwares, as well as scripting possibilities with CADINP [36], the scripting language native to SOFiSTiK.

The results from analysis in SOFiSTiK were evaluated in the program module Wingraf, which is designed to display the analysis results visually [37]. However this tool reads the results directly from a database which is generated each time the analysis is run. Due to the parametric nature of this study, the results were thus not saved when the input parameters are changed. This was solved by developing stand-alone tools for graphical evaluation, however Wingraf was used as a means to verify these tools.

In SOFiSTiK it is possible to either define the FE model using CADINP code, or to create geometrical elements in external CAD softwares, and assign structural properties to these using SOFiSTiK's built in interface with these softwares. When assigning structural properties it is necessary to understand the terminology for structural and geometrical elements used in SOFiSTiK. Below follows a short description of geometrical and structural elements in SOFiSTiK which are used in this study.

SLN - Structural line

Structural lines, **SLN**, can either be straight lines or curves, and are commonly used to create truss, beam or cable elements.

SAR - Structural area

Structural areas, **SAR**, are commonly used to create plate or shell elements, but can also be used to define areas for load application.

SPT - Structural point

Structural points, **SPT**, are often used for supports, but can also be used to define springs or kinematic couplings.

QUAD - Quadrilateral 2D elements

In SOFiSTiK shell elements are modelled with **QUAD** elements. These elements are defined by four points and are typically analysed using the Mindlin-Reissner Plate Theory.

4.2.4 Structural analysis using MATLAB

MATLAB® is a computer program and programming language [38] developed by MathWorks. It was useful in his study, due to the simplicity of performing matrix operations and calculations. In this study a number of already existing MATLAB functions, for analysis of FRP composites, were used with permission [39] to establish constitutive equations for different laminates and to perform simple structural analysis, see Appendix B.1.

4.2.4.1 MATLAB programs for structural analysis using Classical Lamination Theory

A number of MATLAB programs were written, see Appendix B.1, using the functions mentioned above, to evaluate assumptions made for different types of laminates.

5

THEORETICAL BACKGROUND

5.1 Fibre reinforced plastic composites

A composite material is a material which consists of two, or more, distinct constituent materials, or phases, where the phases have significantly different properties [19, pg. 1]. In this text the focus will be on fibre composites, or more specifically, **uni-directional** FRP composites.

5.1.1 Uni-directional fibre composites

Uni-directional FRP composites consist of a discontinuous fibre phase dispersed in a continuous polymer phase. The fibre phase is referred to as **reinforcement**, as it is usually the stronger phase, and the polymer phase is usually called the **matrix** [19, pg. 2]. Figure 5.1a shows a principal cross section of a uni-directional FRP composite where fibres vary in diameter and are randomly distributed throughout the matrix, in analysis it will however be assumed that the fibres have uniform properties and diameters and are evenly distributed throughout the matrix as in Figure 5.1b [19, pg. 63].

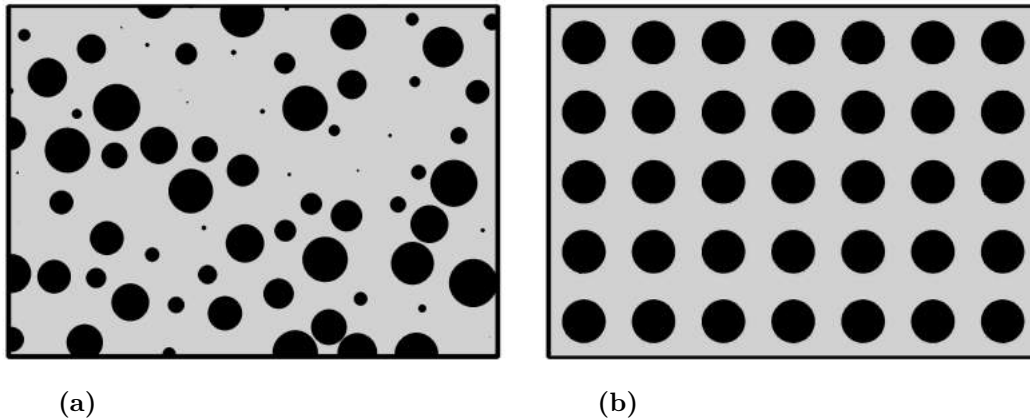


Figure 5.1: Principal cross sections of uni-directional fibre composites. Adapted from Figure 3-2 [19, pg. 64].

- (a) In reality the fibres have different diameters and are randomly distributed throughout the matrix.
- (b) When deriving elastic engineering constants for a uni-directional FRP composite it is assumed that the fibres have uniform properties and diameters and that they are evenly distributed throughout the matrix.

In Figure 5.2, a principal representation of a uni-directional FRP composite is shown. The composite material can be described by three mutually perpendicular planes of symmetry and three main directions, the **longitudinal direction**, $L(1)$, the **transverse direction**, $T(2)$ and the **transverse direction perpendicular to the lamina plane**, $T'(3)$ [19, pg. 63]. The two transverse directions T and T' exhibit nearly identical mechanical properties due to the random distribution of fibres as in Figure 5.1 and the plane $TT'(23)$ can therefore be said to be isotropic. The longitudinal and transverse directions have significantly different properties, due to this the material can be said to be **transversely isotropic**, where the $TT'(23)$ plane is isotropic and the $LT(12)$ and LT' planes are equal in properties and orthotropic.

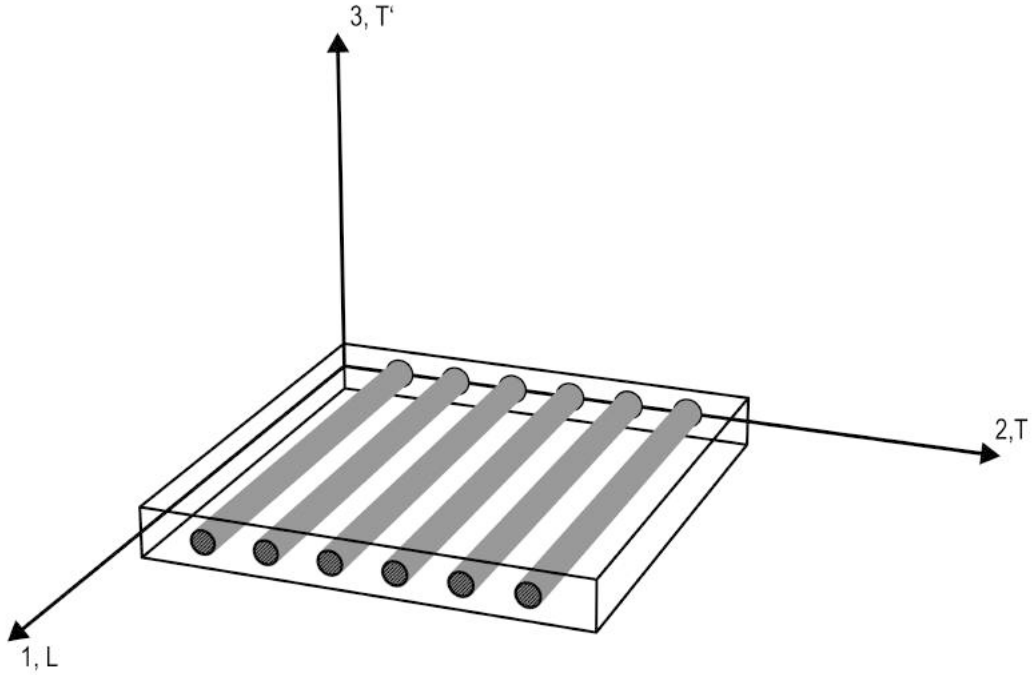


Figure 5.2: Principal representation of a uni-directional fibre composite. Adapted from Figure 3-1 [19, pg. 63].

- (1) Longitudinal direction in composite plane, denoted by L or 1 in the following text.
- (2) Transverse direction in composite plane, denoted by T or 2 in the following text.
- (3) Transverse direction perpendicular to composite plane, denoted by T' or 3 in the following text.

5.1.2 Mechanical properties of FRP composites

The mechanical properties in the longitudinal and transverse directions are dependent on the two constituent phases. Each of these phases have significantly different mechanical properties, which will affect the final structural behaviour of the composite material. However, it is not only the mechanical properties which determine the final composite but also the ratio of the two materials - the **volume fractions** of the fibre and matrix phases, V_f and V_m . The volume fractions are defined as ratios of the constituent material volumes, v_f and v_m , and the total composite volume, v_c , see Equations 5.1 to 5.3 [19, pg. 64-67].

$$v_c = v_f + v_m \quad [\text{m}^3] \quad (5.1)$$

$$V_f = \frac{v_f}{v_c} \quad (5.2)$$

$$V_m = \frac{v_m}{v_c} \quad (5.3)$$

5.1.2.1 Longitudinal stiffness

To determine the longitudinal stiffness, E_L , of a uni-directional composite it is assumed that the fibres are uniformly and continuously distributed throughout the composite parallel to the longitudinal material axis, with a uniform diameter as in Figure 5.2.

Further it is assumed the material properties of the fibres are also uniform and that the bonding between the fibres and matrix is perfect, which means that no slippage can occur and the strains of the composite, ε_c , and the sum of the strains of the constituent materials, ε_f and ε_m , are equal, see Equation 5.4 [19, pg. 68].

$$\varepsilon_c = \varepsilon_f = \varepsilon_m \quad (5.4)$$

For a longitudinally loaded composite, the load carried in the composite, P_L , must thus be evenly distributed, and the sum of the loads carried by the fibres and matrix, P_{fL} and P_{mL} respectively, must equal the total applied load as in equation 5.5.

$$P_L = P_{fL} + P_{mL} \quad (5.5)$$

This means that the longitudinal stiffness of the laminate can be directly determined from the volume fractions, and the stiffness of the fibre and matrix phases, E_f and E_m , as in equation 5.6. This kind of relation is called the **Rule of Mixtures**, **ROM**. For derivation of this expression see Agarwal [19, pg. 69].

$$E_L = E_f V_f + E_m V_m \quad [\text{GPa}] \quad (5.6)$$

5.1.2.2 Transverse stiffness

The transverse stiffness, E_T can be derived in a similar manner as the longitudinal stiffness and is expressed as in Equation 5.7. Here it is assumed that the stress is constant over the cross section perpendicular to the direction of loading for a transversely loaded composite. For derivation of this expression see Agarwal [19, pg. 80].

$$\frac{1}{E_T} = \frac{V_f}{E_f} + \frac{V_m}{E_m} \quad (5.7)$$

Experiments have however shown that the transverse modulus is better determined experimentally, as the actual distribution of fibres throughout the composite is not uniform as in Figure 5.2 but rather random as in Figure 5.1a [19, pg. 83]. A better estimation of the transverse modulus has been proposed by Halpin and Tsai and the equation for transverse stiffness can be expressed using Equations 5.8 and 5.9. The term ξ is a factor depending on several parameters, but can be assumed to be 2 for rectangular or circular cross sections [19, pg. 85].

$$\frac{E_T}{E_m} = \frac{1 + \xi \eta V_f}{1 - \eta V_f} \quad (5.8)$$

$$\eta = \frac{(E_f/E_m) - 1}{(E_f/E_m) + \xi} \quad (5.9)$$

5.1.2.3 Shear stiffness

The in-plane shear stiffness, G_{LT} , of a composite may be determined in the same way as the transverse stiffness was determined in equation 5.7. For detailed derivation of the transverse stiffness as given in Equation 5.10 see Agarwal [19, pg. 91].

$$\frac{1}{G_{LT}} = \frac{V_f}{G_f} + \frac{V_m}{G_m} \quad (5.10)$$

Again a better estimation for the shear stiffness has been proposed by Halpin and Tsai, as in Equations 5.11 and 5.12, where it can be assumed that $\xi = 1$.

$$\frac{G_{LT}}{G_m} = \frac{1 + \xi\eta V_f}{1 - \eta V_f} \quad (5.11)$$

$$\eta = \frac{(G_f/G_m) - 1}{(G_f/G_m) + \xi} \quad (5.12)$$

5.1.2.4 Poisson's ratio

The Major Poisson's ratio, ν_{LT} for the composite material can be determined from the **Rule of Mixtures for the Major Poisson's ratio**, see Equation 5.13. The Minor Poisson's ratio, ν_{TL} can be expressed with the previously established values for the longitudinal and transverse stiffness, E_L and E_T , see equation 5.14. For detailed derivation see Agarwal [19, pg. 95-96].

$$\nu_{LT} = \nu_f V_f + \nu_m V_m \quad (5.13)$$

$$\frac{\nu_{LT}}{E_L} = \frac{\nu_{TL}}{E_T} \quad (5.14)$$

5.1.2.5 Thermal expansion coefficients

Thermal expansion coefficients, α_L and α_T , for uni-directional FRP composites have been derived by Schapery [19, pg. 111], see equations 5.15 and 5.16

$$\alpha_L = \frac{1}{E_L}(\alpha_f E_f V_f + \alpha_m E_m V_m) \quad [1/^\circ\text{C}] \quad (5.15)$$

$$\alpha_T = (1 + \nu_f)\alpha_f V_f + (1 + \nu_m)\alpha_m V_m - \alpha_L \nu_{LT} \quad [1/^\circ\text{C}] \quad (5.16)$$

5.2 Mechanical properties of FRP laminae

One layer of a uni-directional FRP composite is called **lamina** or **ply**. Several laminae, or plies, are stacked on top each other to form a FRP laminate, see Section 5.3. In Section 5.1.1 it was stated that all uni-directional FRP are transversely isotropic, this means that four independent engineering constants are needed to relate stresses and strains in a lamina [19, pg. 160]. It is practical to express this relation in terms of a reference coordinate system as in Figure 5.3. When the longitudinal and transverse material directions align with the axes of the reference coordinate system the lamina is called a **specialy orthotropic lamina**, when the axes do not align the lamina is called a **generally orthotropic lamina**.

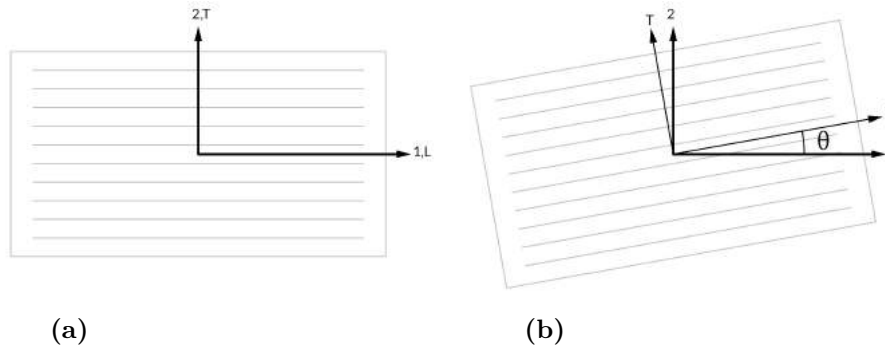


Figure 5.3: Specially and generally orthotropic laminae. Adapted from Figure 5-2 [19, pg. 161].

(a) Specially orthotropic lamina.

(b) Generally orthotropic lamina.

A common linear relationship which relates stresses, σ , and strains, ϵ , is the Generalized Hooke's Law [19, pg. 175], and can be expressed as

$$\sigma_{ij} = E_{ijkl} \epsilon_{kl} \quad [\text{GPa}] \quad (5.17)$$

where E_{ijkl} is a fourth order tensor, represented as a matrix, which contains the elastic constants of the material, see Appendix A.3.1. In the most general case this matrix contains 21 independent components, but in the case of transversely isotropic materials the number of components can be reduced to six, where five are independent [19, pg. 177-180].

5.2.1 Specially orthotropic lamina under plane stress

For a specially orthotropic lamina loaded under plane stress stress strain relationship can be expressed as in Equation 5.18, or on matrix form as in equation 5.19 [19, pg. 182-186].

$$\sigma_{12} = Q \epsilon_{12} \quad [\text{GPa}] \quad (5.18)$$

$$\begin{bmatrix} \sigma_1 \\ \sigma_2 \\ \tau_{12} \end{bmatrix} = \begin{bmatrix} Q_{11} & Q_{12} & Q_{16} \\ & Q_{22} & Q_{26} \\ \text{Sym.} & & Q_{66} \end{bmatrix} \begin{bmatrix} \varepsilon_1 \\ \varepsilon_2 \\ \gamma_{12} \end{bmatrix} \quad [\text{GPa}] \quad (5.19)$$

The \mathbf{Q} matrix is called the lamina stiffness matrix for the composite. The inverse of the stiffness matrix is called the compliance matrix, \mathbf{S} . From the compliance matrix it is possible to derive equations, in terms of the material engineering constants, for the components, Q_{ij} , of the \mathbf{Q} matrix, see Equations 5.20 to 5.24 and Appendix A.3.1.

$$Q_{11} = \frac{E_L}{1 - \nu_{LT}\nu_{TL}} \quad (5.20)$$

$$Q_{22} = \frac{E_T}{1 - \nu_{LT}\nu_{TL}} \quad (5.21)$$

$$Q_{12} = \frac{\nu_{LT}E_T}{1 - \nu_{LT}\nu_{TL}} = \frac{\nu_{TL}E_L}{1 - \nu_{LT}\nu_{TL}} \quad (5.22)$$

$$Q_{66} = G_{LT} \quad (5.23)$$

$$Q_{16} = Q_{26} = 0 \quad (5.24)$$

5.2.2 Generally orthotropic lamina under plane stress

The stresses and strains for a generally orthotropic lamina oriented with the angle θ in the reference coordinate system can be obtained by transformation as in Equations 5.25 and 5.26[19, pg. 189-192]

$$\begin{bmatrix} \sigma_L \\ \sigma_T \\ \tau_{LT} \end{bmatrix} = \boldsymbol{\sigma}_{LT} = [\mathbf{T}_1]_{\theta} \boldsymbol{\sigma}_{12} \quad (5.25)$$

$$\begin{bmatrix} \varepsilon_L \\ \varepsilon_T \\ \gamma_{LT} \end{bmatrix} = \boldsymbol{\epsilon}_{LT} = [\mathbf{T}_2]_{\theta} \boldsymbol{\epsilon}_{12} \quad (5.26)$$

The matrices \mathbf{T}_1 and \mathbf{T}_2 are transformation matrices with regard to θ , see Appendix A.3.2 [19, pg. 190]. The stresses for the lamina in the reference coordinate system can therefore be expressed as in Equations 5.27 and 5.28, where $\bar{\mathbf{Q}}$ is the transformed stiffness matrix for the lamina.

$$\boldsymbol{\sigma}_{12} = [\mathbf{T}_1]_{\theta}^{-1} \mathbf{Q} [\mathbf{T}_2]_{\theta} \boldsymbol{\epsilon}_{12} \quad (5.27)$$

$$\boldsymbol{\sigma}_{12} = \bar{\mathbf{Q}}_{\theta} \boldsymbol{\epsilon}_{12} \quad (5.28)$$

5.3 Constitutive equations for FRP laminates

A FRP **lamin**ate consists of laminae, or plies, stacked on top of each other as in Figure 5.4a. A local coordinate system is used to describe each lamina in relation to the mid-plane of the laminate as in Figure 5.4b. A laminate with thickness t is constructed from n number of plies where the laminate reference coordinate system is placed in the mid-plane of the laminate. The bottom position related to the local z axis, for a lamina k , is given as h_k . The thickness of an individual lamina is given as t_k .

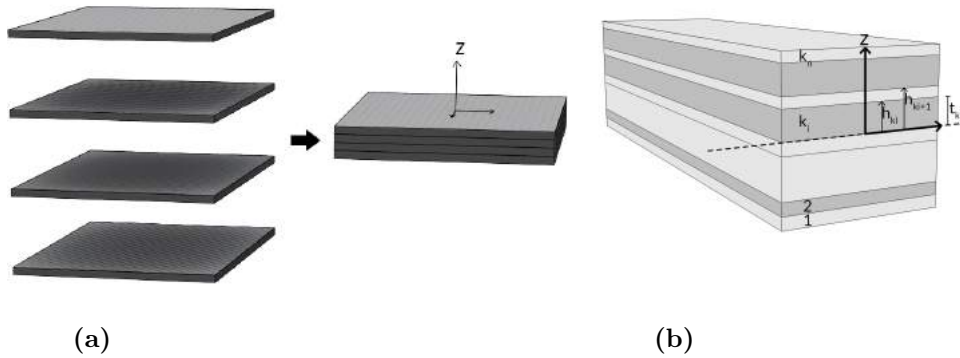


Figure 5.4: Description of a FRP laminate and terminology. Adapted from Figures 6-1 and 6-5 [19, pg. 215,219].

- (a) A FRP laminate consists of FRP laminae stacked on top of each other.
- (b) A laminate with thickness t is constructed from n number of plies where the laminate reference coordinate system is placed in the mid-plane of the laminate. The bottom position related to the local z axis, for a lamina k , is given as h_k . The thickness of an individual lamina is given as t_k .

Since the laminae in a laminate may have unique orientations with regard to the reference coordinate system it is necessary to establish a system which describes the individual laminae and their orientations, θ , and position in a laminate, a **Laminate Orientation Code**, LOC [19, pg. 225-226], which can also be referred to as **layup**. The system is explained below and an example is shown in Figure 5.5.

Laminate Orientation Code, LOC

Orientation

The orientation of a lamina is given as a positive or negative angle relative to the reference coordinate system, ranging from -90° to 90° .

Sequence

The laminae in the laminate are ordered from bottom to top, where the start and end of the LOC is marked by brackets. Each individual lamina is separated from the others with a backslash if the orientations are different, see Figure 5.5.

Number of laminae

If two or more laminae in sequence have the same orientation the number of laminae is given as a numerical subscript.

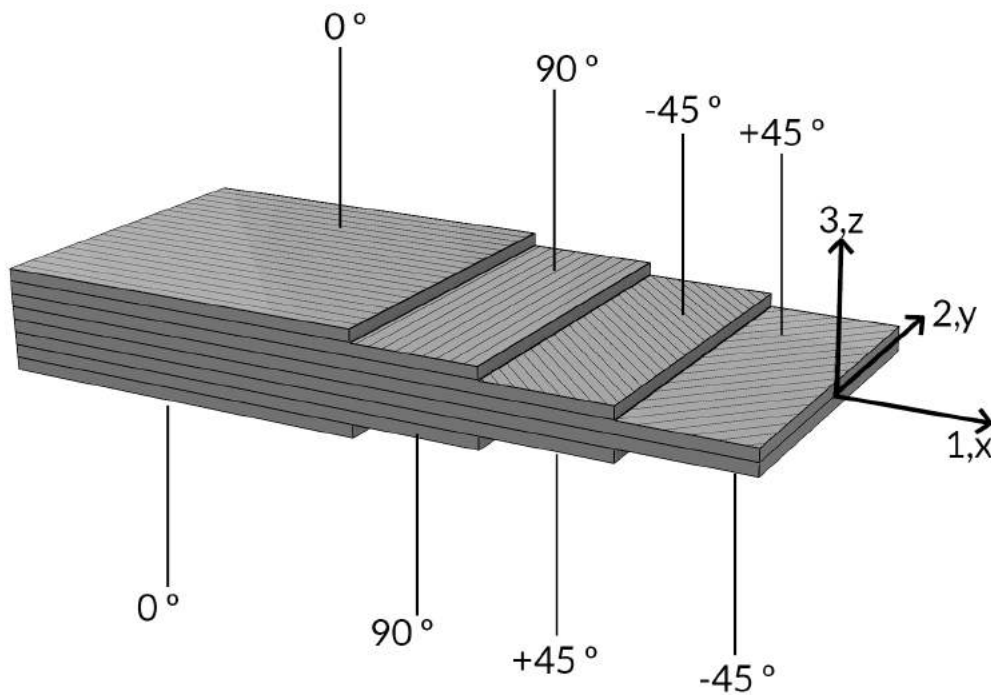


Figure 5.5: A laminate with orientation code $[0\backslash 90\backslash +45\backslash -45\backslash +45\backslash -45\backslash 90\backslash 0]$. Adapted from Figure A3-1 [19, pg. 543].

5.3.1 Classical lamination theory for FRP laminates

The constitutive equations for a laminate can be derived using **Classical Lamination Theory, CLT**. Here it is assumed that the bond between two laminae in a laminate is perfect, thus the entire laminate will behave as a plate where the variation of the strains vary linearly over the thickness of the laminate, however due to the varying orientations of each lamina the stresses will vary through the thickness, see Figure 5.6. (p 213 -216)

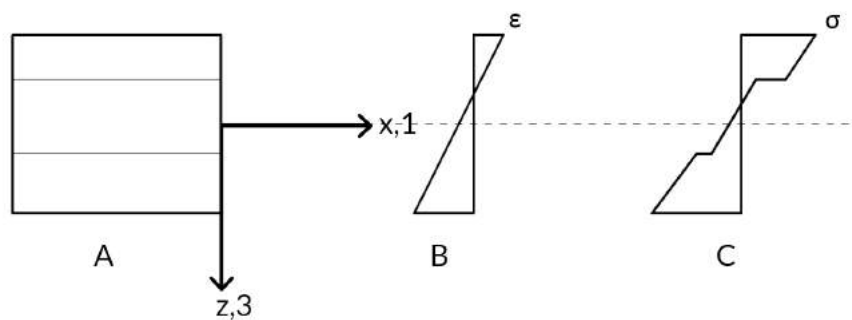


Figure 5.6: Strain and strain variation in a principal FRP laminate. Adapted from Figure 6-3 [19, pg. 217].

- (A) A principal laminae with three laminae.
- (B) Strain variation of a principal laminate.
- (C) Stress variation of a principal laminate.

5. THEORETICAL BACKGROUND

A laminated plate which undergoes a deformation is considered, see Figure 5.7. It is assumed that the line AB is initially straight and perpendicular to the plate mid-plane, and will remain straight and perpendicular to the mid-plane also in the deformed state. This means that any shear deformations in the xz and yz planes are neglected.

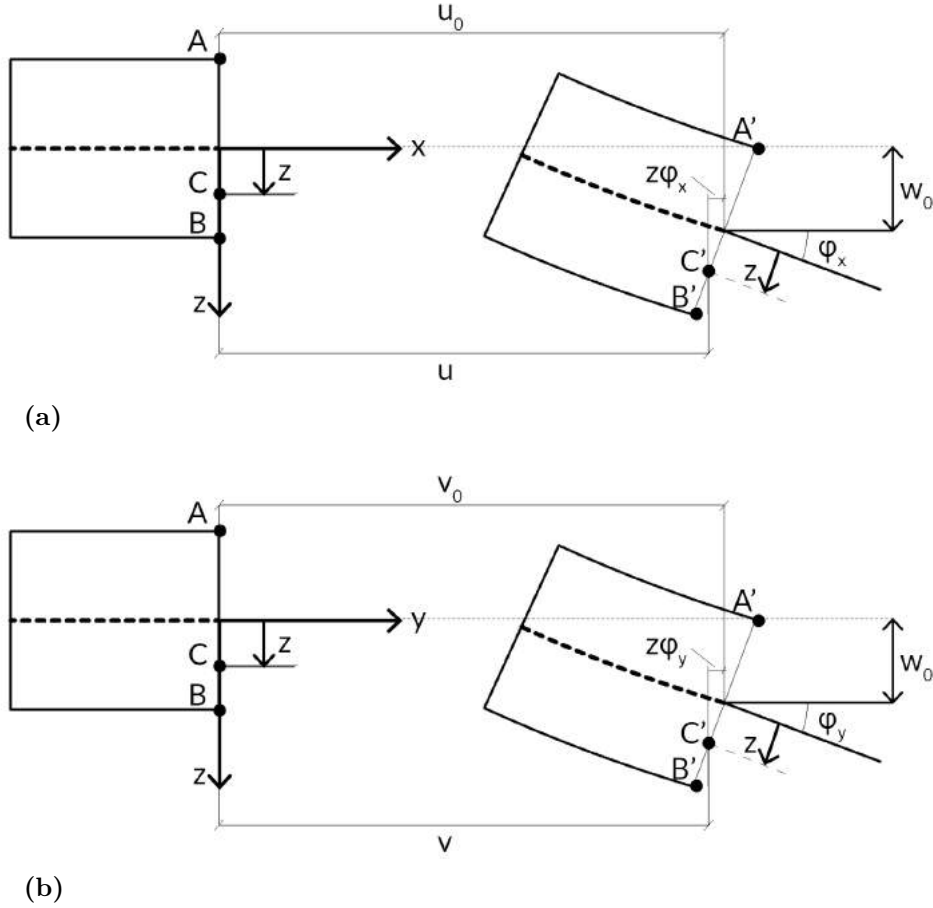


Figure 5.7: Deformation and displacements of a FRP laminate. Adapted from Figure 6-2 [19, pg. 215].

- (a) Deformation and displacements of a laminate in the xz plane.
- (a) Deformation and displacements of a laminate in the yz plane.

The displacement in the x -direction, u , of the point C (see Figure 5.7a) can be expressed in terms of the mid-plane displacement in the x -direction, u_0 , and slope of the mid-plane in the x -direction, φ_x , as in Equation 5.29. (p. 214).

$$u = u_0 - z \sin \varphi_x \approx u_0 - z \varphi_x = \frac{\partial w_0}{\partial x} \quad [\text{m}] \quad (5.29)$$

Similarly the displacement of any point in the y -direction (see Figure 5.7b), v , can be expressed in terms of the mid-plane displacement in the y -direction, v_0 , and slope of the mid-plane in the y -direction, φ_y , as in Equation 5.30.

$$v = v_0 - z \sin \varphi_y \approx v_0 - z \varphi_y = \frac{\partial w_0}{\partial y} \quad [\text{m}] \quad (5.30)$$

It is also assumed that the stretching of the normal of the plate (AB) is insignificant and thus the displacements in the z -direction is assumed to be equal to the mid-plane displacement in the z -direction, w_0 . The strains of the laminate can therefore be expressed as in Equations 5.31 to 5.33.

$$\varepsilon_x = \frac{\partial u}{\partial x} = \frac{\partial u_0}{\partial x} - z \frac{\partial \varphi_x}{\partial x} \quad (5.31)$$

$$\varepsilon_y = \frac{\partial v}{\partial y} = \frac{\partial v_0}{\partial y} - z \frac{\partial \varphi_y}{\partial y} \quad (5.32)$$

$$\gamma_{xy} = \frac{\partial u}{\partial y} + \frac{\partial v}{\partial x} = \frac{\partial u_0}{\partial y} + \frac{\partial v_0}{\partial x} - z \left(\frac{\partial \varphi_x}{\partial y} + \frac{\partial \varphi_y}{\partial x} \right) \quad (5.33)$$

The strain and displacement can now be expressed in terms of the mid-plane strains, $\boldsymbol{\epsilon}^0$, and plate curvature, $\boldsymbol{\kappa}$, in the laminate reference coordinate system as in Equations 5.34 and 5.35.

$$\begin{bmatrix} \varepsilon_x \\ \varepsilon_y \\ \gamma_{xy} \end{bmatrix} = \begin{bmatrix} \varepsilon_x^0 \\ \varepsilon_y^0 \\ \gamma_{xy}^0 \end{bmatrix} + \begin{bmatrix} \kappa_x \\ \kappa_y \\ \kappa_{xy} \end{bmatrix} z \quad \text{or} \quad \begin{bmatrix} \varepsilon_1 \\ \varepsilon_2 \\ \gamma_{12} \end{bmatrix} = \begin{bmatrix} \varepsilon_1^0 \\ \varepsilon_2^0 \\ \gamma_{12}^0 \end{bmatrix} + \begin{bmatrix} \kappa_1 \\ \kappa_2 \\ \kappa_{12} \end{bmatrix} z \quad (5.34)$$

$$\boldsymbol{\epsilon} = \boldsymbol{\epsilon}^0 + \boldsymbol{\kappa}z \quad (5.35)$$

The strains and stresses in each lamina can be independently expressed in relation to the mid-plane strains and plate curvature of the laminate as in Equation 5.36.

$$\begin{bmatrix} \sigma_1 \\ \sigma_2 \\ \tau_{12} \end{bmatrix}_k = \bar{\mathbf{Q}}_k \begin{bmatrix} \varepsilon_1^0 \\ \varepsilon_2^0 \\ \gamma_{12}^0 \end{bmatrix} + \bar{\mathbf{Q}}_k \begin{bmatrix} \kappa_1 \\ \kappa_2 \\ \kappa_{12} \end{bmatrix} z = \bar{\mathbf{Q}}_k \{ \boldsymbol{\epsilon}^0 + \boldsymbol{\kappa}z \} \quad (5.36)$$

Due to the varying stress in each lamina it can be convenient to express the relationship between stresses and strains in terms of resultant forces, \mathbf{N} , and resultant moments, \mathbf{M} , which can be summed by integration over the height of the laminate as in Equations 5.37 and 5.38.

$$\begin{bmatrix} N_1 \\ N_2 \\ N_{12} \end{bmatrix} = \int_{-h/2}^{h/2} \begin{bmatrix} \sigma_1 \\ \sigma_2 \\ \tau_{12} \end{bmatrix} dz = \sum_{k=1}^n \int_{h_{k-1}}^{h_k} \begin{bmatrix} \sigma_1 \\ \sigma_2 \\ \tau_{12} \end{bmatrix}_k dz \quad [\text{N/m}] \quad (5.37)$$

$$\begin{bmatrix} M_1 \\ M_2 \\ M_{12} \end{bmatrix} = \int_{-h/2}^{h/2} \begin{bmatrix} \sigma_1 \\ \sigma_2 \\ \tau_{12} \end{bmatrix} z dz = \sum_{k=1}^n \int_{h_{k-1}}^{h_k} \begin{bmatrix} \sigma_1 \\ \sigma_2 \\ \tau_{12} \end{bmatrix}_k z dz \quad [\text{Nm/m}] \quad (5.38)$$

5. THEORETICAL BACKGROUND

With Equation 5.36 these two equations can be written as Equation 5.39 and 5.40.

$$\mathbf{N} = \left[\sum_{k=1}^n \bar{\mathbf{Q}}_k \int_{h_{k-1}}^{h_k} dz \right] \boldsymbol{\epsilon}^0 + \left[\sum_{k=1}^n \bar{\mathbf{Q}}_k \int_{h_{k-1}}^{h_k} z dz \right] \boldsymbol{\kappa} \quad (5.39)$$

$$\mathbf{M} = \left[\sum_{k=1}^n \bar{\mathbf{Q}}_k \int_{h_{k-1}}^{h_k} z dz \right] \boldsymbol{\epsilon}^0 + \left[\sum_{k=1}^n \bar{\mathbf{Q}}_k \int_{h_{k-1}}^{h_k} z^2 dz \right] \boldsymbol{\kappa} \quad (5.40)$$

By introducing

$$\mathbf{A} = \sum_{k=1}^n \bar{\mathbf{Q}}_k \int_{h_{k-1}}^{h_k} dz \quad [\text{Pa}\cdot\text{m}] \quad (5.41)$$

$$\mathbf{B} = \sum_{k=1}^n \bar{\mathbf{Q}}_k \int_{h_{k-1}}^{h_k} z dz \quad [\text{Pa}\cdot\text{m}^2] \quad (5.42)$$

$$\mathbf{D} = \sum_{k=1}^n \bar{\mathbf{Q}}_k \int_{h_{k-1}}^{h_k} z^2 dz \quad [\text{Pa}\cdot\text{m}^3] \quad (5.43)$$

the constitutive equation for a laminate can thus now be expressed as

$$\begin{bmatrix} \mathbf{N} \\ \mathbf{M} \end{bmatrix} = \begin{bmatrix} \mathbf{A} & \mathbf{B} \\ \mathbf{B} & \mathbf{D} \end{bmatrix} \begin{bmatrix} \boldsymbol{\epsilon}^0 \\ \boldsymbol{\kappa} \end{bmatrix} \quad (5.44)$$

where \mathbf{A} , \mathbf{B} and \mathbf{D} are called the extensional stiffness matrix, the coupling stiffness matrix and the bending stiffness matrix. These matrices are 3×3 matrices and are all symmetric, see Equations 5.45 to 5.47

$$\mathbf{A} = \begin{bmatrix} A_{11} & A_{12} & A_{16} \\ & A_{22} & A_{26} \\ \text{Sym.} & & A_{66} \end{bmatrix} \quad (5.45)$$

$$\mathbf{B} = \begin{bmatrix} B_{11} & B_{12} & B_{16} \\ & B_{22} & B_{26} \\ \text{Sym.} & & B_{66} \end{bmatrix} \quad (5.46)$$

$$\mathbf{D} = \begin{bmatrix} D_{11} & D_{12} & D_{16} \\ & D_{22} & D_{26} \\ \text{Sym.} & & D_{66} \end{bmatrix} \quad (5.47)$$

5.4 Mechanical coupling in FRP laminates

The components of the \mathbf{A} , \mathbf{B} and \mathbf{D} matrices are directly related to the orientation, thickness and the layup sequence of the plies in the laminate. The laminate can therefore be designed in such a way that certain elements of these matrices can be made zero, or non-zero, and thus exhibit or eliminate certain structural behaviours.

Two special types of laminates which can be very useful, are symmetric and balanced laminates, see Sections 5.4.1 and 5.4.2, because they eliminate **mechanical coupling** between in-plane extension and shear as well as out-of-plane coupling between extension and bending, see Figures 5.8 and 5.9.

Laminates which have no coupling behaviours are called un-coupled laminates, or Fully Orthotropic Laminates, see Section 5.5. Even though symmetric and balanced laminates are not entirely un-coupled these are often used in aerospace applications, where it is assumed that the coupling effects may be safely disregarded in laminates with a large number of plies [40].

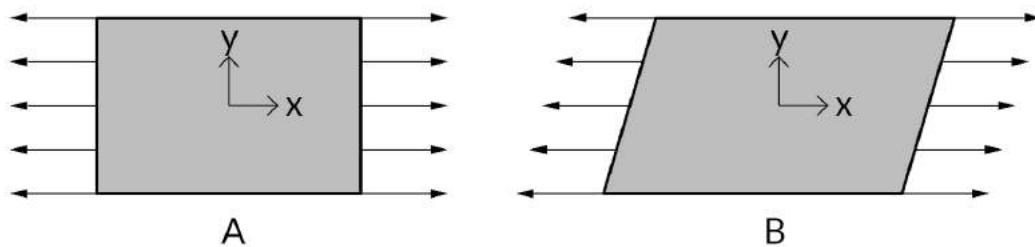


Figure 5.8: A laminate is said to be coupled with regard to in-plane extension and shear if an axially applied load gives rise to shear deformation.

(A) An axially loaded laminate.

(B) Shear deformation in a laminate which is coupled with regard to in-plane extension and shear.

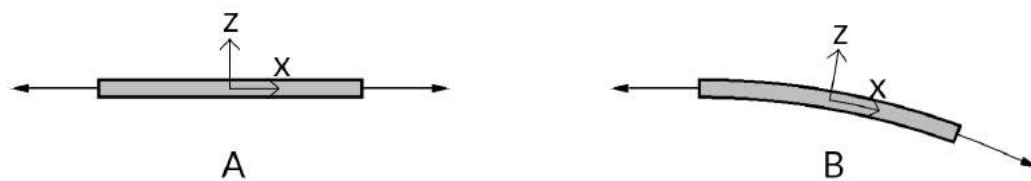


Figure 5.9: A laminate is said to be coupled with regard to in-plane extension and out-of-plane bending if an axially applied load gives rise to plate bending or warping.

(A) An axially loaded laminate.

(B) Deformation in a laminate which is coupled with regard to in-plane extension and out-of-plane bending.

5.4.1 Symmetric laminates

A **symmetric laminate** is always symmetric about the mid-plane, and for each lamina with an orientation θ and thickness t_k at a certain distance z from the mid-plane there must also exist one lamina with the same thickness t_k with an orientation θ at a distance $-z$ from the mid-plane [19], see Figure 5.10.

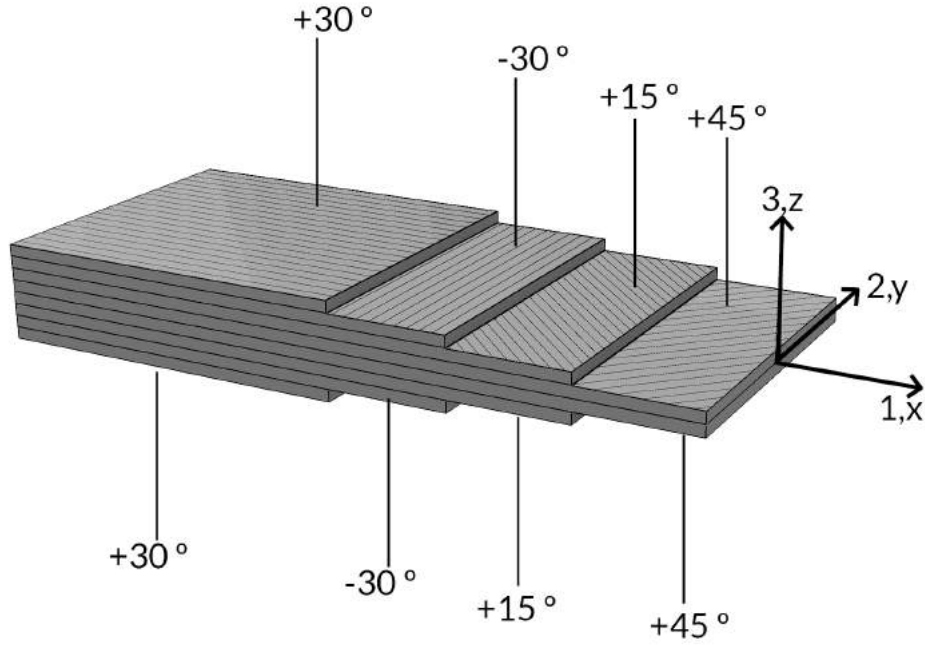


Figure 5.10: A symmetric laminate with LOC $[30\backslash-30\backslash15\backslash45\backslash45\backslash15\backslash-30\backslash30]$ or $[30\backslash-30\backslash15\backslash45]_s$. Adapted from Figure A3-1 [19, pg. 543].

In these laminates the components B_{ij} of the \mathbf{B} matrix will always be zero, and the matrix is therefore denoted as \mathbf{B}_0 [40]. In some cases, even a non-zero \mathbf{B} matrix can be considered non-coupled, if it's small enough [41].

$$\mathbf{B}_0 = \begin{bmatrix} B_{11} & B_{12} & B_{16} \\ & B_{22} & B_{26} \\ \text{Sym.} & & B_{66} \end{bmatrix} = \begin{bmatrix} 0 & 0 & 0 \\ 0 & 0 & 0 \\ 0 & 0 & 0 \end{bmatrix} \quad (5.48)$$

The \mathbf{B} matrix is called the coupling stiffness matrix because it relates the extension and bending of a laminate mathematically, see Equation 5.44. This means that it relates the mid-plane strains and plate curvatures in the laminate. Thus, a load applied in the plane of the laminate can cause the laminate to bend or warp out of plane, if the elements of the coupling matrix \mathbf{B} are non-zero [19, pg. 221]. In a symmetric laminate there will therefore be no out-of-plane extension and bending coupling.

In these laminates the components, A_{ij} , of the \mathbf{A} matrix, and components, D_{ij} , of the \mathbf{D} matrix may all be finite (non-zero), in which case these are denoted as \mathbf{A}_f and \mathbf{D}_f . The most general symmetric laminate is thus designated as $\mathbf{A}_f\mathbf{B}_0\mathbf{D}_f$ [42].

5.4.2 Balanced laminates

A **balanced laminate** can be constructed in three different ways [19, pg. 228-228]. **Angle-ply laminates** are constructed such that there for every lamina with a thickness h and orientation θ exist an other lamina with the same thickness and orientation, $-\theta$, see Figure 5.11. In the following text the term balanced laminate will refer to angle-ply laminates unless it is stated otherwise. The other two balanced types are **uni-directional laminates**, which consist only of laminae with the same orientation, and **cross-ply laminates** which consist of laminae with the orientations $\pm 0^\circ$ or $\pm 90^\circ$ only.

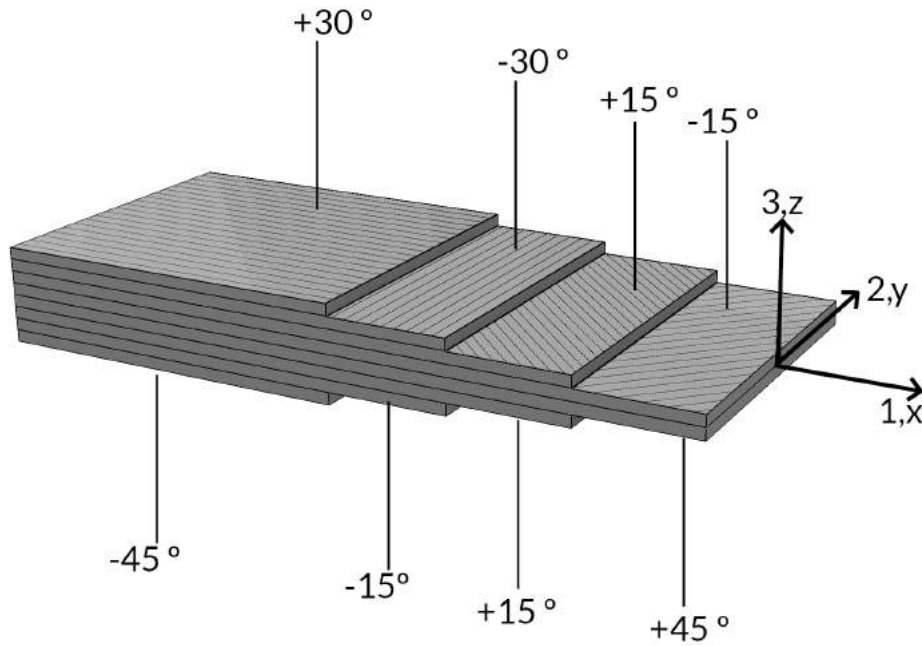


Figure 5.11: A balanced laminate with LOC $[30 \setminus -30 \setminus 15 \setminus -15 \setminus 45 \setminus 15 \setminus -15 \setminus -45]$. Adapted from Figure A3-1 [19, pg. 543].

A laminate is said to be balanced if the A_{16} and A_{26} components of the \mathbf{A} matrix are zero, in which case it is denoted as \mathbf{A}_s , see Equation 5.49.

$$\mathbf{A}_s = \begin{bmatrix} A_{11} & A_{12} & 0 \\ & A_{22} & 0 \\ \text{Sym.} & & A_{66} \end{bmatrix} \quad (5.49)$$

The \mathbf{A} matrix describes the in-plane behaviour of a laminate. If the terms A_{16} and A_{26} are non-zero there will be in-plane shear coupling effects, meaning that an axially loaded laminate will also be subjected to shear deformation. A balanced laminate will therefore not have any in-plane extension and shear coupling.

In these laminates, the components, B_{ij} , of the \mathbf{B} matrix may all be finite (non-zero), in which case the matrix is denoted as \mathbf{B}_f . In the most general case the components D_{ij} of the \mathbf{D} matrix will be non-zero, but in some cases the D_{16} and D_{26} components may be zero, it will therefore be denoted as \mathbf{D}_s . The most general balanced laminate is thus designated as $\mathbf{A}_s \mathbf{B}_f \mathbf{D}_f$ [42].

5.5 Equivalent material parameters for Fully Orthotropic Laminates

A **Fully Orthotropic Laminate**, **FOL**, will be fully un-coupled, meaning it will not display either in-plane extension and shear coupling, nor out-of-plane extension and bending coupling. A laminate of this type is designated as $\mathbf{A}_s\mathbf{B}_0\mathbf{D}_s$ [42]. These laminates generally minimise distortion which may occur during manufacturing and increase compression buckling strength in comparison with symmetric and balanced laminates [40]. This type of laminate will also have the same mechanical behaviour as a uni-directional laminae, and thus the mechanical properties of this type of laminate can be described by elastic engineering constants, which can be derived from the laminate constitutive equation.

5.5.1 Stress-strain relation in fully orthotropic laminates - Effective elastic engineering constants

Efficient elastic engineering constants for a FOL can be derived from the stress-strain relation in a laminate, the process for this is described below. For the derivation it is assumed that the laminate is transversely isotropic, meaning that both the strains and stress is linearly distributed over the laminate height. This assumption is not true for FOL with laminae with orientations $\theta \neq 0^\circ$, however for the sake of the derivation of efficient engineering constants this assumption is assumed to be valid as the mechanical behaviour of the laminate is transversely isotropic.

By letting $N_1 \neq 0$ and $N_2 = N_{12} = 0$ the constitutive equation for this type of laminate can be simplified as in Equation 5.50.

$$N_1 = A_{11}\varepsilon_1 + A_{12}\varepsilon_2 \quad (5.50)$$

Since the stress is assumed to be uniform over the height, this equation can be re-written as

$$\sigma_1 t = A_{11}\varepsilon_1 + A_{12}\varepsilon_2 \quad (5.51)$$

where t is the laminate thickness. By introducing Hooke's Law into Equation 5.51 the expression can now be formulated as in Equation 5.52.

$$E_1 \varepsilon_1 t = A_{11}\varepsilon_1 + A_{12}\varepsilon_2 \quad (5.52)$$

And now the elastic modulus in the main direction can be calculated as in Equation 5.53.

$$E_1 = \frac{A_{11}}{t} + \frac{A_{12}\varepsilon_2}{\varepsilon_1 t} \quad (5.53)$$

The Major Poisson's ration can be calculated as in Equation 5.54.

$$\nu_{12} = \frac{-\varepsilon_2}{\varepsilon_1} \quad (5.54)$$

The transverse modulus, and Minor Poisson's ratio can be calculated in the same way by letting $N_2 \neq 0$ and $N_1 = N_{12} = 0$.

$$E_2 = \frac{A_{21}\varepsilon_1}{\varepsilon_2 t} + \frac{A_{22}}{t} \quad (5.55)$$

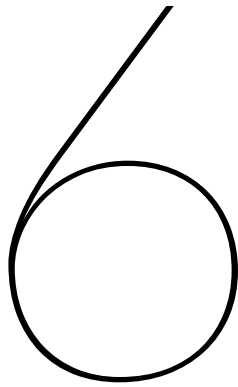
$$\nu_{21} = \frac{-\varepsilon_1}{\varepsilon_2} \quad (5.56)$$

The shear modulus is calculated directly from the A matrix as in Equation 5.57.

$$G_{12} = \frac{A_{66}}{t} \quad (5.57)$$

Finally the thermal expansion coefficient are calculated using the transformation matrix \mathbf{T}_2 and the α_L and α_T for the laminate, see Equation 5.58.

$$\begin{bmatrix} \alpha_1 \\ \alpha_2 \\ \alpha_{12} \end{bmatrix} = T_2^{-1} \begin{bmatrix} \alpha_L \\ \alpha_T \\ 0 \end{bmatrix} \quad (5.58)$$



MATERIAL PARAMETERS FOR STRUCTURAL ANALYSIS

6. MATERIAL PARAMETERS FOR STRUCTURAL ANALYSIS

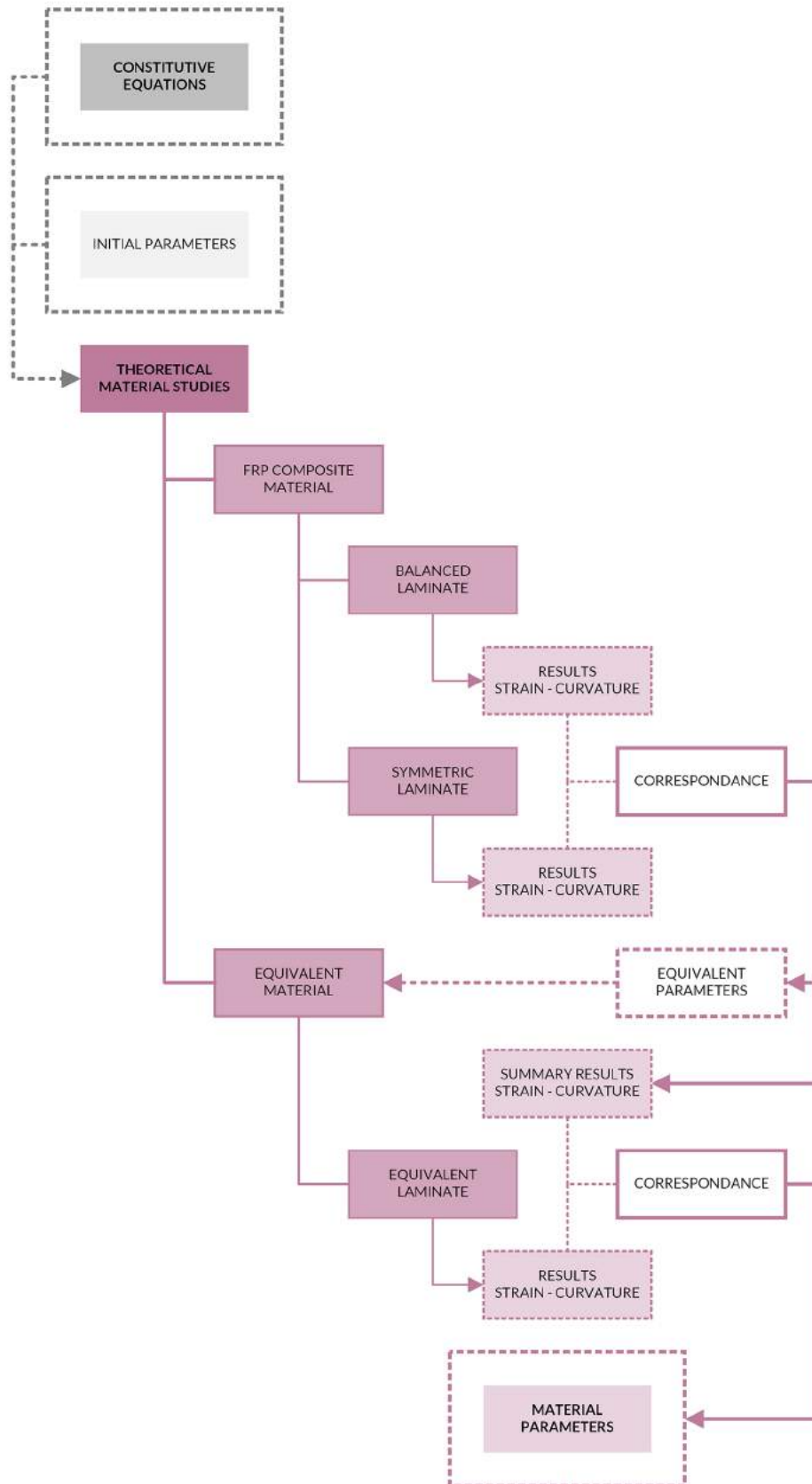


Figure 6.1: Flowchart describing the methodology used for the case studies presented in Chapter 6 - Material parameters for structural analysis.

6.1 Analysis of FRP composites

The possibilities to analyse anisotropic materials in SOFiSTiK are limited. It is possible to define fibrous or layered materials with orthotropic material properties, for instance ply-wood [43]. However in the case of uni-directional FRP composites it can be difficult to define suitable material formulations, due to for instance a large number of laminae, a Poisson's ratio > 0.5 or large differences in stiffness in different orientations. This will be seen later in Chapter 7, Section 7.2. Due to these reasons it is convenient to use simplified material definitions for analysis in SOFiSTiK, in order to establish a stable and reliable parametric analysis approach.

In Chapter 5 the constitutive equations for laminated FRP composites were derived, and the principal mechanical behaviours of balanced, symmetric and fully orthotropic laminates were explained. It was seen that the components of the \mathbf{A} , \mathbf{B} and \mathbf{D} matrices are linked to the lamina orientations, number of laminae as well as lamina thickness.

The FRP module which is the topic of study, as well as the node discontinuity zones in Figure 1.7, are recalled from Chapter 1. It is clear that the theory presented in the previous chapter mainly applies to the node zones at the intersections between the fibre bundles. These areas are already potential instability and stress concentration zones due to change of stiffness as well as geometric discontinuities. In addition to this, it is also now known that these zones may give rise to additional instability modes due to mechanical coupling effects.

By design the fibre bundles of the FRP module cannot be constructed such that the node zones will have fully orthotropic laminate layups, however the layup will always be either symmetric or balanced with alternating lamina orientations $\pm\theta$, see Appendix A.1. If the number of laminae in these laminates is large enough, it may be possible to neglect the coupling effects, see Section 5.4.

Instabilities and stress concentrations due to geometric discontinuities have been excluded from the scope of this study, however it is still necessary to determine if it is possible to also exclude the coupling effects of the node zones in order to be able to simplify the material formulations in SOFiSTiK.

The pre-normative design guidelines, mentioned in Section 1.1.1 proposes methods in which characteristic material values for FRP composites can be determined. It can be done by using CLT, conducting tests on a similar laminate or by laboratory tests which are specified in the EN1990 [6]. It is also recommended to apply a symmetric and balanced laminate design, which is not the case in the studied FRP module.^{1,2}

In this chapter a number of assumptions are presented, and a number of case studies were conducted in order to evaluate and verify these assumptions. The principal method and work flow for these case studies can be seen in Figure 6.1.

¹ In the pre-normative design guidelines the term balanced laminate (or bi-directional laminate) refers to only cross ply laminates (with $\pm 0^\circ$ and $\pm 90^\circ$ orientations) [6]. This type of laminate will always be a FOL.

² It should be noted that a laminate which is simultaneously symmetric and balanced may not be fully orthotropic, due to the fact that the \mathbf{D} matrix could be finite (\mathbf{D}_f). An example of a laminate which is symmetric and balanced, but not a FOL is $[30/-45/-15/15/45/-30]_s$.

6.1.1 Assumptions

The assumptions made in this chapter apply to thick laminates with balanced or symmetric layups and alternating lamina orientations $\pm\theta$, see Figure 6.2 and Appendix A.1. These types of laminates have been chosen based on assumptions made regarding the manufacturing of the FRP modules, where layers of FRP will be either wound or stacked, in such a manner that the orientations of the layers will be alternating. In the case of the symmetric laminate the number of laminae will always be uneven, and in the case of the balanced laminate the number of laminae will always be even.

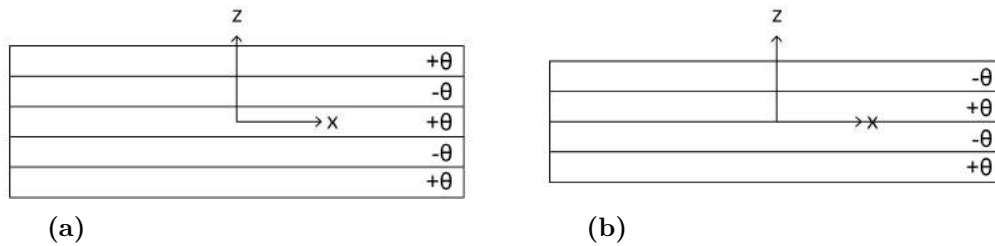


Figure 6.2: Symmetric and balanced laminates with alternating lamina orientations.

- (a) Symmetric laminate with alternating lamina orientations and an uneven number of laminae. LOC $[\pm\theta \setminus -\theta]_s$.
- (b) Balanced laminate with alternating lamina orientations and an even number of laminae. LOC $[\pm\theta]$.

Out-of-plane coupling effects can be neglected

In balanced laminates the \mathbf{B} matrix will be non-zero, however the only non-zero terms will be B_{16} and B_{26} . Due to the nearly symmetric layup, only one lamina will contribute to these terms, and as such it is assumed that the coupling effects will decrease for an increasing number of laminae and will be so small that it can be neglected.

Shear coupling effects can be neglected

In symmetric laminates the A_{16} and A_{26} components of the \mathbf{A} matrix are non-zero, however the contributions to these terms will be cancelled out for all laminae except for one in the laminates studied due to the nearly balanced layup. Therefore only one lamina will contribute to in plane shear and extension coupling effects, and for thick laminates this is assumed to be so small that it can be neglected.

6.1.2 MATLAB programs

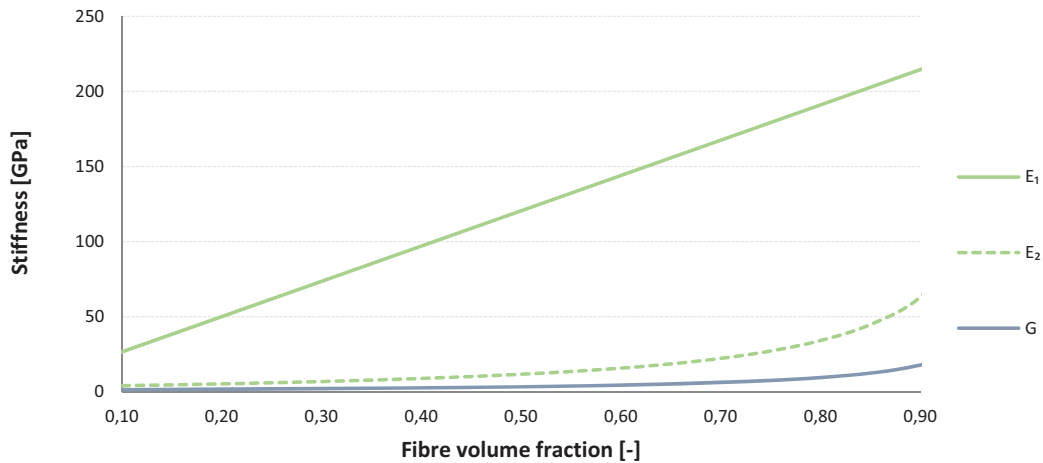
Already existing MATLAB functions were used to create a number of MATLAB programs which were written for the case studies in this chapter. These programs are described in Appendix B.1.

6.2 Mechanical response of FRP laminae

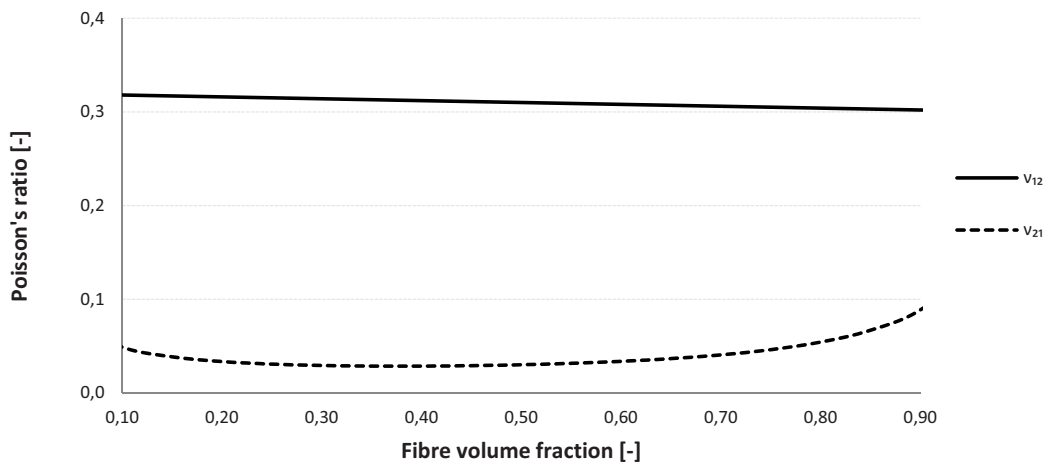
The relation between fibre volume fraction, stiffness and in-plane-shear coupling was studied to evaluate which fibre volume fractions and lamina orientations are most critical with regard to coupling. The material parameters which were used to establish the lamina engineering constants can be found in Tables 4.2 and 4.3.

6.2.1 Engineering constants for different laminae

Engineering constants were calculated using the MATLAB program *EvalLamina.m*, see Appendix B.1. The longitudinal modulus E_1 was calculated using the Rule of Mixtures and the transverse modulus, E_2 , and the shear modulus, G were calculated using the Halpin-Tsai method, see Chapter 5. The factor ξ for the transverse modulus was set to 2, and for the shear modulus it was set to 1. The calculated engineering constants as a function of the volume fraction, V_f , for the composite material can be seen in Figure 6.3.



(a) Longitudinal, transverse and shear moduli.



(b) Major and Minor Poisson's ratio.

Figure 6.3: Engineering constants for CFRP laminae as a function of the volume fraction, V_f .

6.2.2 Mechanical coupling in different laminae

For each fibre volume fraction, $0.05 \leq V_f \leq 0.95$, and lamina orientation, $\pm 0^\circ \leq \theta \leq \pm 45^\circ$, the $\bar{\mathbf{Q}}$ matrix was calculated and the \bar{Q}_{16} components were compared for the different laminae. The largest value of the \bar{Q}_{16} component was found for a fibre volume fraction of 0.85 and lamina orientation $\pm 30^\circ$. The \bar{Q}_{16} for all other laminae were then compared to this value, see Equation 6.1, Figure 6.4 and Table 6.1.

$$\bar{Q}_{16,rel} = \frac{\bar{Q}_{16,\pm\theta}}{\bar{Q}_{16,\pm 30^\circ}} \quad (6.1)$$

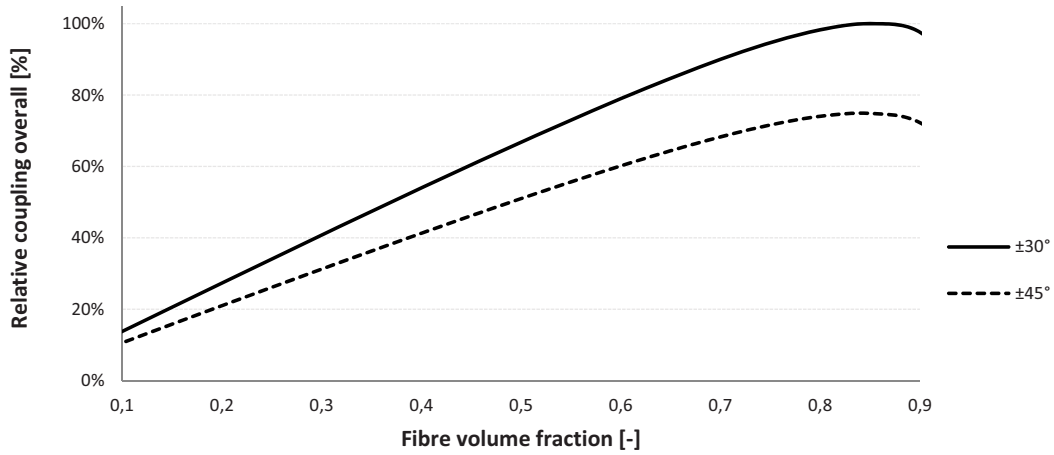


Figure 6.4: The calculated ratio $\bar{Q}_{16,rel}$, for $\pm 30^\circ$ and $\pm 45^\circ$ lamina orientations.

Table 6.1: The calculated values for $\bar{Q}_{16,rel}$, which compares the \bar{Q}_{16} term of the $\bar{\mathbf{Q}}$ matrix for all lamina orientations and volume fractions, to the overall maximum \bar{Q}_{16} .

$\theta \backslash V_f$	0.05	0.15	0.25	0.35	0.45	0.55	0.65	0.75	0.85	0.95
$\pm 0^\circ$	0%	0%	0%	0%	0%	0%	0%	0%	0%	0%
$\pm 5^\circ$	2%	5%	9%	13%	16%	19%	23%	25%	27%	23%
$\pm 10^\circ$	4%	11%	17%	24%	31%	37%	44%	49%	52%	44%
$\pm 15^\circ$	5%	15%	25%	34%	44%	53%	61%	68%	73%	61%
$\pm 20^\circ$	6%	18%	30%	42%	53%	64%	74%	83%	88%	74%
$\pm 25^\circ$	7%	20%	33%	46%	59%	71%	82%	92%	97%	82%
$\pm 30^\circ$	7%	21%	34%	47%	60%	73%	85%	95%	100%	84%
$\pm 35^\circ$	7%	20%	33%	46%	59%	71%	82%	92%	96%	80%
$\pm 40^\circ$	6%	18%	30%	42%	54%	65%	75%	83%	88%	72%
$\pm 45^\circ$	5%	16%	26%	36%	46%	56%	64%	72%	75%	60%

For each lamina orientation and fibre volume fraction the \bar{Q}_{16} component was also compared to the \bar{Q}_{11} component of the same lamina. It was seen here that for a lamina orientation of $\pm 45^\circ$ the ratio between these two component was the highest for each fibre volume fraction, see Figure 6.5 and Table 6.2. This was taken to mean that the coupling tendency relative the lamina stiffness will always be most critical for laminae with a $\pm 45^\circ$ orientation.

$$\bar{Q}_{\pm\theta\text{rel}} = \frac{\bar{Q}_{16,\pm\theta}}{\bar{Q}_{11,\pm\theta}} \quad (6.2)$$

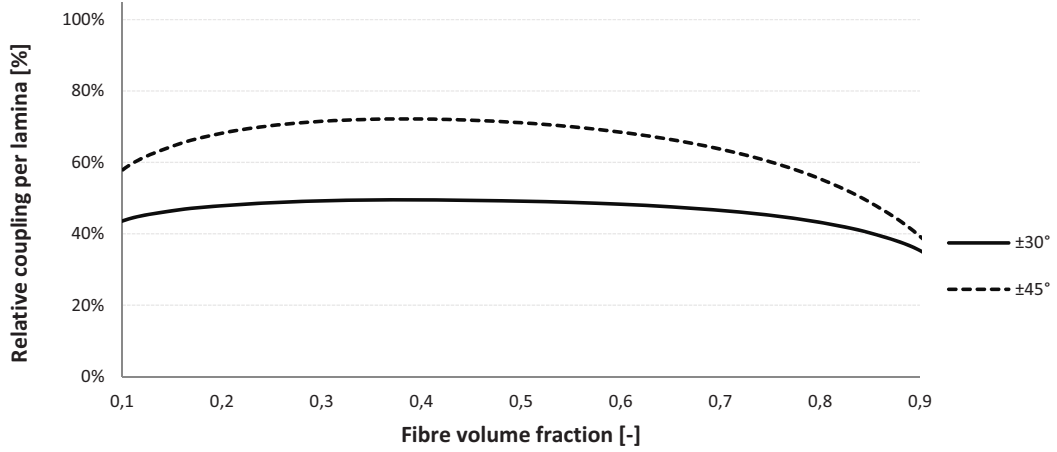


Figure 6.5: The calculated ratio $\bar{Q}_{\pm\theta\text{rel}}$, for $\pm 30^\circ$ and $\pm 45^\circ$ lamina orientations.

Table 6.2: The calculated values for $\bar{Q}_{\pm\theta\text{rel}}$, which compares the \bar{Q}_{16} and \bar{Q}_{11} terms of the \bar{Q} matrix for each lamina orientation and fibre volume fraction.

$\theta \backslash V_f$	0.05	0.15	0.25	0.35	0.45	0.55	0.65	0.75	0.85	0.95
$\pm 0^\circ$	0%	0%	0%	0%	0%	0%	0%	0%	0%	0%
$\pm 5^\circ$	7%	8%	8%	8%	8%	8%	8%	8%	7%	5%
$\pm 10^\circ$	13%	15%	16%	16%	16%	16%	16%	15%	14%	10%
$\pm 15^\circ$	19%	23%	24%	24%	24%	24%	24%	23%	21%	15%
$\pm 20^\circ$	26%	31%	32%	33%	33%	32%	32%	30%	28%	20%
$\pm 25^\circ$	31%	39%	40%	41%	41%	41%	40%	38%	34%	23%
$\pm 30^\circ$	37%	46%	49%	49%	49%	49%	48%	45%	40%	26%
$\pm 35^\circ$	41%	54%	57%	58%	58%	57%	55%	52%	45%	27%
$\pm 40^\circ$	43%	60%	64%	66%	66%	64%	62%	57%	48%	27%
$\pm 45^\circ$	44%	65%	70%	72%	72%	70%	66%	60%	49%	25%

6.3 Mechanical response of FRP laminates

Mechanical coupling in different types of laminates were studied to evaluate how the lamina orientations, as well as the number of laminae affects the coupling tendencies of a laminate. Here the fibre volume fraction, V_f was set to 0.52, see Tables 4.2 and 4.3.

6.3.1 Mechanical coupling in different types of laminates

The symmetric and balanced laminates presented in Tables 6.3 to 6.4 were studied using the MATLAB functions and the program *MechanicalCoupling.m*, see Appendix B.1.

Table 6.3: Thin laminates with lamina orientations $\pm 0^\circ \leq \theta \leq \pm 45^\circ$.

Laminate type	Thickness [mm]		Count [-]
	Laminate	Lamina	Layers
6.3.1 Symmetric thin	0.3	≈ 0.1	3
6.3.1 Balanced thin	0.1	≈ 0.1	2

Table 6.4: Thick laminates with lamina orientations $\pm 30^\circ$ and $\pm 45^\circ$.

Laminate type	Thickness [mm]		Count [-]
	Laminate	Lamina	Layers
6.3.1 Symmetric 10	10	$3.3 \gtrapprox t \gtrapprox 0.1$	$3 \leq n \leq 101$
6.3.1 Symmetric 15	15	$5 \gtrapprox t \gtrapprox 0.3$	$3 \leq n \leq 151$
6.3.1 Balanced 10	10	$5 \gtrapprox t \gtrapprox 0.1$	$2 \leq n \leq 100$
6.3.1 Balanced 15	15	$7.5 \gtrapprox t \gtrapprox 0.3$	$2 \leq n \leq 150$

6.3.1.1 Mechanical coupling in symmetric laminates

The \mathbf{A} , \mathbf{B} and \mathbf{D} matrices were calculated for the thin symmetric laminate in Table 6.3, for lamina orientations $\pm 0^\circ \leq \theta \leq \pm 45^\circ$. In Figure 6.6 the components of the extensional stiffness matrix, \mathbf{A} , are plotted. Here it can be seen that the largest contributions overall to the A_{16} and A_{26} components are for $\pm 30^\circ$ orientations. It can also be seen that the largest contributions to these components relative the laminate stiffness are for $\pm 45^\circ$.

The \mathbf{A} , \mathbf{B} and \mathbf{D} matrices were then calculated for the thick symmetric laminates in Table 6.4 with lamina orientations $\pm 30^\circ$ and $\pm 45^\circ$ for an increasing number of plies. In Figure 6.7 it can be seen that the contribution to the A_{16} and A_{26} components of the extensional stiffness matrix for the 15 mm thick laminate decreased for an increasing number of plies, and that these terms are small compared to the other components of the \mathbf{A} matrix, especially when the number of plies is larger than approximately 25. The same results were seen in the 10 mm laminate.

In Figure 6.8 it can be seen that the A_{16} component appear to decrease exponentially with an increasing number of plies and that the reduction of these terms is approximately 94% when the number of laminae has reached 51, and that the decrease rate appears to approach a constant value. The decrease rate was also calculated for the A_{26} component and the same decrease rate was seen here. For the 10 mm laminate the decrease rate followed the same pattern.

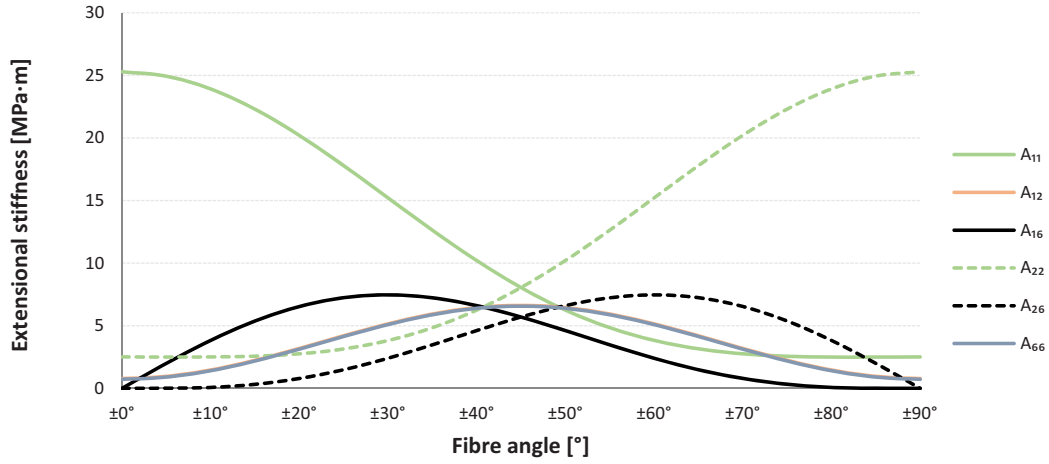


Figure 6.6: Components of the extensional stiffness matrix, \mathbf{A} , for a thin symmetric laminates with varying ply orientations.

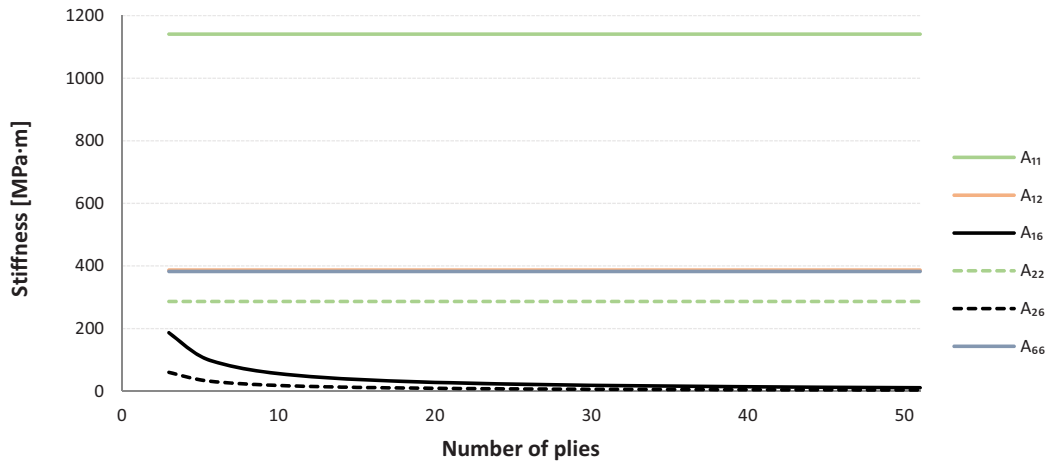


Figure 6.7: Components of the extensional stiffness matrix, \mathbf{A} , for a symmetric laminate with lamina orientations $\pm 30^\circ$ for an increasing number of plies.

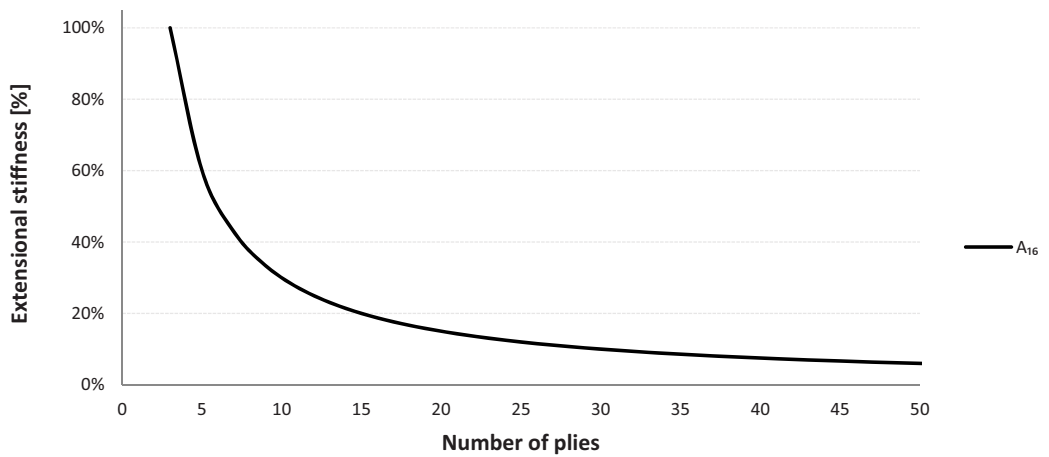


Figure 6.8: Decrease rate of A_{16} component of the extensional stiffness matrix, \mathbf{A} , for a symmetric laminate with lamina orientations $\pm 30^\circ$ for an increasing number of plies.

6.3.1.2 Mechanical coupling in balanced laminates

The \mathbf{A} , \mathbf{B} and \mathbf{D} matrices were also calculated for a thin balanced laminate, with two laminae, see Table 6.3. In Figure 6.9 the components of the coupling stiffness matrix for this laminate is shown. Here the coupling tendency can be observed in the B_{16} and B_{26} components of the \mathbf{B} matrix. The largest contribution overall to the B_{16} and B_{26} components are for $\pm 30^\circ$ orientations, and it can be seen that the largest contribution to these components relative the laminate stiffness is for $\pm 45^\circ$.

The \mathbf{A} , \mathbf{B} and \mathbf{D} matrices were calculated for laminates with orientations $\pm 30^\circ$ and $\pm 45^\circ$ and an increasing number of plies, see Table 6.4. In Figures 6.10 and 6.11 it can be seen that the contributions to the B_{16} and B_{26} components decreased for an increasing number of plies for a 15 mm thick laminate. In Figure 6.11 the decrease of the B_{16} component is shown for the same laminate. The reduction of this terms is approximately 96% for a number of 50 plies compared to 2 plies, the same decrease rate was found for the B_{26} component. Again compared to the overall stiffness the contributions to the coupling terms B_{26} and B_{26} are very small for a number of laminae larger than approximately 25, and the results of the 10 mm laminate followed the same pattern.

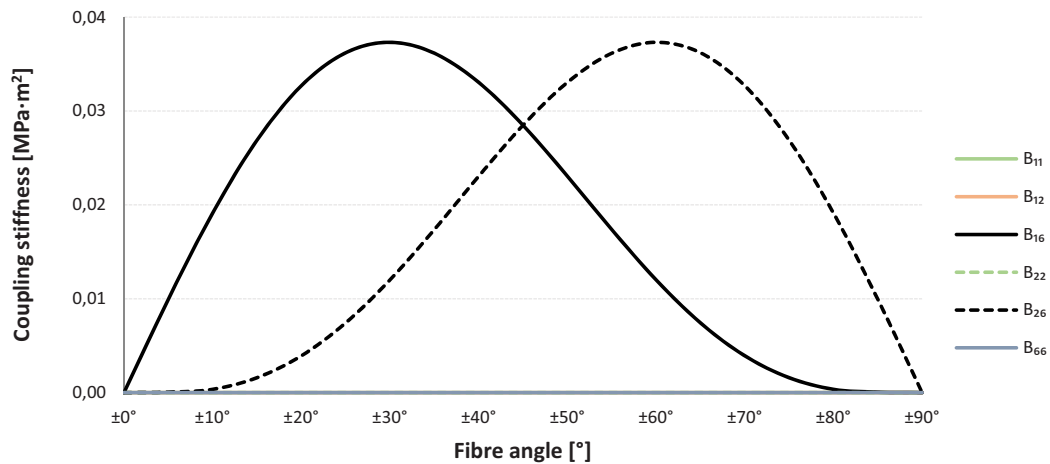


Figure 6.9: Components of the coupling stiffness matrix, \mathbf{B} , for a thin balanced laminates with varying ply orientations.

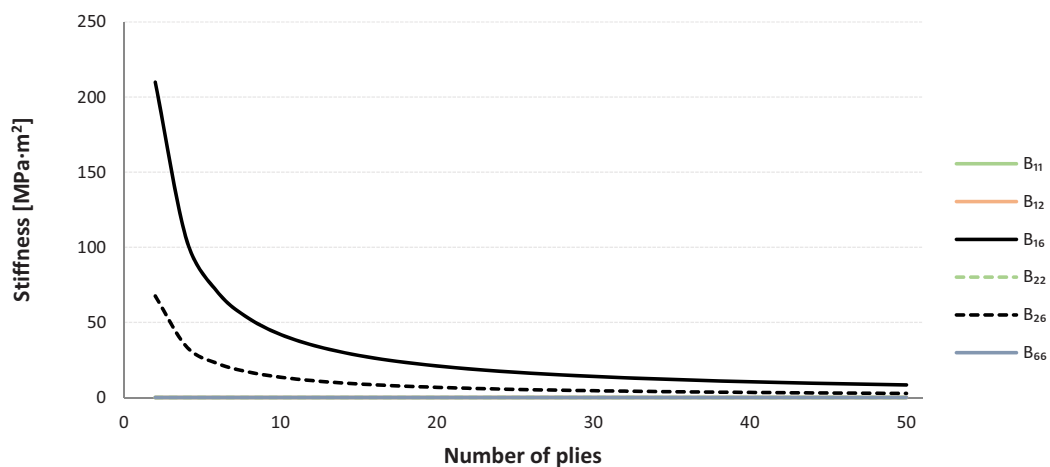


Figure 6.10: Components of the coupling stiffness matrix, \mathbf{B} , for a balanced laminate with lamina orientations $\pm 30^\circ$ for an increasing number of plies.

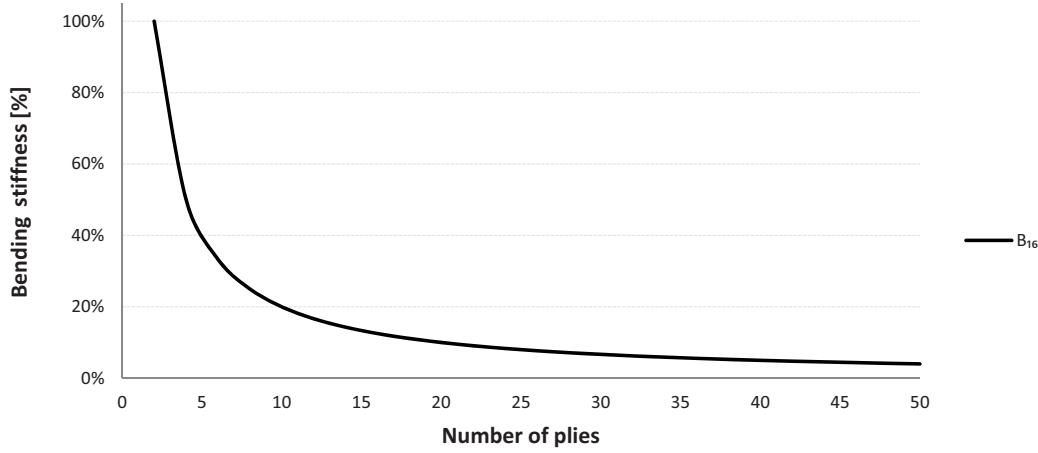


Figure 6.11: Decrease rate of B_{16} component of the coupling stiffness matrix, B , for a balanced laminate with lamina orientations $\pm 30^\circ$ for an increasing number of plies.

6.3.2 Mechanical response in different laminates

In order to evaluate whether the deformations which arise due to mechanical coupling are so small that these effects are negligible a study was conducted comparing the strain and curvature response in thin and thick (symmetric and balanced) laminates, shown in Table 6.5. These studies were conducted using the MATLAB program *EvalLaminate.m*, see Appendix B.1.

Table 6.5: Thin and thick symmetric and balanced laminate layups. These laminates were studied for lamina orientations $\pm 30^\circ$ and $\pm 45^\circ$.

Laminate type	Thickness [mm]		Count [-]
	Laminate	Lamina	Layers
6.3.2 Symmetric 1	1	≈ 0.1	11
6.3.2 Symmetric 10	10	≈ 0.1	101
6.3.2 Symmetric 1.5	1.5	≈ 0.3	51
6.3.2 Symmetric 15	15	≈ 0.3	5
6.3.2 Balanced 1	1	≈ 0.1	10
6.3.2 Balanced 10	10	≈ 0.1	100
6.3.2 Balanced 1.5	1.5	≈ 0.3	6
6.3.2 Balanced 15	15	≈ 0.3	50

The laminates were subjected to axially applied loads uniformly distributed over the laminate height, and resulting strains were then calculated for each load case, Equations 6.3 and 6.4 to 6.6. The load magnitude was determined so that the results could be directly compared for the thin and thick laminates. The applied load was thus proportional to the laminate height, see Equation 6.3, where $F = 1 \text{ kN m}^{-1}$, and t is the laminate thickness in metres.

$$N_{ij} = Ft \text{ [N]} \quad (6.3)$$

The subscript ij denotes the axis in which the load is applied, in this case the longitudinal (1) and transverse directions (2) as well as the direction of shear (12). To differentiate the results the loads and resulting strains and curvatures related to the thin laminates will be denoted with a prime superscript ($'$).

$$\text{Load case 6.3.2.1:} \quad \mathbf{N}_1 = \begin{bmatrix} F \\ 0 \\ 0 \end{bmatrix} t \quad (6.4)$$

$$\text{Load case 6.3.2.2:} \quad \mathbf{N}_2 = \begin{bmatrix} 0 \\ F \\ 0 \end{bmatrix} t \quad (6.5)$$

$$\text{Load case 6.3.2.3:} \quad \mathbf{N}_3 = \begin{bmatrix} 0 \\ 0 \\ F \end{bmatrix} t \quad (6.6)$$

6.3.2.1 Mechanical response in symmetric laminates

In Table 6.6 the resulting strains for the 10 mm thick and 1 mm thin laminates, subjected to uniform loads N_1 and N_1' are shown. In both laminates the lamina thickness was set to approximately 0.1 mm. Here it can be seen that the shear deformations which arise due to coupling are small relative the extensional strains. It can also be seen that the thin and thick laminate have nearly identical strain response in the longitudinal (1) and transverse directions (2). Here it can also be seen that the reduction in shear deformations is approximately 89% in the thick laminate compared to the thin laminate. The results for remaining load cases followed the same trend. The study was also conducted for laminates with 1.5 and 15 mm thickness, with lamina thickness of approximately 0.3 mm with similar results.

6.3.2.2 Mechanical response in balanced laminates

The curvature which occurs when a balanced laminate is loaded axially was evaluated. The resulting curvatures for the 10 mm thick and 1 mm thin laminates, subjected to uniform loads N_{12} and N_{12}' are shown in Table 6.7. Here it can be seen that the out of plane deformation in the thick laminates is less than 1% of the out-of-plane deformation for thin laminates. The results for remaining load cases followed the same trend. The study was also conducted for laminates with 1.5 and 15 mm thickness, with lamina thickness of approximately 0.3 mm with similar results.

Table 6.6: Strains for a 10 mm thick symmetric laminate (ϵ_1 , ϵ_2 , γ_{12}) compared to the strains (ϵ'_1 , ϵ'_2 , γ'_{12}) for a 1 mm thick symmetric laminate subjected to a uniform load N_1 and N'_1 respectively.

θ °	ϵ'_1 [10^{-9}]	ϵ'_2 [10^{-9}]	γ'_{12} [10^{-9}]	ϵ_1 [10^{-9}]	ϵ_2 [10^{-9}]	γ_{12} [10^{-9}]	$\frac{\epsilon_1}{\epsilon'_1}$ [%]	$\frac{\epsilon_2}{\epsilon'_2}$ [%]	$\frac{\gamma_{12}}{\gamma'_{12}}$ [%]
$\pm 0^\circ$	8.0	2.5	0.0	8.0	2.5	0.0	100	100	-
$\pm 5^\circ$	8.1	3.1	1.7	8.1	3.1	0.2	100	100	11
$\pm 10^\circ$	8.7	5.1	2.1	8.7	5.0	0.2	100	100	11
$\pm 15^\circ$	9.9	8.6	2.1	9.8	8.5	0.2	100	100	11
$\pm 20^\circ$	12.2	14.0	2.0	12.1	14.0	0.2	99	100	11
$\pm 25^\circ$	16.5	22.0	1.9	16.4	22.0	0.2	100	100	11
$\pm 30^\circ$	24.3	32.8	1.8	24.3	32.8	0.2	100	100	11
$\pm 35^\circ$	37.4	45.8	1.7	37.3	45.8	0.2	100	100	11
$\pm 40^\circ$	56.1	57.7	1.5	56.0	57.7	0.2	100	100	11
$\pm 45^\circ$	76.5	62.8	1.1	76.5	62.9	0.1	100	100	11

Table 6.7: Curvatures for a 10 mm thick balanced laminate (κ_1 , κ_2 , κ_{12}) compared to the curvatures (κ'_1 , κ'_2 , κ'_{12}) for a 10 mm thick symmetric laminate subjected to a uniform load N_{12} and N'_{12} respectively.

θ °	κ'_1 [$\frac{10^{-6}}{\text{rad}}$]	κ'_2 [$\frac{10^{-6}}{\text{rad}}$]	κ'_{12} [$\frac{10^{-6}}{\text{rad}}$]	κ_1 [$\frac{10^{-6}}{\text{rad}}$]	κ_2 [$\frac{10^{-6}}{\text{rad}}$]	κ_{12} [$\frac{10^{-6}}{\text{rad}}$]	$\frac{\kappa_1}{\kappa'_1}$ [%]	$\frac{\kappa_2}{\kappa'_2}$ [%]	$\frac{\kappa_{12}}{\kappa'_{12}}$ [%]
$\pm 0^\circ$	0.0	0.0	0.0	0.0	0.0	0.0	-	-	-
$\pm 5^\circ$	10.9	4.7	0.0	0.1	0.0	0.0	0.99	0.99	-
$\pm 10^\circ$	14.2	5.9	0.0	0.1	0.1	0.0	0.99	0.99	-
$\pm 15^\circ$	14.1	5.3	0.0	0.1	0.1	0.0	0.98	0.98	-
$\pm 20^\circ$	13.3	4.3	0.0	0.1	0.0	0.0	0.98	0.98	-
$\pm 25^\circ$	12.8	3.1	0.0	0.1	0.0	0.0	0.98	0.98	-
$\pm 30^\circ$	12.3	1.5	0.0	0.1	0.0	0.0	0.98	0.98	-
$\pm 35^\circ$	11.6	0.8	0.0	0.1	0.0	0.0	0.98	0.98	-
$\pm 40^\circ$	10.0	3.9	0.0	0.1	0.0	0.0	0.98	0.98	-
$\pm 45^\circ$	7.2	7.2	0.0	0.1	0.1	0.0	0.98	0.98	-

6.4 Equivalent material parameters

In the possible layups which has been assumed for this FRP module, see Table A.1, the smallest possible number of laminae will be 33. In the study presented in Section 6.3.1 it was seen that the coupling effects are very small for a number of laminae larger than approximately 25. In Section 6.3.2 it was seen that the shear deformation of the thick laminate was approximately 10% of the shear deformation of the thin laminate. It may not seem like a significant decrease, however considering that the shear deformations are very small in comparison with the extensional strains it is here assumed that these coupling effects are insignificant. It was therefore assumed that the laminates will be fully orthotropic and efficient engineering constants can be derived following the procedure in Section 5.5.

6.4.1 Engineering constants

Efficient engineering constants were calculated for the previously studied laminates, using the MATLAB program *EvalLaminate.m*, see Appendix B.1. The results were within the same range for all laminates. In Figures 6.12 and 6.13 as well as Table 6.8 the engineering constants which were derived for a 10 mm thick symmetric laminate are shown.

Table 6.8: Derived engineering constants for a 10 mm thick symmetric laminate with varying lamina orientations.

θ °	E_1 [GPa]	E_2 [GPa]	G_{12} [GPa]	ν_{12} [-]	ν_{21} [-]	α_{12} [10 ⁻⁶]	α_{21} [10 ⁻⁶]
±0°	125.25	12.41	3.59	0.31	0.03	0.2	31.35
±5°	122.89	12.33	4.47	0.38	0.04	0.44	31.11
±10°	115.35	12.1	7.01	0.58	0.06	1.14	30.41
±15°	101.78	11.73	10.89	0.87	0.1	2.29	29.26
±20°	82.59	11.26	15.66	1.16	0.16	3.84	27.7
±25°	60.86	10.76	20.73	1.34	0.24	5.76	25.78
±30°	41.22	10.35	25.5	1.35	0.34	7.99	23.56
±35°	26.79	10.26	29.39	1.23	0.47	10.45	21.1
±40°	17.85	10.93	31.92	1.03	0.63	13.07	18.48
±45°	13.07	13.07	32.8	0.82	0.82	15.77	15.77
±50°	10.93	17.85	31.92	0.63	1.03	18.48	13.07
±55°	10.26	26.79	29.39	0.47	1.23	21.1	10.45
±60°	10.35	41.22	25.5	0.34	1.35	23.56	7.99
±65°	10.76	60.86	20.73	0.24	1.34	25.78	5.76
±70°	11.26	82.59	15.66	0.16	1.16	27.7	3.84
±75°	11.73	101.78	10.89	0.1	0.87	29.26	2.29
±80°	12.1	115.35	7.01	0.06	0.58	30.41	1.14
±85°	12.33	122.89	4.47	0.04	0.38	31.11	0.44
±90°	12.41	125.25	3.59	0.03	0.31	31.35	0.2

6. MATERIAL PARAMETERS FOR STRUCTURAL ANALYSIS

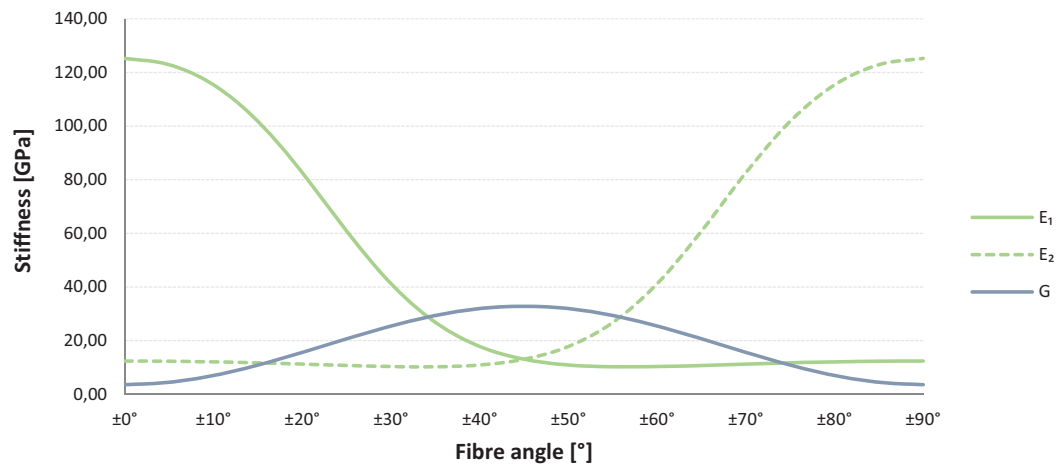


Figure 6.12: Equivalent orthotropic elastic moduli derived for a 10 mm thick symmetric laminate with varying lamina orientations.

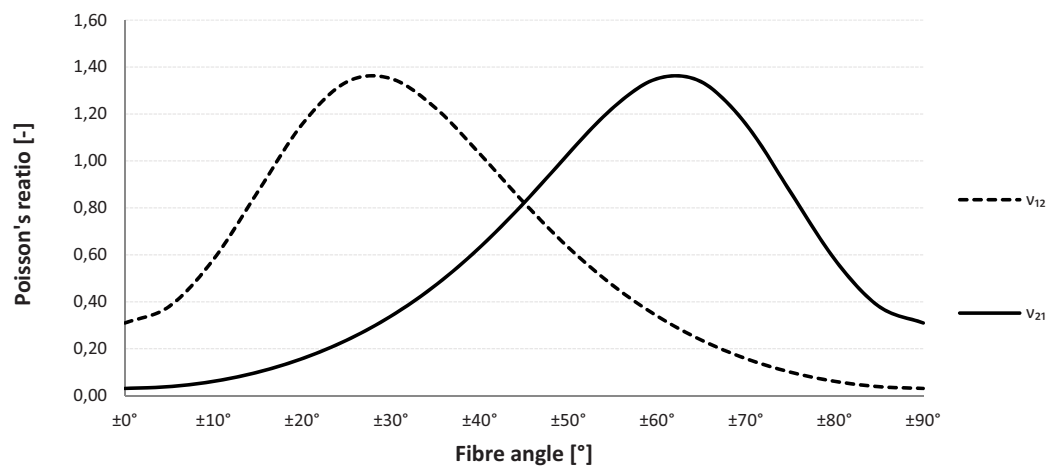


Figure 6.13: Equivalent orthotropic Poisson's ratio derived for a 10 mm thick symmetric laminate with varying lamina orientations.

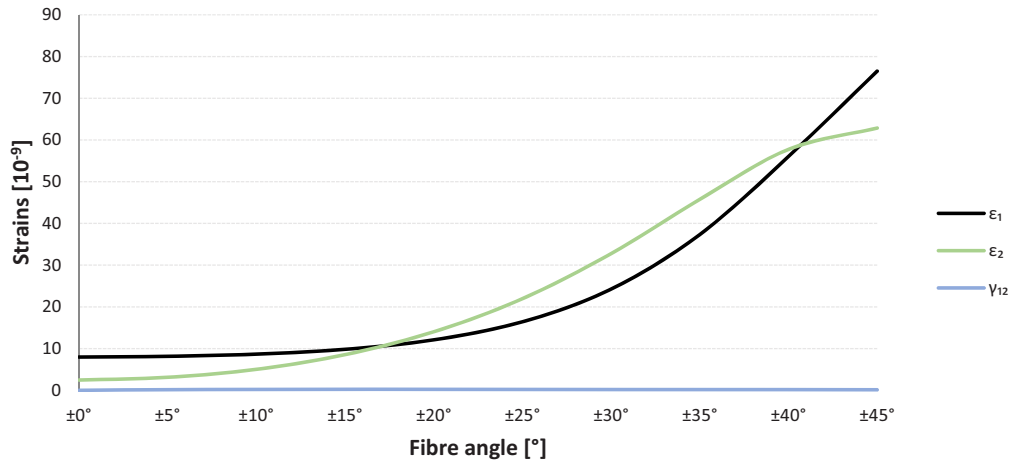
6.4.2 Verification of equivalent material parameters

A study was conducted to verify the calculated engineering constants, using the MATLAB program *OrthotropicLaminate.m*, see Appendix B.1. For each lamina orientation in Table 6.8 a fictional fully orthotropic laminate was constructed, see Table 6.9.

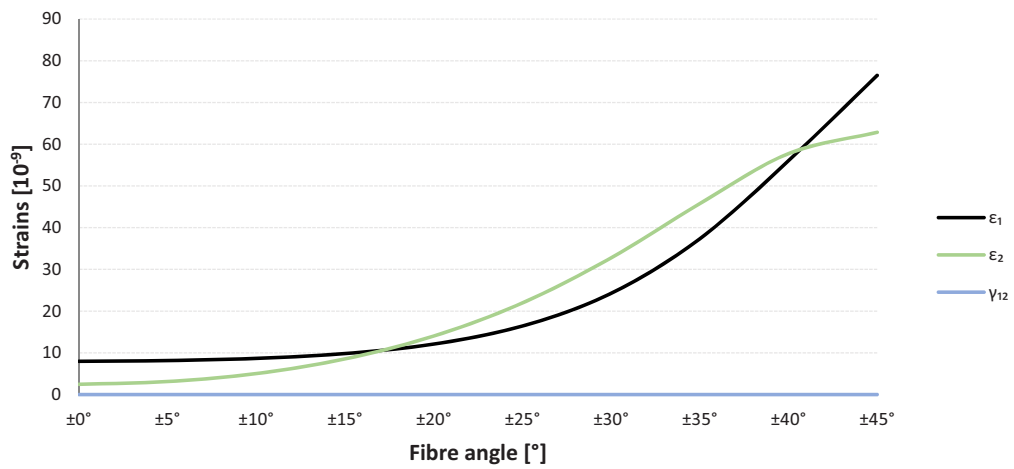
Table 6.9: Thin and thick fully orthotropic laminates studied with equivalent orthotropic material parameters derived for lamina orientations $\pm 0^\circ$ to $\pm 45^\circ$.

Laminate type	Thickness [mm]		Count [-]
	Laminate	Lamina	Layers
6.4.2 Orthotropic 1	1	≈ 0.1	11
6.4.2 Orthotropic 10	10	≈ 0.1	101
6.4.2 Orthotropic 1.5	1.5	≈ 0.3	51
6.4.2 Orthotropic 15	15	≈ 0.3	5

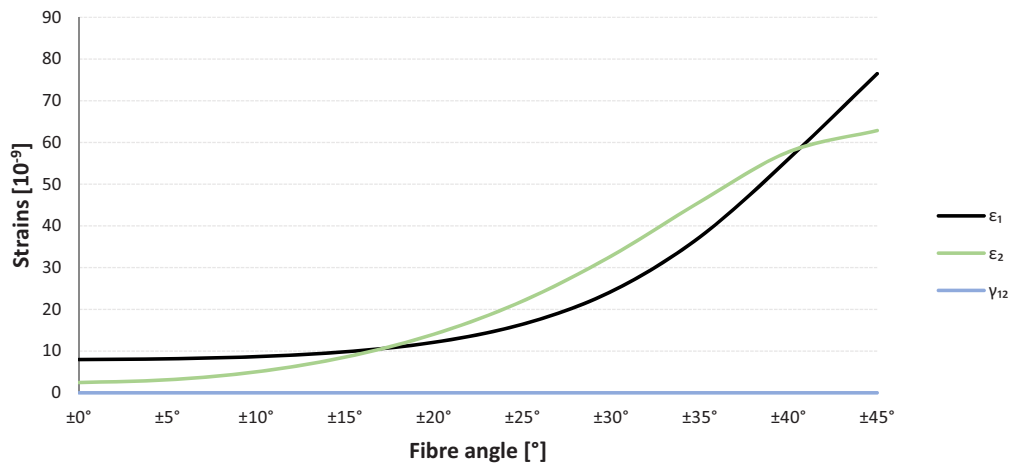
For these fictional laminates, the mechanical response was evaluated in the same manner as the laminates studied in Section 6.3.2. In Figure 6.14 the strains for symmetric, balanced and fully orthotropic laminates with a thickness of 10 mm are shown, where each laminate was subjected to a uniform load N_1 . Here it can be seen that the strains are nearly identical for all laminates. The same pattern could be seen for the remaining load cases and laminate configurations. The assumption that coupling effects can be neglected and that the laminates can be assumed to be transversely isotropic was thus considered sufficiently accurate.



(a) Symmetric laminate



(b) Balanced laminate



(c) Equivalent orthotropic laminate

Figure 6.14: Strains for different laminates with 10 millimeter thickness subjected to a load N_1 .

7

MATERIAL PARAMETERS FOR FE
ANALYSIS

7. MATERIAL PARAMETERS FOR FE ANALYSIS

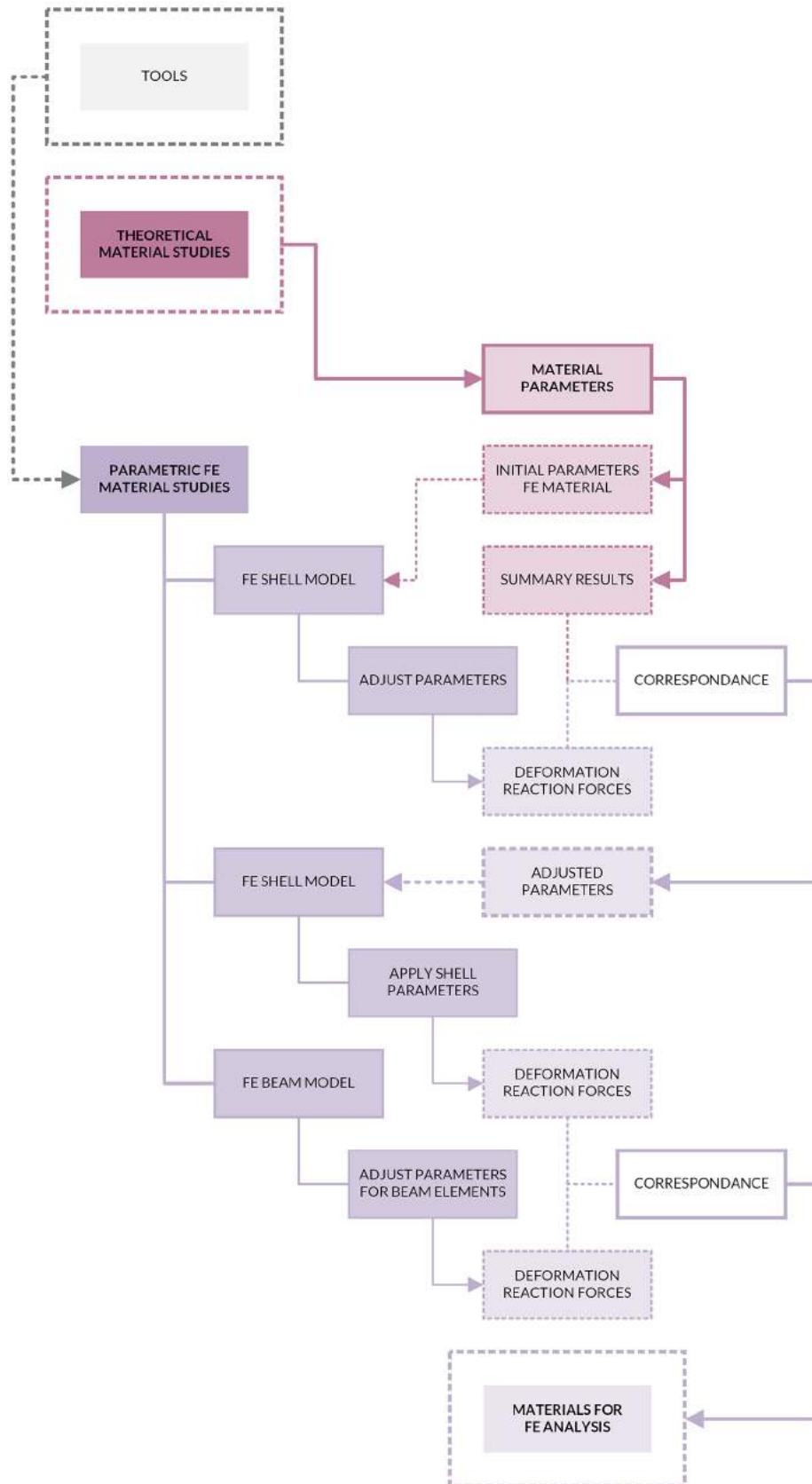


Figure 7.1: Flowchart describing the methodology used for the case studies presented in Chapter 7 - Material parameters for FE analysis.

7.1 Parametric QUAD and beam models for verification of material parameters

In Chapter 6 material parameters were derived for a CFRP material with varying fibre orientations. These material parameters were analysed and verified using Classical Laminate Theory, however the aim of this study is to establish a parametric approach for FE analysis. In order to verify that the material parameters could also be used in FE analysis for SOFiSTiK QUAD and beam elements a number of case studies were conducted. The outline of these case studies are illustrated in Figure 7.1.

Two parametric models were developed, a QUAD model and a beam model, see Figures 7.2 to 7.5. The geometry and FE topology were generated in Grasshopper using these parametric model definitions and were then exported to SOFiSTiK as CADINP code. In both model definitions weak springs were added as supports at the boundaries to prevent rigid body motions in analysis.

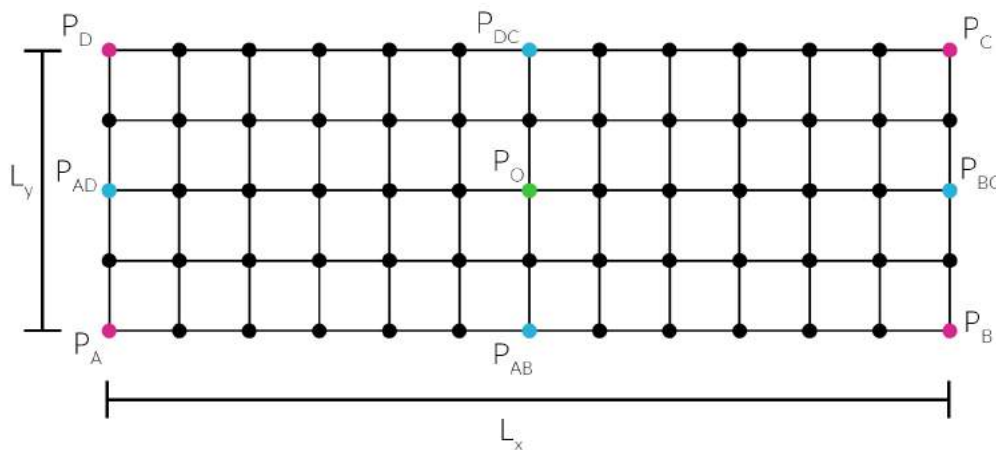


Figure 7.2: Definition of parametric model used for QUAD models. The geometry and FE topology was generated in Grasshopper and Rhinoceros 3D using this definition.

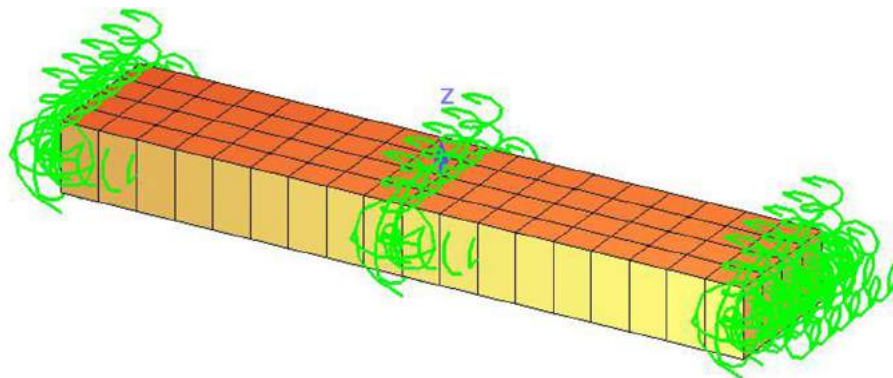


Figure 7.3: Parametric FE QUAD model in SOFiSTiK. Here the thickness of the 2D quad elements is shown as well as springs (in green colour) which are used as boundary supports.

7. MATERIAL PARAMETERS FOR FE ANALYSIS

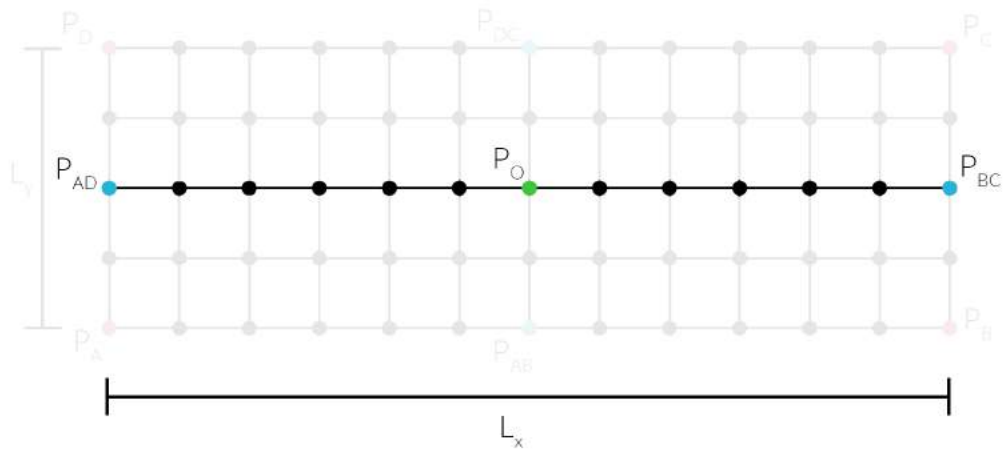


Figure 7.4: Definition of parametric model used for beam models. The geometry and FE topology was generated in Grasshopper and Rhinoceros 3D using this definition.

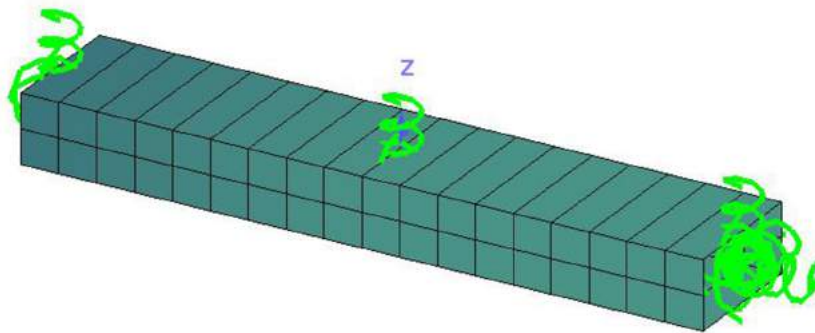
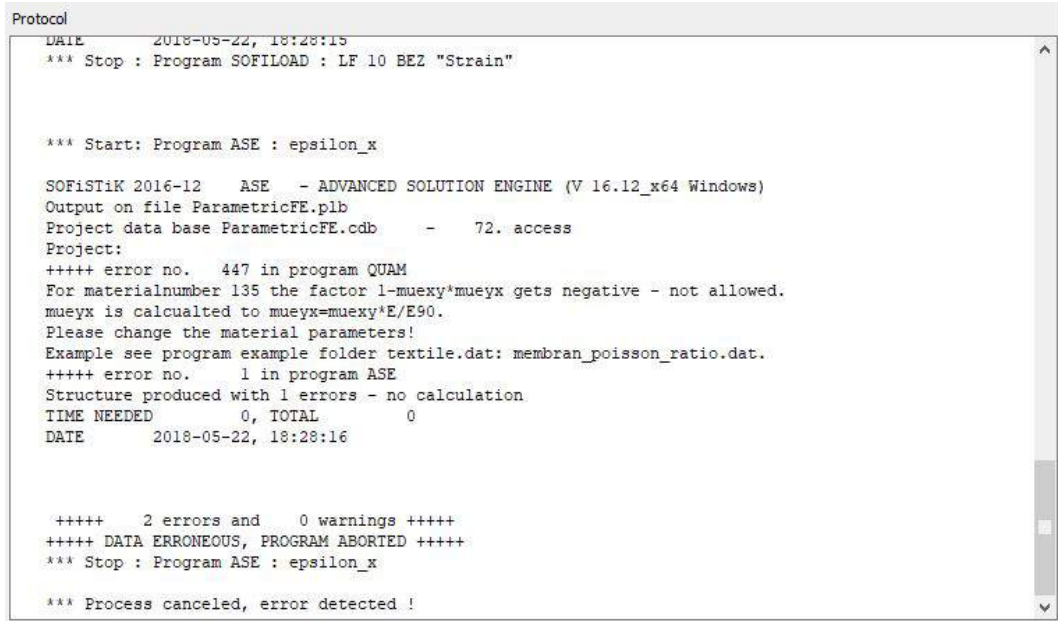


Figure 7.5: Parametric FE beam model in SOFiSTiK. Here the cross sections of the beam elements are shown as well as springs (in green colour) which are used as boundary supports.

7.2 Adaptations of material parameters for FE analysis

Nine orthotropic materials were defined in SOFiSTiK, using the material parameters in Table 6.8 for the fibre orientations $\pm 0^\circ$ to $\pm 45^\circ$. The orthotropic FRP material was modelled as a timber material in SOFiSTiK because this material can be used to define transversely isotropic materials. In SOFiSTiK this material also allows a Poisson's ratio larger than 0.49 [43]. Poisson's ratio is typically theoretically limited to -1 to 0.5, however in the case of anisotropic materials such as CFRP it can be well above 0.5 [44], which was seen in Chapter 6. Before applying the materials in analysis it was however necessary to make adaptations to the material parameters, due to limitations in SOFiSTiK. The relation in Equation 7.1, must always be true, otherwise SOFiSTiK will not be able to use the material in analysis, see Figure 7.6.

$$1 - \nu_{xy}\nu_{yx} > 0 \quad \implies \quad \begin{cases} \nu_{xy} > 0, & \nu_{yx} < \frac{1}{\nu_{xy}} \\ \nu_{xy} < 0, & \nu_{yx} > \frac{1}{\nu_{xy}} \end{cases} \quad (7.1)$$



```

Protocol
DATE      2018-05-22, 18:28:15
*** Stop : Program SOFILOAD : LF 10 BEZ "Strain"

*** Start: Program ASE : epsilon_x

SOFiSTiK 2016-12   ASE   - ADVANCED SOLUTION ENGINE (V 16.12_x64 Windows)
Output on file ParametricFE.plb
Project data base ParametricFE.cdb - 72. access
Project:
+++++ error no. 447 in program QUAM
For materialnumber 135 the factor 1-mueyx*mueyx gets negative - not allowed.
mueyx is calculated to mueyx=mueyx*E/E90.
Please change the material parameters!
Example see program example folder textile.dat: membran_poisson_ratio.dat.
+++++ error no. 1 in program ASE
Structure produced with 1 errors - no calculation
TIME NEEDED 0, TOTAL 0
DATE      2018-05-22, 18:28:16

+++++ 2 errors and 0 warnings +++++
+++++ DATA ERRONEOUS, PROGRAM ABORTED +++++
*** Stop : Program ASE : epsilon_x

*** Process canceled, error detected !

```

Figure 7.6: The error "447" will occur during analysis in SOFiSTiK if the relation in Equation 7.1 is not fulfilled.

In SOFiSTiK the Minor Poisson's ratio, ν_{yx} is calculated from the elastic moduli of the material, see Equation 7.2 [43]. The relation in Equation 7.3 must also be true, however in Figure 7.7a it can be seen that it is not the case for the material parameters in Table 6.8. This can be solved by adapting the Poisson's ratios as in Figure 7.7b (compare with Figure 6.13) and applying a material rotation, ψ , of 90° , see Figure 7.8. This rotation corresponds to the third Euler angle [43], which describes a 90° rotation about the local material z -axis.

$$\nu_{yx} = \frac{\nu_{12}E_1}{E_2} \quad (7.2)$$

$$\frac{\nu_{12}E_1}{E_2} < \frac{1}{\nu_{12}} \quad (7.3)$$

7. MATERIAL PARAMETERS FOR FE ANALYSIS

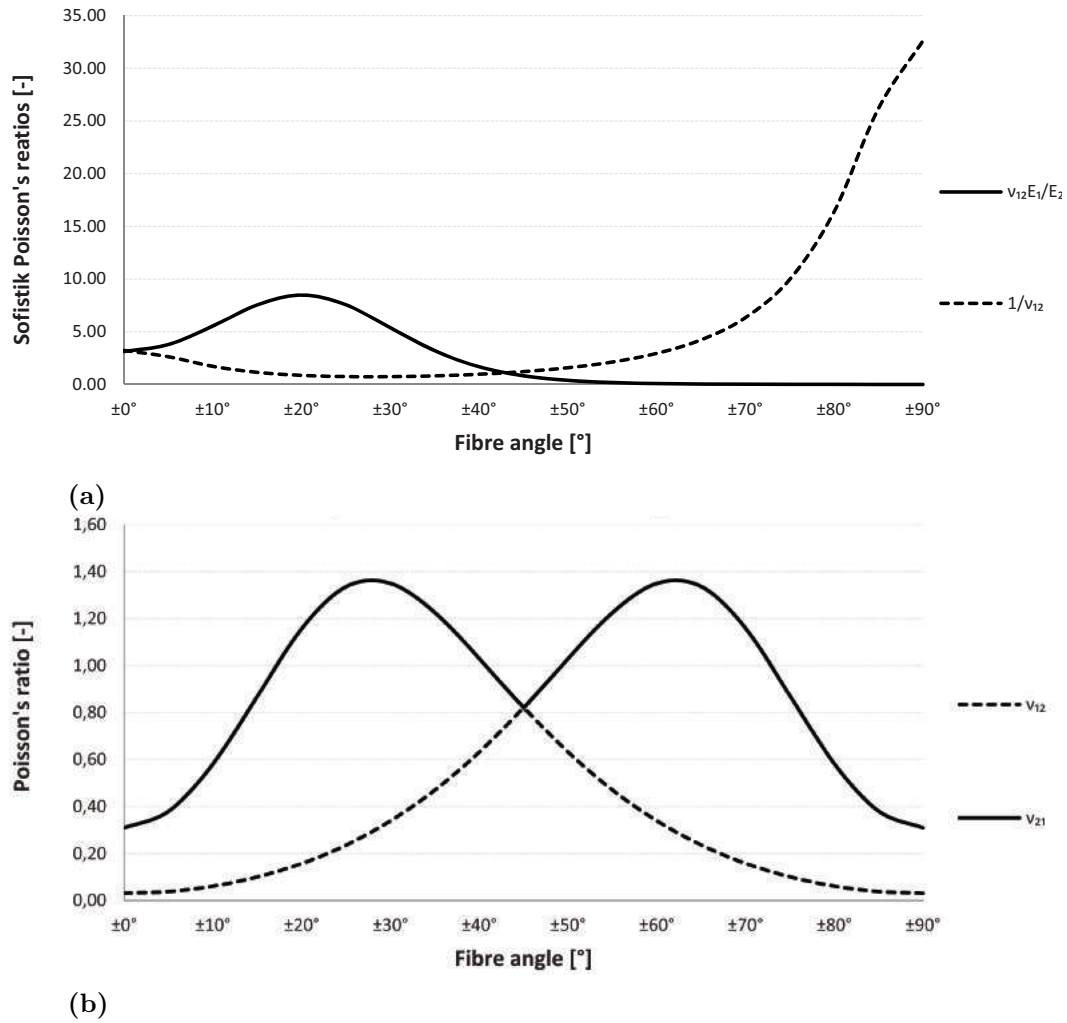


Figure 7.7: Diagrams showing the relation between the Poisson's ratios calculated for fully orthotropic laminates in Chapter 6 and the adaptations required for analysis in SOFiSTiK.

- (a) The black solid line should always be below the black dashed line, it can be seen here that this is not the case for the material parameters established in Chapter 6.
- (b) The Major and Minor Poisson's ratios were adapted as in (b), and an Euler angle, ψ , of 90° was added to the material definition in SOFiSTiK.

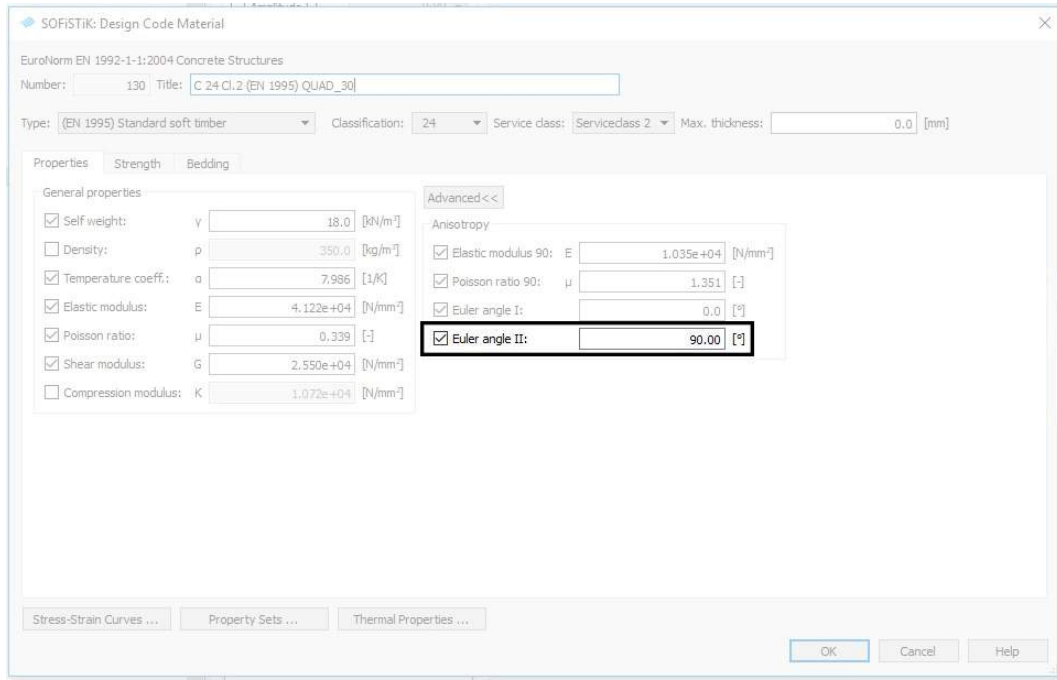


Figure 7.8: A rotation, ψ , of 90° , is applied in the cases where Poisson's ratio has been adjusted. This rotation corresponds to the third Euler angle [43] and describes a 90° rotation about the local z-axis.

Table 7.1: Nine materials were defined for FE analysis of QUAD elements in SOFiSTiK. The name of the material in SOFiSTiK is defined by which fibre orientation the material corresponds to. The elastic moduli E and E_{90} correspond to E_1 and E_2 , and G corresponds to G_{12} . The Poisson's ratios have been adapted so that ν corresponds to ν_{21} , and ν_{90} corresponds to ν_{12} . The thermal expansion coefficient α has been taken as α_1 . The angle ψ corresponds to the third Euler angle.

Name	E [GPa]	E_{90} [GPa]	G [GPa]	ν [-]	ν_{90} [-]	α [10^{-6}]	ψ [°]
CFRP 100	125.25	12.41	3.59	0.03	0.31	0.2	90
CFRP 105	122.89	12.33	4.47	0.04	0.38	0.44	90
CFRP 110	115.35	12.1	7.01	0.06	0.58	1.14	90
CFRP 115	101.78	11.73	10.89	0.1	0.87	2.29	90
CFRP 120	82.59	11.26	15.66	0.16	1.16	3.84	90
CFRP 125	60.86	10.76	20.73	0.24	1.34	5.76	90
CFRP 130	41.22	10.35	25.5	0.34	1.35	7.99	90
CFRP 135	26.79	10.26	29.39	0.47	1.23	10.45	90
CFRP 140	17.85	10.93	31.92	0.63	1.03	13.07	90
CFRP 145	13.07	13.07	32.8	0.82	0.82	15.77	90

7.2.1 Mesh convergence study

A mesh convergence study was conducted to find a suitable mesh size before analysis. The parametric model definition for QUAD elements was used to model a plate with dimensions $100 \times 100 \times 10$ mm. The plate was fixed on one end and loaded with a uniform load of on the other end, see Figure 7.9. The mesh size was decreased in four steps and displacements were compared for each mesh size, see Figure 7.10. The increase in displacement for each mesh size was less than 0.001 mm and the mesh was assumed to be fine enough for a side length of 10 mm, see Figure 7.10d.

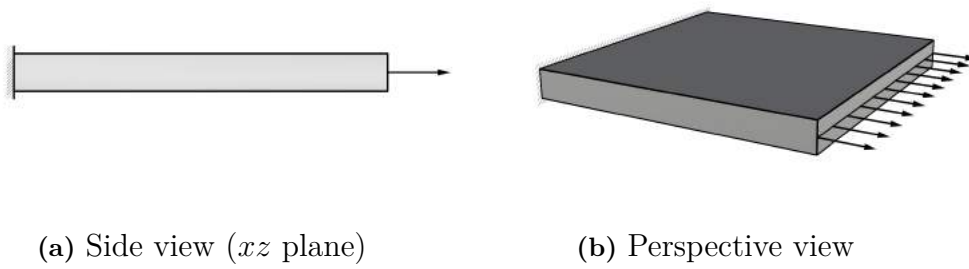


Figure 7.9: Application of loads in mesh convergence study.

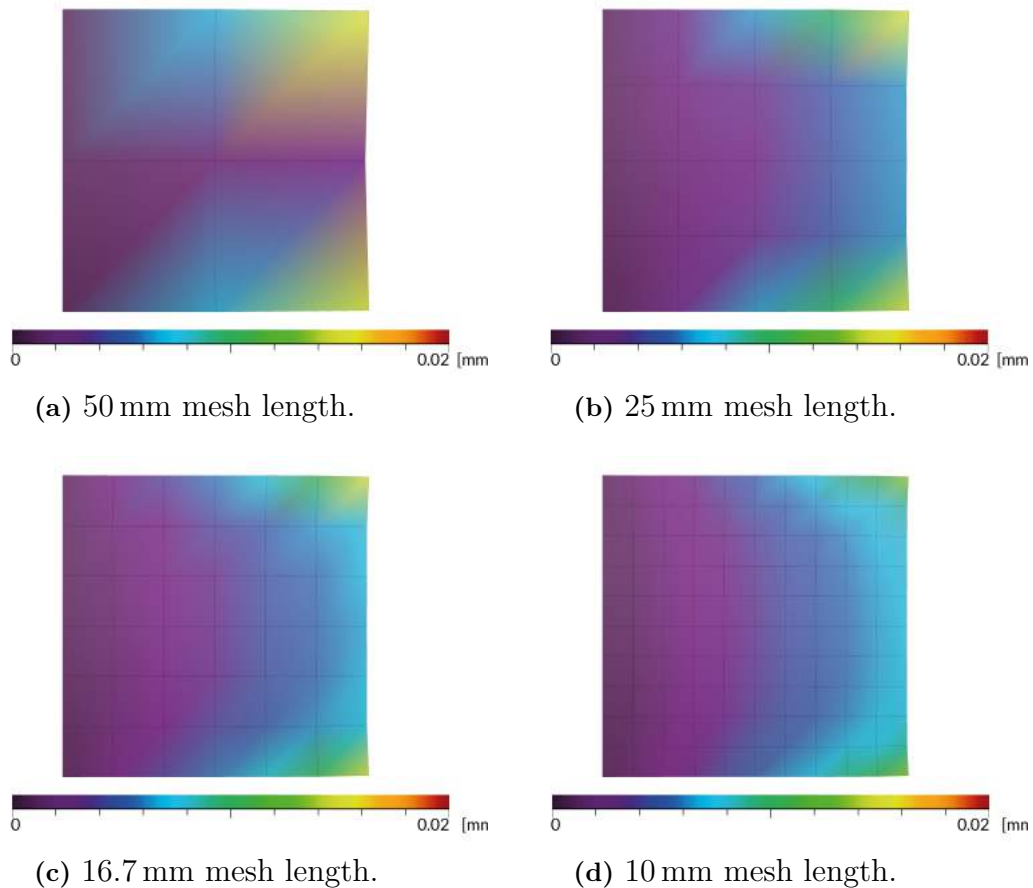


Figure 7.10: Displacement plots of mesh convergence study in SOFiSTiK for a quadratic plate with dimensions $100 \times 100 \times 10$ mm, and decreasing mesh side lengths.

7.3 Verification of material parameters for QUAD elements

A study was conducted in SOFiSTiK to verify the defined materials for QUAD elements in SOFiSTiK. For each material in Table 7.1 a plate with dimensions $100 \times 100 \times 10$ mm was evaluated in SOFiSTiK for six load cases, see Figure 7.11 and Table 7.2. In each load case a displacement was applied to the boundary so that the resulting strain or curvature of the in the load direction would be 10^{-3} .

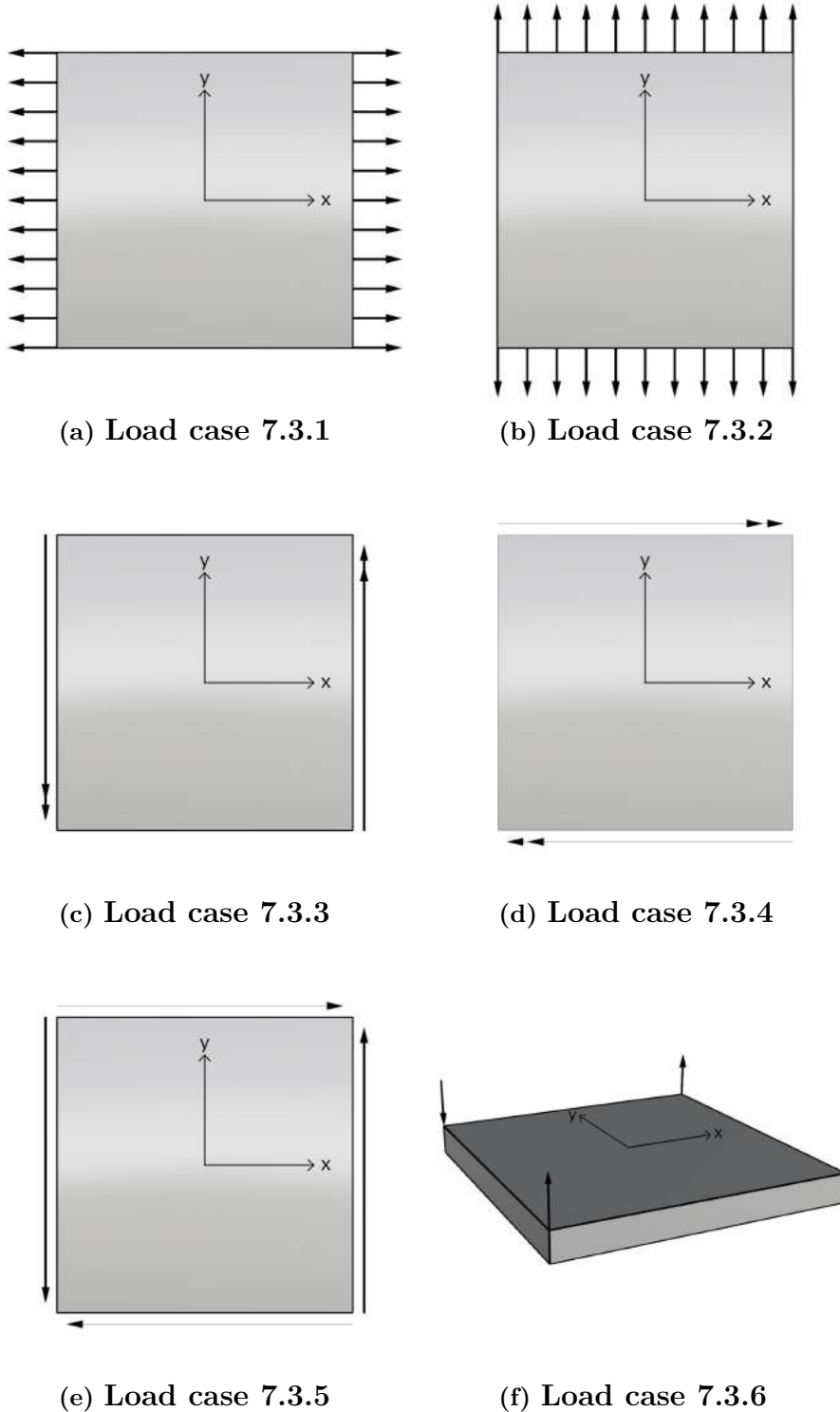


Figure 7.11: Load cases used in QUAD model case studies.

Table 7.2: Applied strains and curvatures in loadcases 7.3.1 to 7.3.6

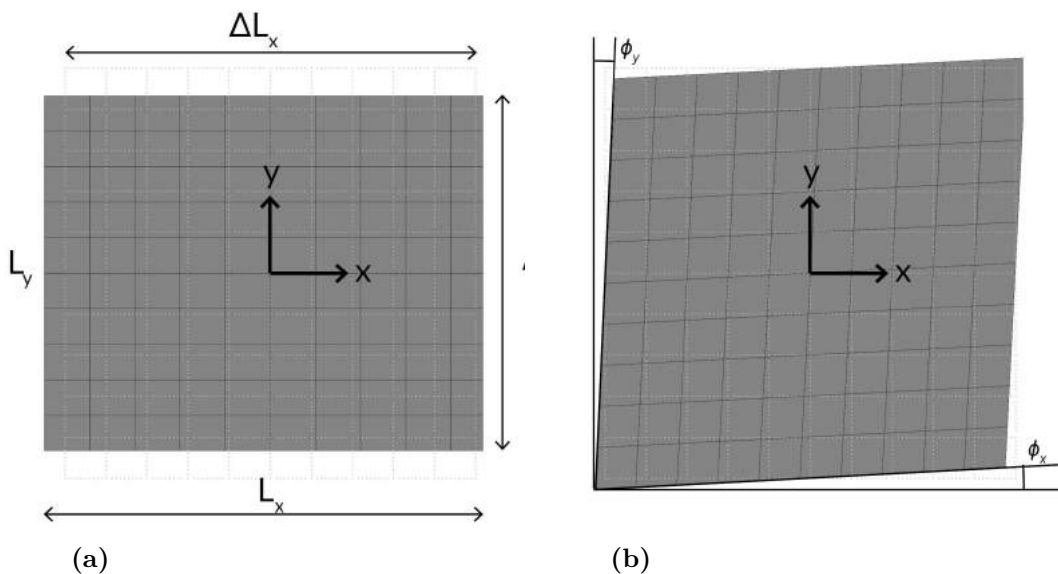
Load case Name	Strains [10^{-3}]			Curvature [10^{-3}]		
	ε_x	ε_y	ε_{xy}	κ_x	κ_y	κ_{xy}
Load case 7.3.1	1	-	-	-	-	-
Load case 7.3.2	-	1	-	-	-	-
Load case 7.3.3	-	-	1	-	-	-
Load case 7.3.4	-	-	-	1	-	-
Load case 7.3.5	-	-	-	-	1	-
Load case 7.3.6	-	-	-	-	-	1

7.3.1 Strains and curvatures for QUAD elements

For each load case the resulting strains and curvatures were compared to results from a study conducted in MATLAB using the same materials, load cases and laminate thickness. The MATLAB study was conducted using the MATLAB program *EquivalentLaminate.m*, see Appendix B.1.

7.3.1.1 Calculation of strains and curvatures in Grasshopper

To simplify the comparison and evaluation of the strains and curvature results from FE analysis in SOFiSTiK a parametric tool, *PlotStrainCurvature*, was developed for Grasshopper and Rhinoceros 3D, see Appendix B.2. The strains and curvatures were calculated using the Equations 7.4 and 7.6, with the lengths, L and radii, R defined in Figures 7.12 and 7.13.

**Figure 7.12**

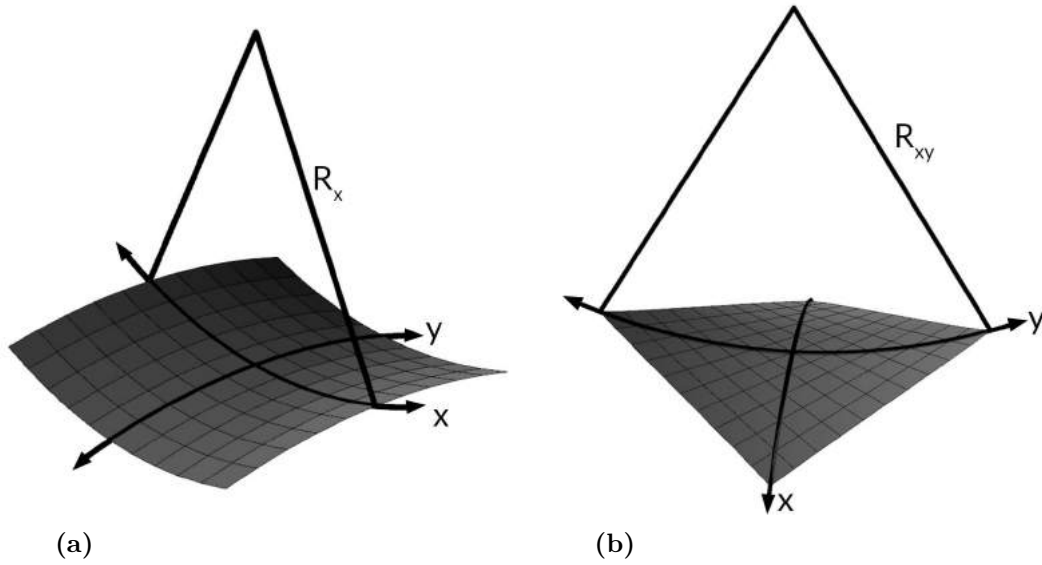


Figure 7.13

$$\varepsilon = \frac{\Delta L}{L} \quad (7.4)$$

$$\gamma = \phi_x + \phi_y \quad (7.5)$$

$$\kappa = \frac{1}{R} \quad (7.6)$$

7.3.1.2 Evaluation of displacements in Grasshopper

The *PlotStrainCurvature* tool, which was used to calculate strains and curvatures was further developed and an additional tool, *PlotDisplacements*, was created to show the displaced FE mesh in Rhino. With this tool it was also possible to visualise the displacements using colour gradients, as was seen in Figure 7.10. This tool is described further in Appendix B.2.

7.3.1.3 Comparison of strains and curvature

In all six load cases and for all nine materials the calculated strains and curvatures in SOFiSTiK and MATLAB had a correspondence of nearly 100%. The results for each load case and material can be found in Tables 7.3 to 7.8.

The displacement results were imported into Grasshopper and plotted using the *PlotDisplacements* tool, and it could also be seen here that the strains and curvatures were uniform over the whole plate, see Figures 7.14 to 7.16.

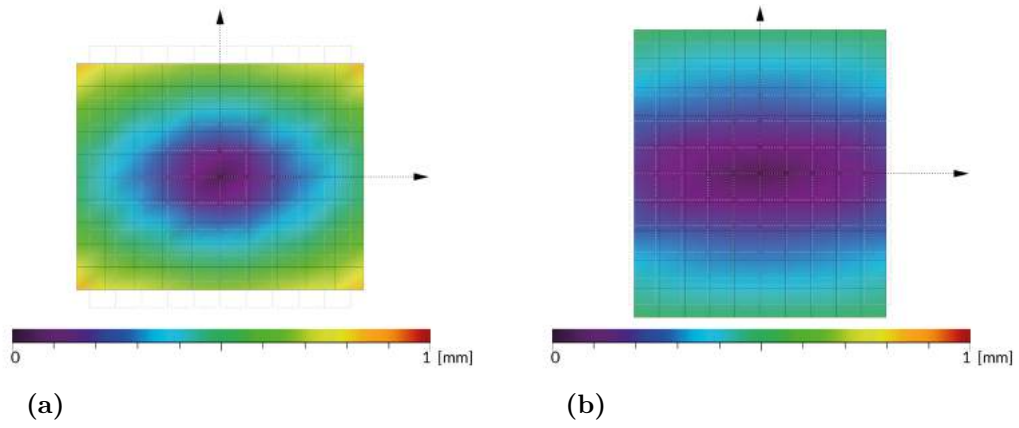


Figure 7.14: Displacement plots for axial strains, for CFRP 130.
 (a) Displacements for plate with a strain ε_x applied.
 (b) Displacements for plate with a strain ε_y applied.

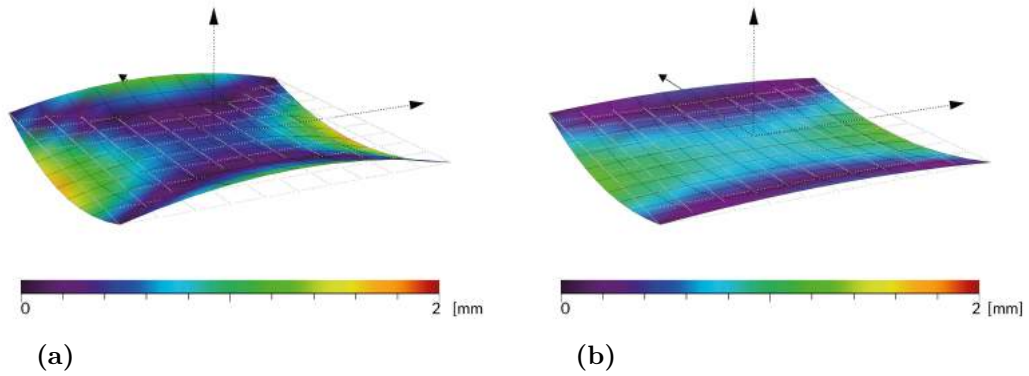


Figure 7.15: Displacement plots for plate curvatures, for CFRP 130.
 (a) Displacements for plate with a curvature κ_x applied.
 (b) Displacements for plate with a curvature κ_y applied.

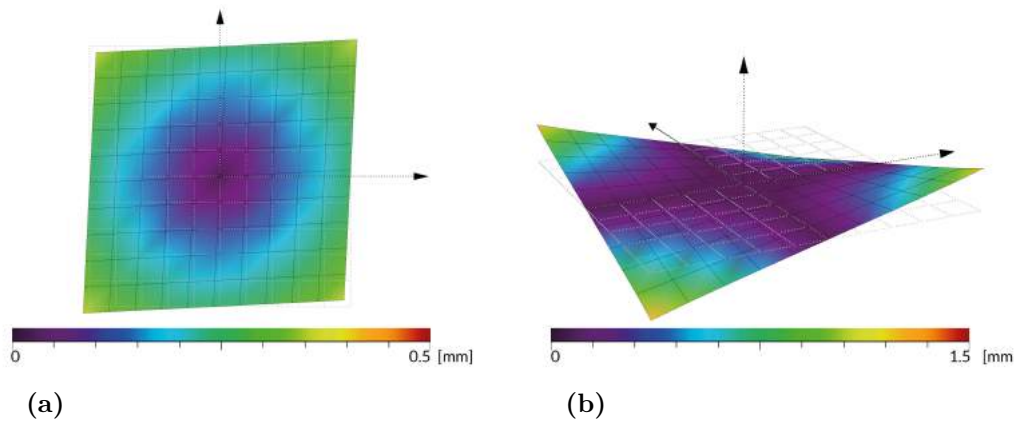


Figure 7.16: Displacement plots for shear strain and curvature, for CFRP 130.
 (a) Displacements for plate with a shear strain γ_{xy} applied.
 (b) Displacements for plate with a shear curvature κ_{xy} applied.

7.3.2 Stress distribution in QUAD elements

The stresses for QUAD elements were calculated in SOFiSTiK on the top, bottom and centre planes of the QUAD element. In this study the normal stresses in the local x - and y -directions as well as shear stress in the xy -plane were evaluated.

7.3.2.1 Evaluation of stress results in Grasshopper

The *PlotDisplacements* tool were further developed into a new tool *PlotStresses*, which could display stress results on the bottom, top and centre planes of QUAD elements, see Appendix B.2.

7.3.2.2 Comparison of stresses

The average stresses calculated in SOFiSTiK for each load case and material were compared to the stresses calculated in MATLAB, see Tables 7.3 to 7.8. Here it could be seen that the correspondence was nearly 100% for all materials and load cases. The stress results were imported into Grasshopper, see Figures 7.21 to 7.23, and it could be seen here that the stress distribution is uniform over the whole plate, except for in **Load case 7.3.6**. However, in this load case, stress concentrations appeared due to the fact that the displacements were applied to the corner points and not uniformly along the boundary, see Figure 7.11f. The overall stress in this load case were however uniform, see Figure 7.17, and the average stress had a near 100% correspondence with the results from the MATLAB analysis.

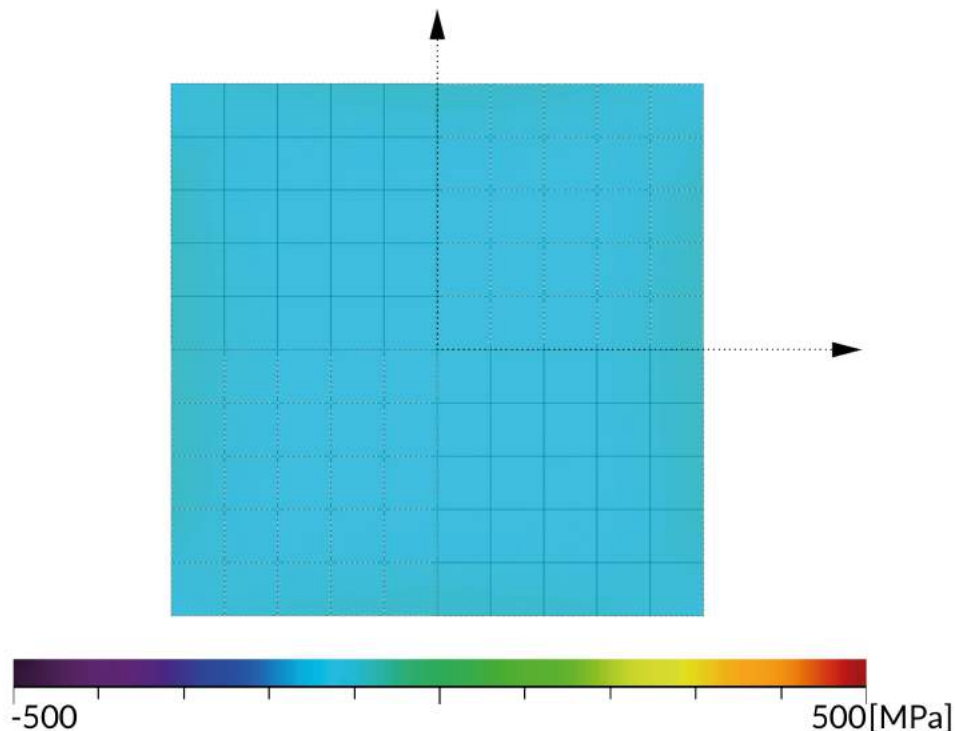


Figure 7.17: Stress plot showing small stress variations for plate subjected to shear bending, however it can be seen that these variations are small and that the overall stress is uniform.

7. MATERIAL PARAMETERS FOR FE ANALYSIS

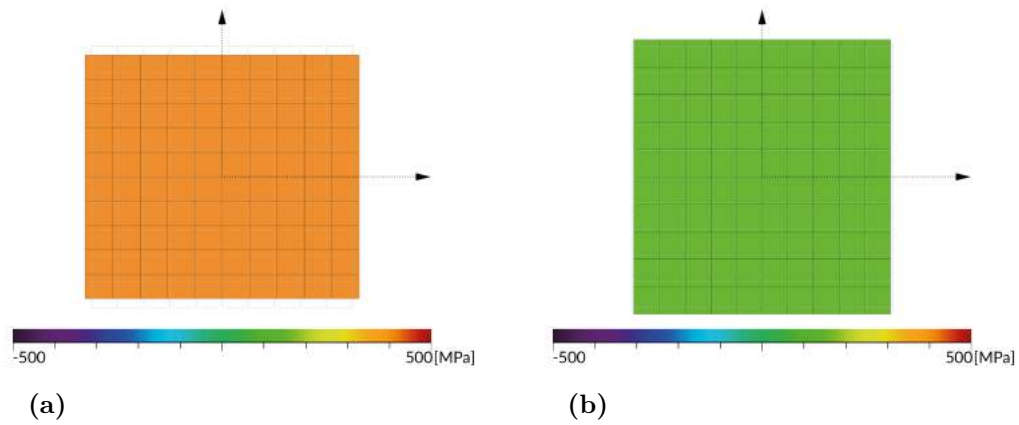


Figure 7.18: Stresses in bottom plane for the material CFRP 130.

(a) Load case 7.3.1

(b) Load case 7.3.1

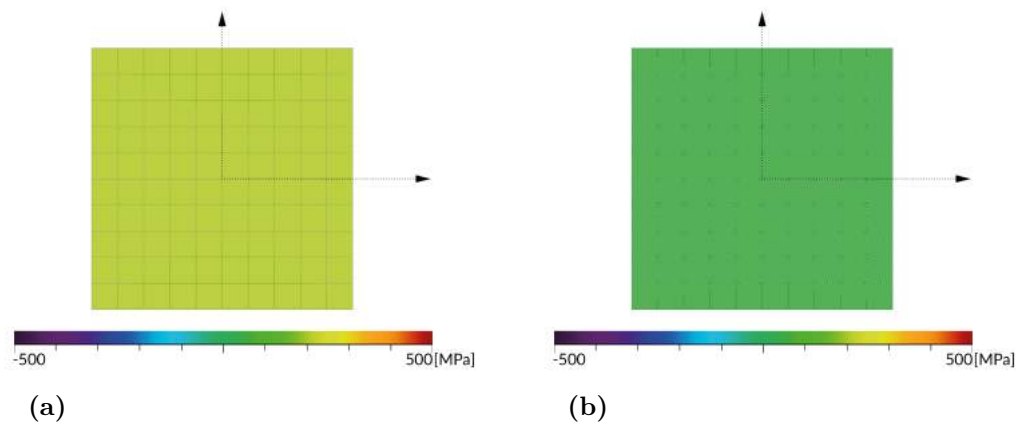


Figure 7.19: Stresses in bottom plane for the material CFRP 130.

(a) Load case 7.3.3

(b) Load case 7.3.3

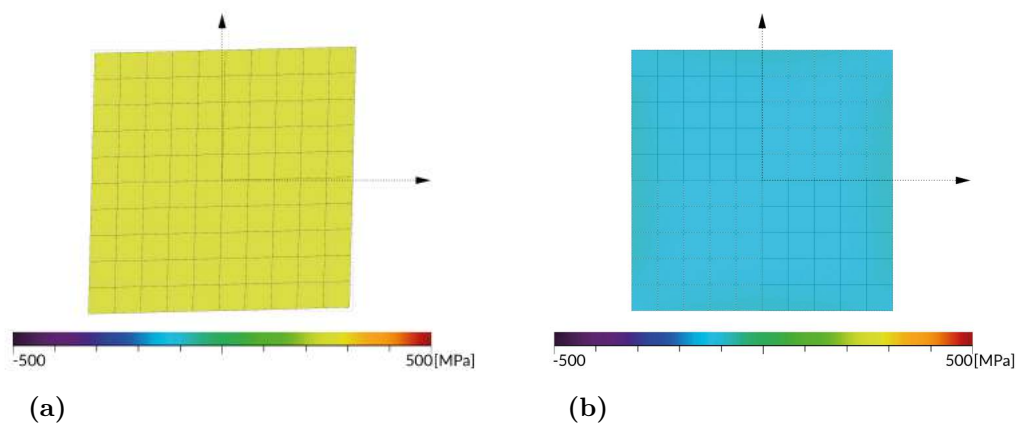


Figure 7.20: Stresses in bottom plane for the material CFRP 130.

(a) Load case 7.3.5

(b) Load case 7.3.6

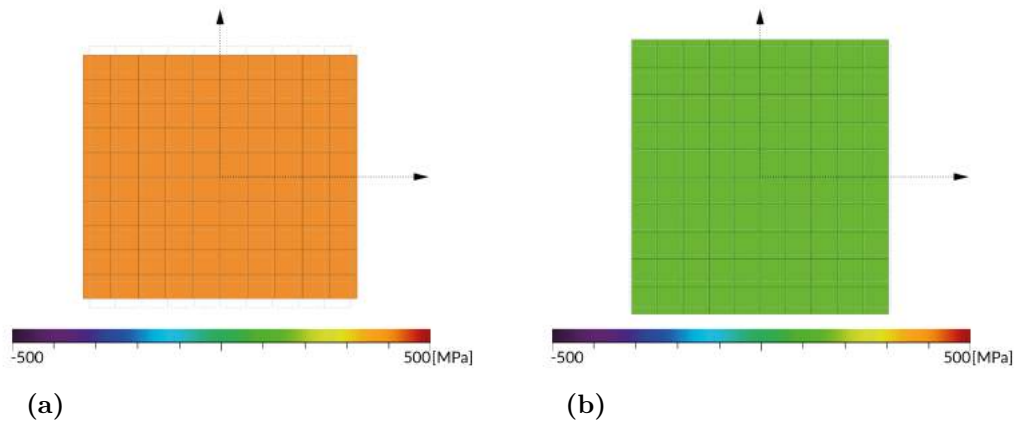


Figure 7.21: Stresses in centre plane for the material CFRP 130.

(a) Load case 7.3.1

(b) Load case 7.3.2

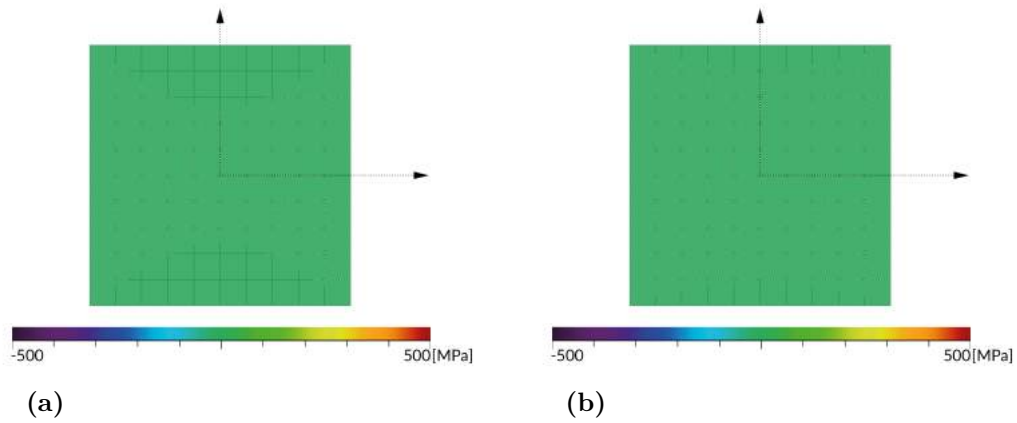


Figure 7.22: Stresses in centre plane for the material CFRP 130.

(a) Load case 7.3.3

(b) Load case 7.3.4

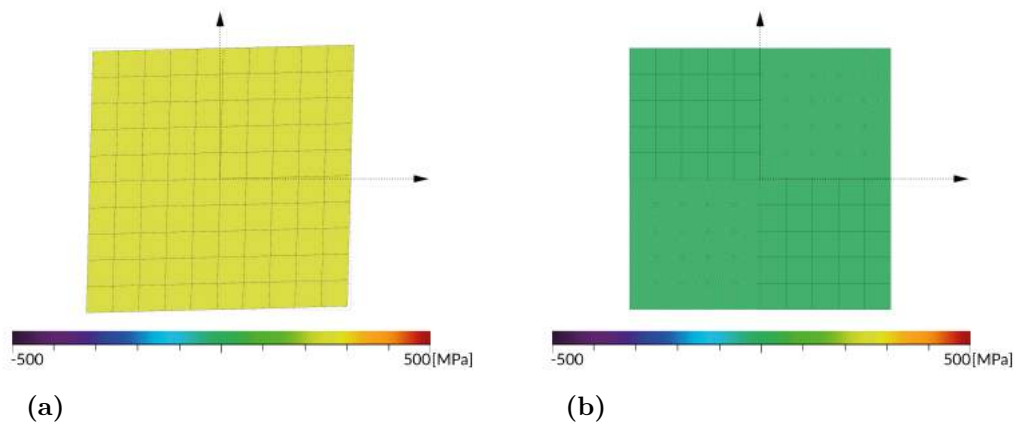


Figure 7.23: Stresses in centre plane for the material CFRP 130.

(a) Load case 7.3.5

(b) Load case 7.3.6

7. MATERIAL PARAMETERS FOR FE ANALYSIS

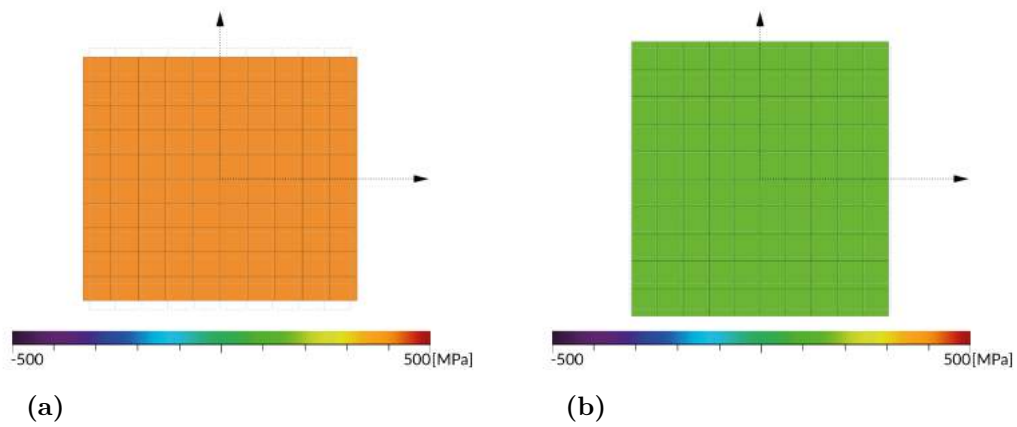


Figure 7.24: Stresses in top plane for the material CFRP 130.

(a) Load case 7.3.1

(b) Load case 7.3.2

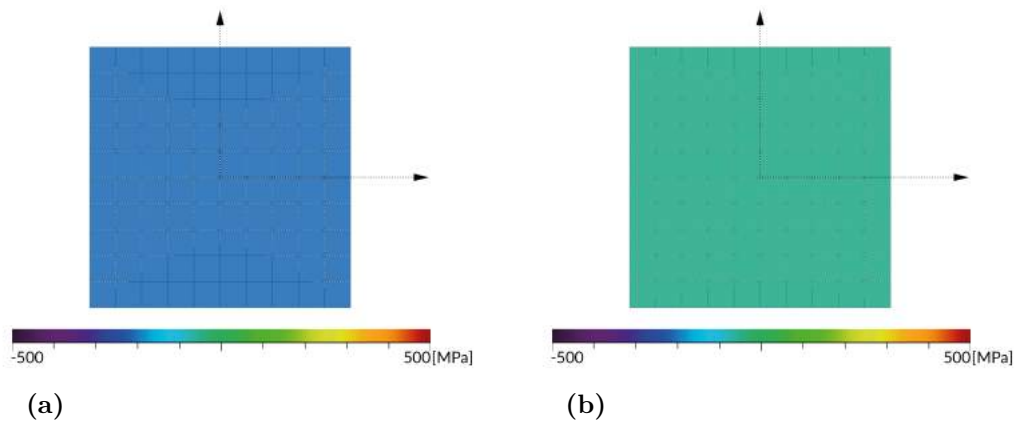


Figure 7.25: Stresses in top plane for the material CFRP 130.

(a) Load case 7.3.3

(b) Load case 7.3.4

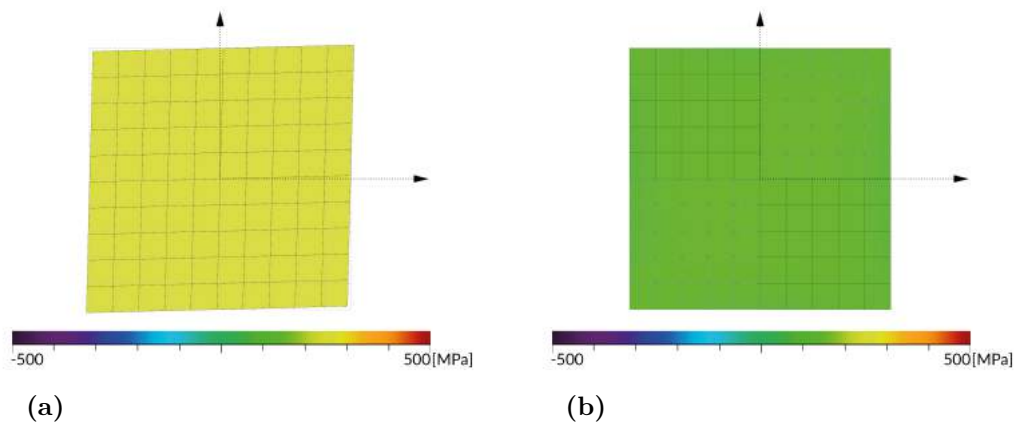


Figure 7.26: Stresses in top plane for the material CFRP 130.

(a) Load case 7.3.5

(b) Load case 7.3.6

Table 7.3: Resulting strains and stresses in MATLAB and SOFiSTiK for Load case 7.3.1.

Angle θ	Strain, ε_2 [10^{-3}]			Stress, σ_1 [MPa]		
	MATLAB	SOFiSTiK	[%]	MATLAB	SOFiSTiK	[%]
$\pm 0^\circ$	0.31	0.31	100.00	1252.48	1252.48	100.00
$\pm 5^\circ$	0.38	0.38	100.01	1228.92	1228.92	100.00
$\pm 10^\circ$	0.58	0.58	99.99	1153.53	1153.52	100.00
$\pm 15^\circ$	0.87	0.87	99.99	1017.87	1017.85	100.00
$\pm 20^\circ$	1.16	1.16	99.99	825.97	825.91	100.01
$\pm 25^\circ$	1.34	1.34	99.99	608.66	608.57	100.01
$\pm 30^\circ$	1.35	1.35	99.99	412.31	412.21	100.03
$\pm 35^\circ$	1.23	1.23	99.99	267.96	267.87	100.03
$\pm 40^\circ$	1.03	1.03	100.00	178.52	178.47	100.03
$\pm 45^\circ$	0.82	0.82	100.00	130.74	130.73	100.00

Table 7.4: Resulting strains and stresses in MATLAB and SOFiSTiK for Load case 7.3.2.

Angle θ	Strains, ε_1 [10^{-3}]			Stress, σ_2 [MPa]		
	MATLAB	SOFiSTiK	[%]	MATLAB	SOFiSTiK	[%]
$\pm 0^\circ$	0.03	0.03	100.00	124.07	124.07	100.00
$\pm 5^\circ$	0.04	0.04	100.01	123.29	123.29	100.00
$\pm 10^\circ$	0.06	0.06	99.98	120.99	120.99	100.00
$\pm 15^\circ$	0.10	0.10	99.99	117.32	117.32	100.00
$\pm 20^\circ$	0.16	0.16	99.99	112.64	112.63	100.01
$\pm 25^\circ$	0.24	0.24	99.99	107.61	107.60	100.01
$\pm 30^\circ$	0.34	0.34	99.99	103.50	103.48	100.02
$\pm 35^\circ$	0.47	0.47	99.99	102.67	102.64	100.03
$\pm 40^\circ$	0.63	0.63	100.00	109.32	109.30	100.02
$\pm 45^\circ$	0.82	0.82	100.00	130.74	130.73	100.00

Table 7.5: Resulting strains and stresses in MATLAB and SOFiSTiK for Load case 7.3.3.

Angle θ	Strains, γ_{12} [10^{-3}]			Stress, τ_{12} [MPa]		
	MATLAB	SOFiSTiK	[%]	MATLAB	SOFiSTiK	[%]
$\pm 0^\circ$	1.00	1.00	100.00	35.88	35.90	99.94
$\pm 5^\circ$	1.00	1.00	100.00	44.69	44.70	99.97
$\pm 10^\circ$	1.00	1.00	100.00	70.05	70.10	99.94
$\pm 15^\circ$	1.00	1.00	100.00	108.92	108.90	100.02
$\pm 20^\circ$	1.00	1.00	100.00	156.59	156.60	100.00
$\pm 25^\circ$	1.00	1.00	100.00	207.33	207.30	100.01
$\pm 30^\circ$	1.00	1.00	100.00	255.00	255.00	100.00
$\pm 35^\circ$	1.00	1.00	100.00	293.87	293.90	99.99
$\pm 40^\circ$	1.00	1.00	100.00	319.24	319.20	100.01
$\pm 45^\circ$	1.00	1.00	100.00	328.05	328.00	100.01

Table 7.6: Resulting curvatures and stress in MATLAB and SOFiSTiK for Load case 7.3.4.

Angle θ	Curvature, κ_2 [10^{-3}]			Stress, σ_1 [MPa]		
	MATLAB	SOFiSTiK	[%]	MATLAB	SOFiSTiK	[%]
$\pm 0^\circ$	0.31	0.31	99.94	626.24	626.24	100.00
$\pm 5^\circ$	0.38	0.38	99.96	614.46	614.46	100.00
$\pm 10^\circ$	0.58	0.58	99.95	576.76	576.76	100.00
$\pm 15^\circ$	0.87	0.87	99.98	508.94	508.92	100.00
$\pm 20^\circ$	1.16	1.16	100.02	412.98	412.96	100.01
$\pm 25^\circ$	1.34	1.34	100.04	304.33	304.28	100.02
$\pm 30^\circ$	1.35	1.35	100.04	206.16	206.10	100.03
$\pm 35^\circ$	1.23	1.23	100.02	133.98	133.93	100.04
$\pm 40^\circ$	1.03	1.03	100.00	89.26	89.23	100.03
$\pm 45^\circ$	0.82	0.82	99.98	65.37	65.36	100.01

Table 7.7: Resulting curvatures and stress in MATLAB and SOFiSTiK for Load case 7.3.5.

Angle θ	Curvature, κ_2 [10^{-3}]			Stress, σ_1 [MPa]		
	MATLAB	SOFiSTiK	[%]	MATLAB	SOFiSTiK	[%]
$\pm 0^\circ$	0.03	0.03	99.93	62.04	62.04	99.99
$\pm 5^\circ$	0.04	0.04	99.95	61.65	61.64	100.01
$\pm 10^\circ$	0.06	0.06	99.93	60.49	60.49	100.01
$\pm 15^\circ$	0.10	0.10	99.68	58.66	58.66	100.00
$\pm 20^\circ$	0.16	0.16	99.93	56.32	56.32	100.00
$\pm 25^\circ$	0.24	0.24	99.93	53.80	53.80	100.01
$\pm 30^\circ$	0.34	0.34	99.94	51.75	51.74	100.02
$\pm 35^\circ$	0.47	0.47	99.94	51.33	51.32	100.03
$\pm 40^\circ$	0.63	0.63	99.96	54.66	54.65	100.02
$\pm 45^\circ$	0.82	0.82	99.98	65.37	65.36	100.01

Table 7.8: Resulting curvatures and stress in MATLAB and SOFiSTiK for Load case 7.3.6.

Angle θ	Curvature, κ_{12} [10^{-3}]			Stress, τ_{12} [MPa]		
	MATLAB	SOFiSTiK	[%]	MATLAB	SOFiSTiK	[%]
$\pm 0^\circ$	1.00	1.00	100.00	17.94	17.95	99.94
$\pm 5^\circ$	1.00	1.00	100.00	22.34	22.35	99.97
$\pm 10^\circ$	1.00	1.00	100.00	35.03	35.05	99.94
$\pm 15^\circ$	1.00	1.00	100.00	54.46	54.45	100.02
$\pm 20^\circ$	1.00	1.00	100.00	78.30	78.30	100.00
$\pm 25^\circ$	1.00	1.00	100.00	103.66	103.65	100.01
$\pm 30^\circ$	1.00	1.00	100.00	127.50	127.50	100.00
$\pm 35^\circ$	1.00	1.00	100.00	146.93	146.95	99.99
$\pm 40^\circ$	1.00	1.00	100.00	159.62	159.60	100.01
$\pm 45^\circ$	1.00	1.00	100.00	164.02	164.00	100.01

7.4 Materials and cross sections for beam elements

To verify if the material parameters also could be used for analysis using beam elements a study was conducted comparing QUAD and beam elements in SOFiSTiK. Four load cases were defined, see Table 7.10 and Figure 7.27. The study was conducted for two geometries, see Table 7.9.

Table 7.9: Beam dimensions used in FE material case studies.

Load case	Length [m]		
Name	L_x	L_y	L_z
Short beam	100	20	10
Long beam	200	20	10

Table 7.10: Loads applied in Load case 7.4.1 to Load case 7.4.4

Load case	Load [kN/m]		
Name	q_x	q_y	q_z
Load case 7.4.1	5		
Load case 7.4.2	-5		
Load case 7.4.3		0.2	
Load case 7.4.4			0.2

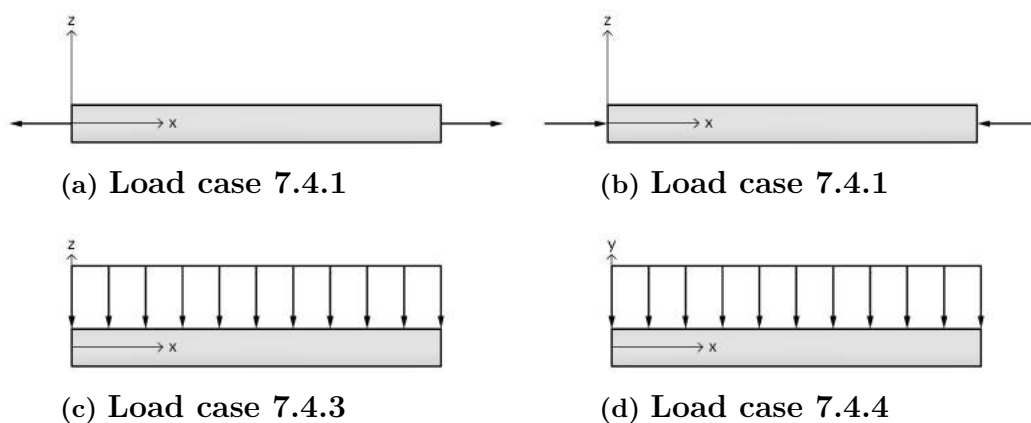


Figure 7.27: Loads applied in Load case 7.4.1 to Load case 7.4.4

7.4.1 Adaptations of parameters for beam elements

For each of the nine materials and load cases the maximum displacements were compared for the QUAD and beam models. In Figures 7.28 to 7.30 the results of a study conducted for a beam with cross section dimensions 20×10 mm and length of 100mm is shown. Here it can be seen that displacements are similar for extension (Figure 7.28) and bending about the local z -axis (Figure 7.30). However for bending about the y -axis (Figure 7.29) the differences are very large and the the differences also increase for the materials based on laminates with fibre orientations larger than $\pm 0^\circ$.

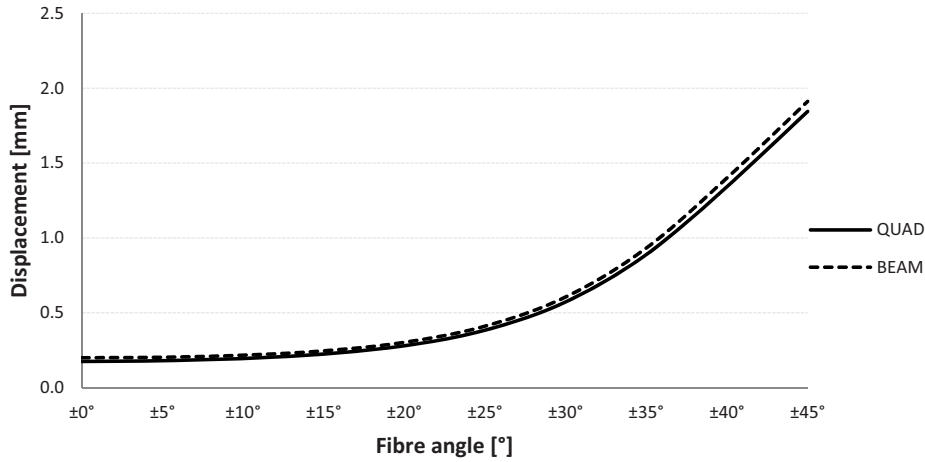


Figure 7.28: Comparison of maximum displacements in the x direction for QUAD and beam elements, with cross section dimensions 20×10 mm and 100mm lengths for **Load case 7.4.1**.

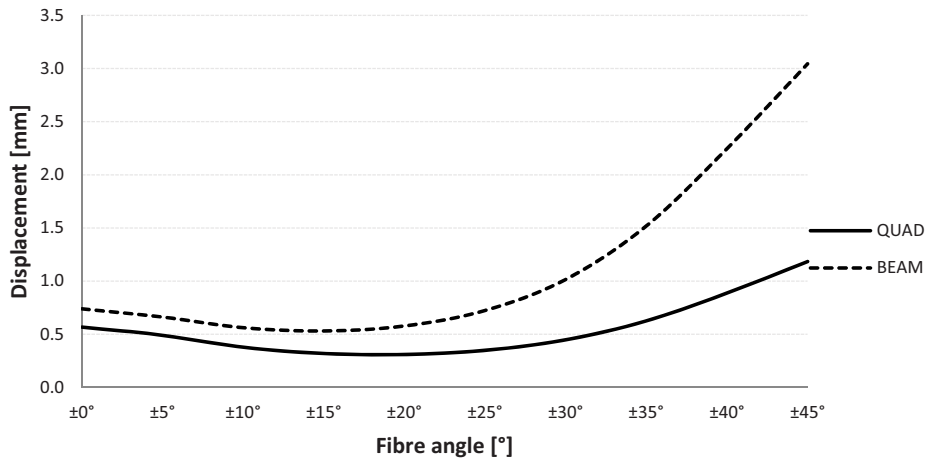


Figure 7.29: Comparison of maximum displacements in the y direction for QUAD and beam elements, with cross section dimensions 20×10 mm and 100mm lengths for **Load case 7.4.4**.

7. MATERIAL PARAMETERS FOR FE ANALYSIS

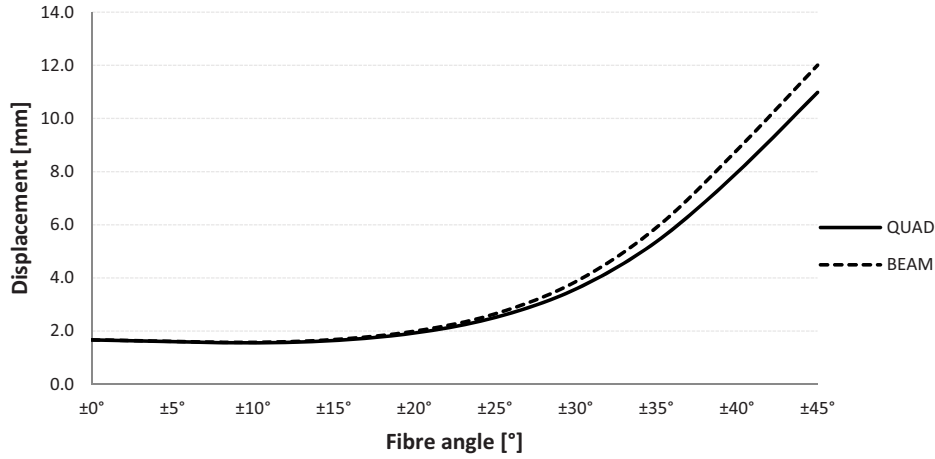


Figure 7.30: Comparison of maximum displacements in the z direction for QUAD and beam elements, with cross section dimensions 20×10 mm and 100mm lengths for **Load case 7.4.3**.

The large difference here is assumed to be due to the fact that the transverse beam deflection are assumed to be uniform across the width of the beam and is a function of x in beam theory. Due to the plate curvatures κ_y and κ_{xy} this deflection is not independent from y . However for beams with a very high length to width ratio, the effect of plate curvatures become so small that it can be neglected [19].

It was attempted to correct the difference in the transverse deflections by adapting the beam cross sections in SOFiSTiK. This was done by defining a shear deformation area, A_y [43]. For each load case in the previous study, the ratio between the transverse deflections for beam and QUAD elements, w_y^b and w_y^Q , were calculated. This was then applied as a factor to the beam cross section area, A , see Equation 7.7. With these cross section adaptations the same study was conducted again, and the results can be seen in Figure 7.31 for load case **Load case 7.4.4**.

$$A_y = \frac{w_y^b}{w_y^Q} A \quad (7.7)$$

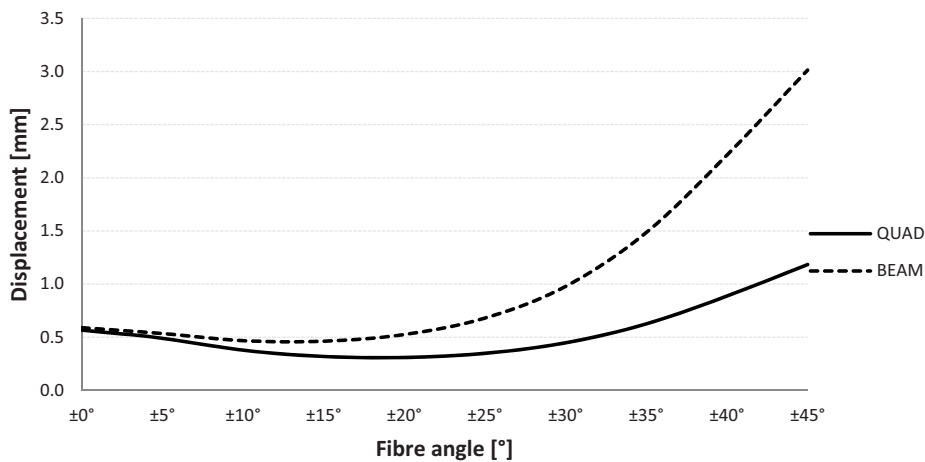


Figure 7.31: Comparison of maximum displacements in y direction QUAD and beam elements with adapted shear deformation areas for **Load case 7.4.4**

Here it can be seen that this factor has a large influence on the transverse deflection for the material defined by the lamina orientation $\pm 0^\circ$, for remaining materials this factor had little or no influence. The displacements in the x and z directions were unaffected by this change.

The study was also conducted for a longer beam element with cross section dimensions 20×10 mm and length of 200mm. Here there was a much better correspondence for the $\pm 0^\circ$ material. The transverse deflections in the y were corresponding very well for all materials, however the deflections in the z direction started to diverge for the two models around $\pm 20^\circ$, see, Figure 7.32 to 7.34. No further attempts to find a better correspondence were made, and all materials, with the exception of the $\pm 0^\circ$ material, were omitted for analysis with beam elements in the following studies.

The displacements were imported into Grasshopper and compared visually in order to evaluate the correspondence of the displacements over the whole width and length of the beam, see Figures 7.35 to 7.38. Here it was observed that the displacements were very similar overall.

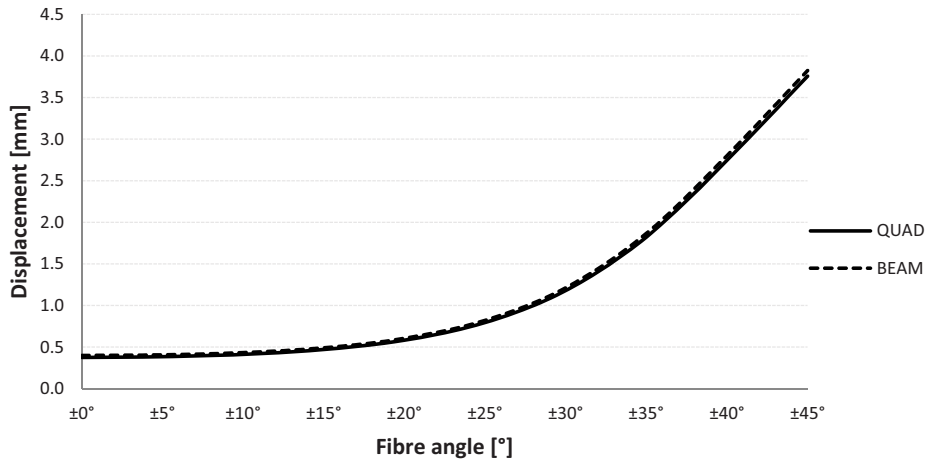


Figure 7.32: Comparison of maximum displacements in the x direction for QUAD and beam elements, with cross section dimensions 20×10 mm and 200mm lengths for **Load case 7.4.1**.

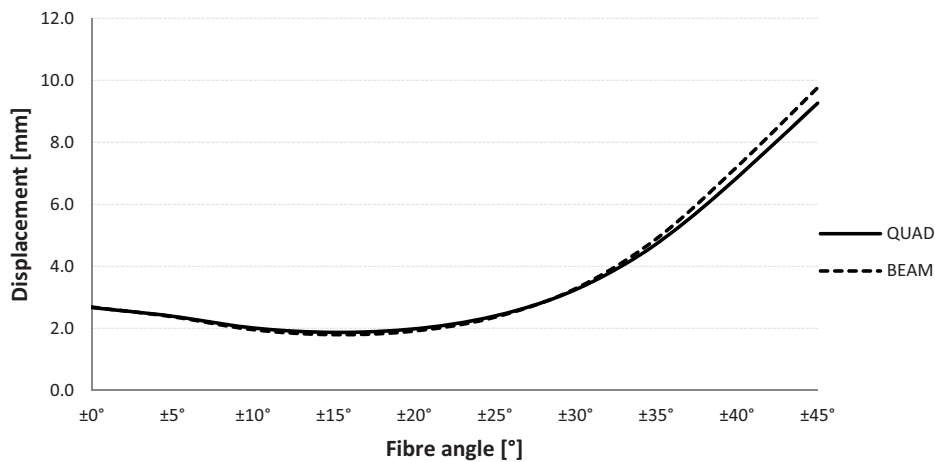


Figure 7.33: Comparison of maximum displacements in the y direction for QUAD and beam elements, with cross section dimensions 20×10 mm and 200mm lengths for **Load case 7.4.4**.

7. MATERIAL PARAMETERS FOR FE ANALYSIS

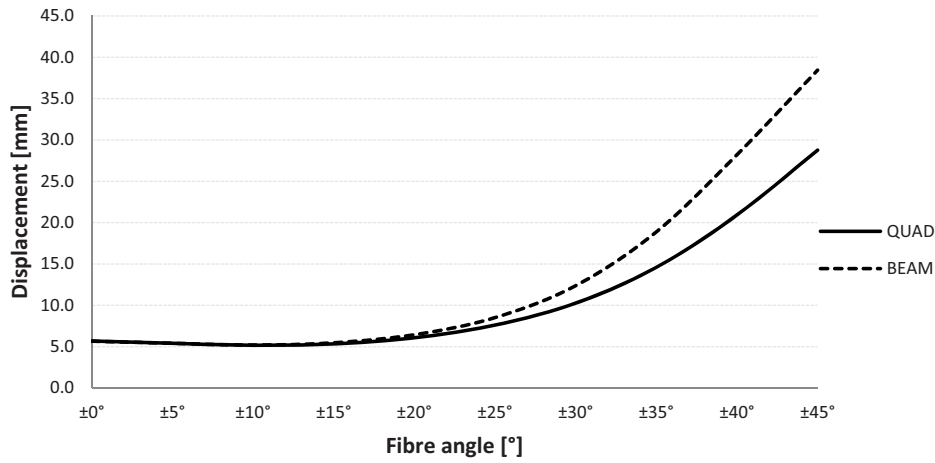


Figure 7.34: Comparison of maximum displacements in the z direction for QUAD and beam elements, with cross section dimensions 20×10 mm and 200mm lengths for **Load case 7.4.3**.

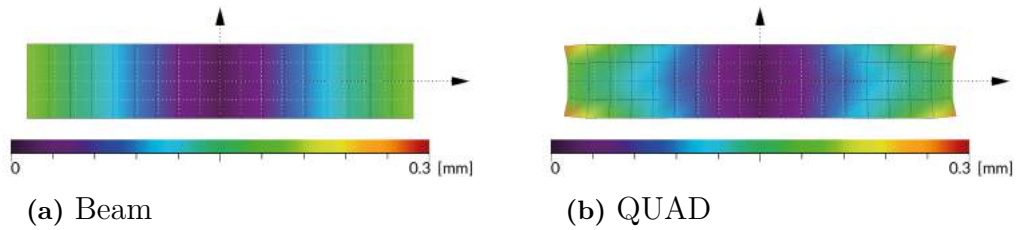


Figure 7.35: Comparison of displacements for **Load case 7.4.1**.

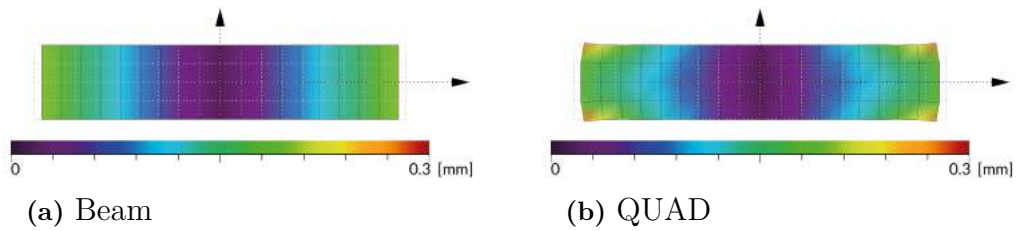


Figure 7.36: Comparison of displacements for **Load case 7.4.2**.

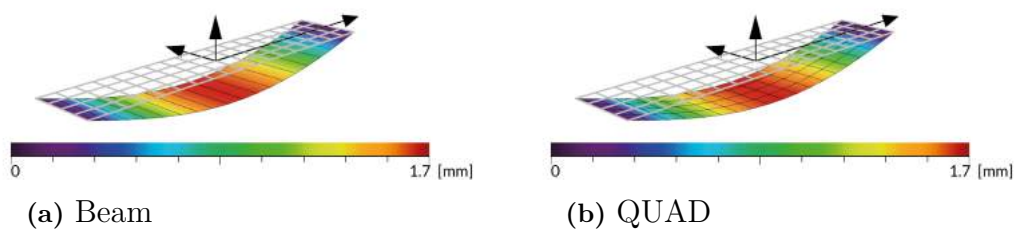


Figure 7.37: Comparison of displacements for **Load case 7.4.3**.

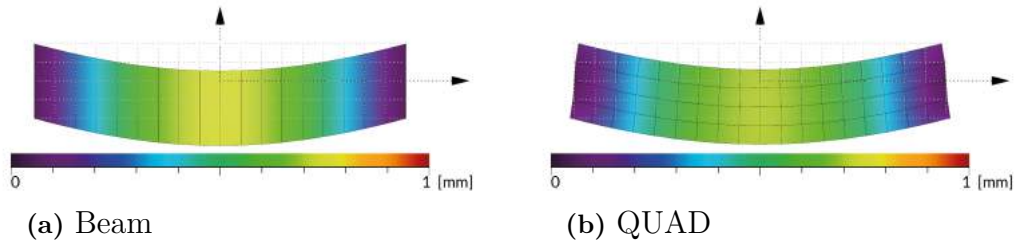


Figure 7.38: Comparison of displacements for **Load case 7.4.4**.

7.4.2 Resulting forces and stresses in QUAD and BEAM elements

Stresses for beams can be calculated using the program module AQB in SOFiSTiK [45], and it is also possible to calculate stresses at certain points in the cross sections [43]. In this study it was however chosen to calculate the stresses from sectional force results, since it simplified the import of the results into Grasshopper with the developed tool *PlotStresses*, and made it possible to directly compare stress results for beam and QUAD models.

7.4.2.1 Calculation of stresses

Normal stresses due to bending about the local y and z axes in the beams were calculated according to Equation 7.8 [46].

$$\sigma_x = \frac{N_x}{A} + \frac{M_y}{I_y}z + \frac{M_z}{I_z}y \quad (7.8)$$

The maximum shear stress in the centre point of the beam was according to Equation 7.9 [46]. Here the shear force, V , is taken as the largest of V_z and V_y . This was compared to the calculated "absolute slab stress" for QUAD elements in SOFiSTiK.

$$\tau_{\max} = \frac{3V}{2A} \quad (7.9)$$

Additionally the shear stress in the xy -plane was calculated for beams according to equation 7.10 for direct comparison with the shear stress in QUAD elements. Shear stress in the xy -plane due to torsion was calculated according to Equations 7.11 and 7.12, where $\beta = 0.246$ and d and b are the beam cross section dimensions [46]. The calculated stresses were verified against comparison with stresses calculated using AQB in SOFiSTiK's Wingraf.

$$\tau_{xy} = \frac{3V_y}{2A} \quad (7.10)$$

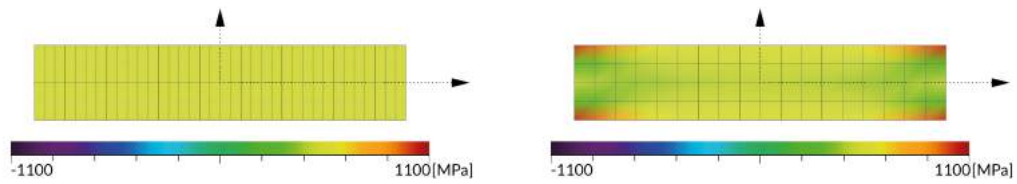
$$\tau_T = \frac{M_T}{W_T} \quad (7.11)$$

$$W_T = \beta db^2, \text{ where } b \leq d \quad (7.12)$$

7.4.2.2 Comparison between QUAD and beams models

In Table 7.11 the minimum and maximum stresses for each load case and the material CFRP 100 are shown. Here it can be seen that there are differences in the minimum and maximum stresses between the two models, due to local stress concentrations in the QUAD model, but the average stress in all cases except for shear were corresponding well.

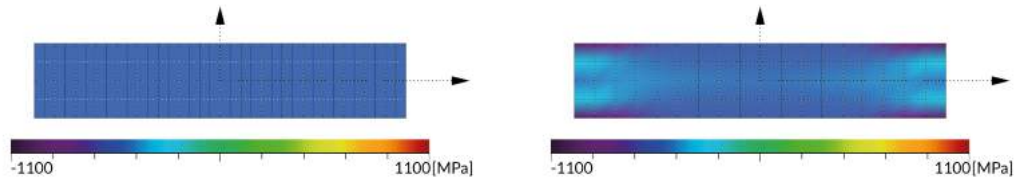
The stresses were imported into Grasshopper and Rhino using the tool *PlotStresses* for visual comparison of the results, see Figures 7.39 to 7.44. Here it can be seen that the stress variation is very similar especially in the centre of the beam for all cases.



(a) Beam

(b) QUAD

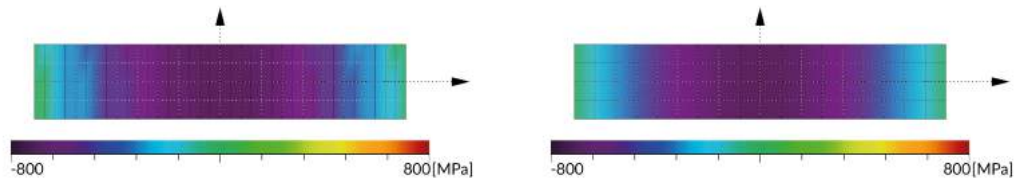
Figure 7.39: Comparison of normal stress σ_r for Load case 7.4.1.



(a) Beam

(b) QUAD

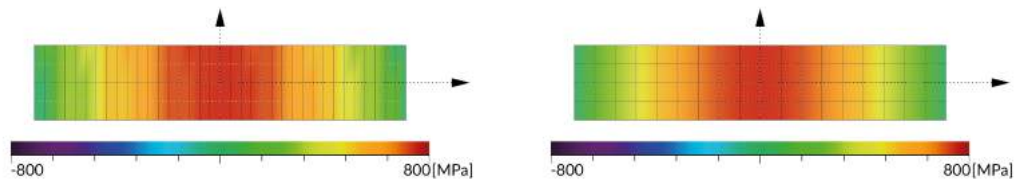
Figure 7.40: Comparison of normal stress σ_x for Load case 7.4.2.



(a) Beam

(b) QUAD

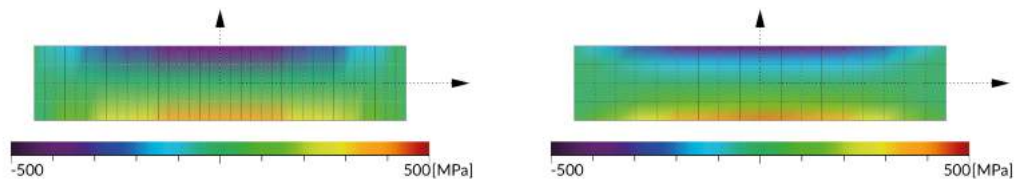
Figure 7.41: Comparison of normal stress σ_x in top plane for Load case 7.4.3.



(a) Beam

(b) QUAD

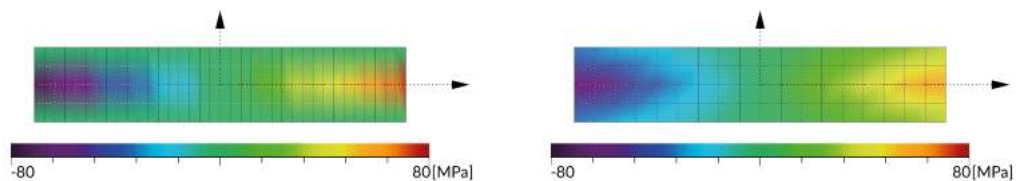
Figure 7.42: Comparison of normal stress σ_x in bottom plane for Load case 7.4.3.



(a) Beam

(b) QUAD

Figure 7.43: Comparison of normal stress σ_x in centre plane for Load case 7.4.4.



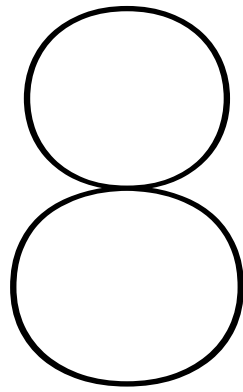
(a) Beam

(b) QUAD

Figure 7.44: Comparison of shear stress τ_{xy} in centre plane for Load case 7.4.4.

Table 7.11: Normal and shear stresses, σ_x and τ_{xy} , in QUAD and beam models for **Load case 7.4.1** to **Load case 7.4.4**.

Load case	Position	σ_x [MPa]		τ_{xy} [MPa]	
		Min	Max	Min	Max
Load case 7.4.1 - QUAD	Center	258.62	1020.06	0.00	0.00
	Top	258.62	1020.06	0.00	0.00
	Bottom	258.62	1020.06	0.00	0.00
Load case 7.4.1 - Beam	Center	500.00	500.00	0.00	0.00
	Top	500.00	500.00	0.00	0.00
	Bottom	500.00	500.00	0.00	0.00
Load case 7.4.2 - QUAD	Center	-1020.06	-258.62	0.00	0.00
	Top	-1020.06	-258.62	0.00	0.00
	Bottom	-1020.06	-258.62	0.00	0.00
Load case 7.4.2 - - Beam	Center	-500.00	-500.00	0.00	0.00
	Top	-500.00	-500.00	0.00	0.00
	Bottom	-500.00	-500.00	0.00	0.00
Load case 7.4.3 - QUAD	Center	0.00	0.00	-71.80	71.80
	Top	-0.78	750.77	0.00	0.00
	Bottom	-750.77	0.78	0.00	0.00
Load case 7.4.3 - Beam	Center	0.00	0.00	-75.00	75.00
	Top	0.00	750.00	0.00	0.00
	Bottom	-750.00	0.00	0.00	0.00
Load case 7.4.4 - QUAD	Center	-420.03	420.03	-61.14	61.14
	Top	0.00	0.00	0.00	0.00
	Bottom	0.00	0.00	0.00	0.00
Load case 7.4.4 - BEAM	Center	-375.00	375.00	-75.00	75.00
	Top	0.00	0.00	0.00	0.00
	Bottom	0.00	0.00	0.00	0.00



DEVELOPMENT OF A PARAMETRIC DESIGN AND ANALYSIS APPROACH

8. DEVELOPMENT OF A PARAMETRIC DESIGN AND ANALYSIS APPROACH

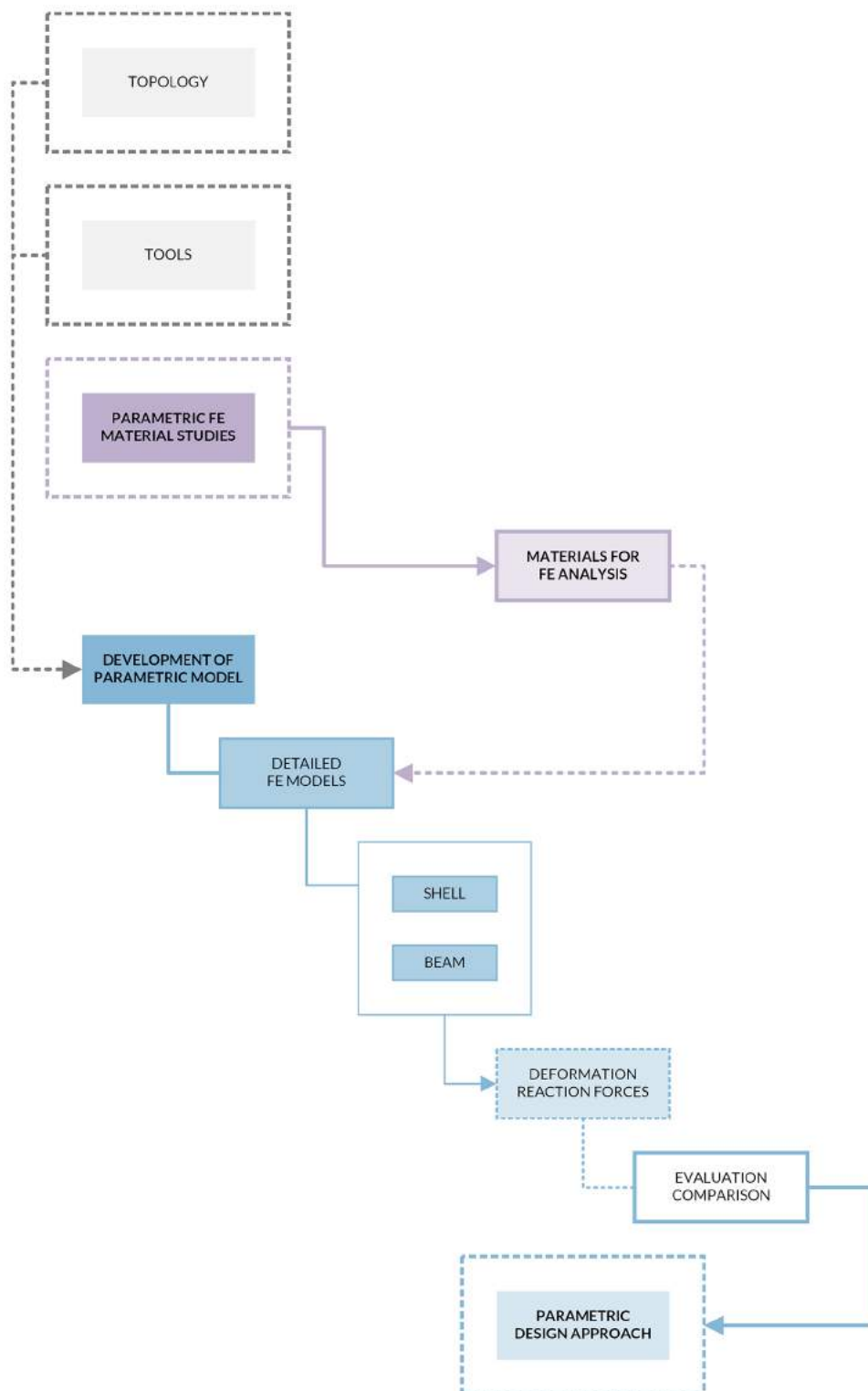


Figure 8.1: Flowchart describing the methodology used for the case studies presented in Chapter 8 - Development of a parametric design and analysis approach.

8.1 Preliminary evaluation of detailed parametric models

Three types of parametric models were developed for the topology of the studied FRP type, a QUAD model, a beam model and a uniform QUAD model, and case studies were carried out as in Figure 8.1. The results from these case studied are presented in this chapter.

8.1.1 Defining structural objects in Grasshopper

The structural information were defined as object attributes, and three Grasshopper components were written using C# in order to generate these attributes for SPT, SLN and SAR objects, see Appendix B.2 for a description of these tools.

8.1.2 Parametric FE models in Grasshopper

The geometry and structural information for the FE models were defined in Grasshopper and a parametric model was developed, see Figure 8.2. The models were defined for a topology mesh segment, with the assumption that the principles applied in this small scale model could also be applied to the actual FRP modules since the topology would be the same. The mesh segment was modelled assuming the mesh segment is planar. In the actual FRP module this is not the case, this will however be further discussed in Chapter 10. Comparison between the three models was done by comparing deflections in the points indicated in Figure 8.2, as well as comparing forces and stresses, mainly in the uni-directional zones.

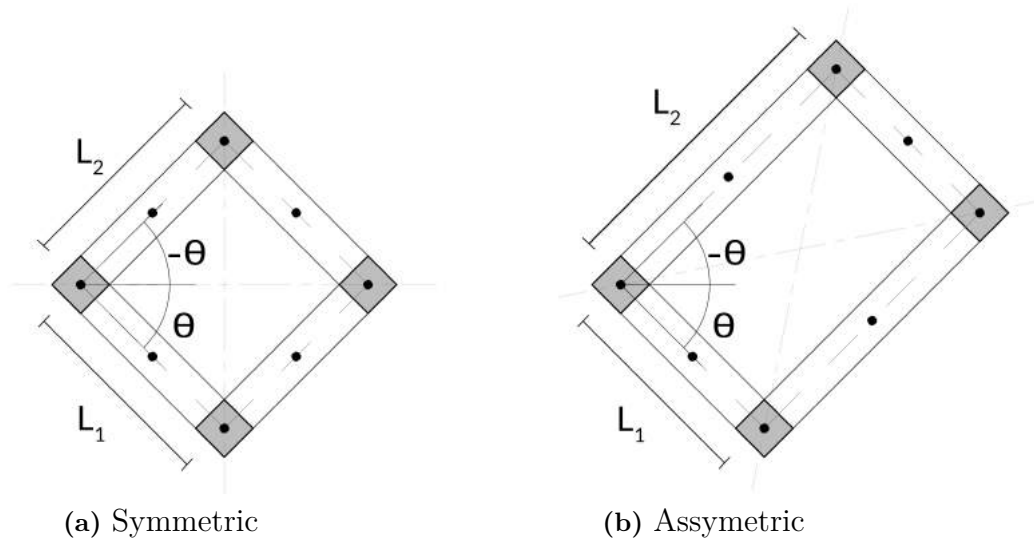


Figure 8.2: Principal illustration of the parametric model developed for a mesh segment.

8.1.2.1 QUAD model for topology mesh segment

The QUAD model was modeled as in Figure 8.3. Both the uni-directional and node zones were considered by applying the CFRP 100 material in the unidirectional zones, and materials based on the angle θ in the node zones, see Table 7.1.

8.1.2.2 Beam model for topology mesh segment

The beam model was modelled as in Figure 8.4. The node zones were not accounted for and the beams were modelled as uniform beams with the material CFRP 100, see Table 7.1, and cross section dimensions shown in Table 4.1 with a modified shear area as in Equation 7.7.

8.1.2.3 Uniform QUAD model for topology mesh segment

The uniform QUAD model was modelled using a uniform QUAD mesh over the whole mesh segment, see Figure 8.5. The reason for this was to evaluate whether the QUAD elements or materials could be adapted in a way such that this model would replicate the behaviour of the QUAD model. If possible this would mean that the parametric model could perhaps be simplified with regard to geometric complexity, number of elements and model parameters.

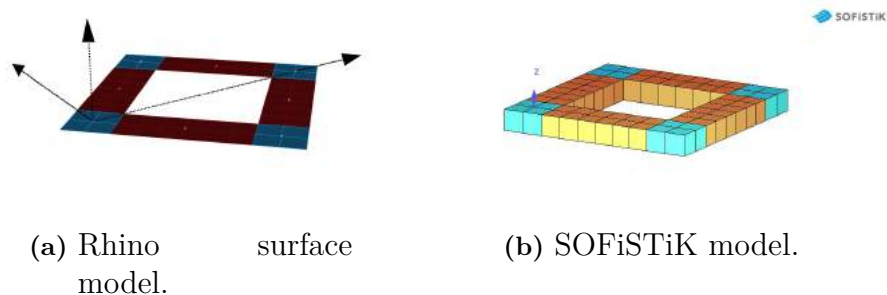


Figure 8.3: Parametric QUAD models.

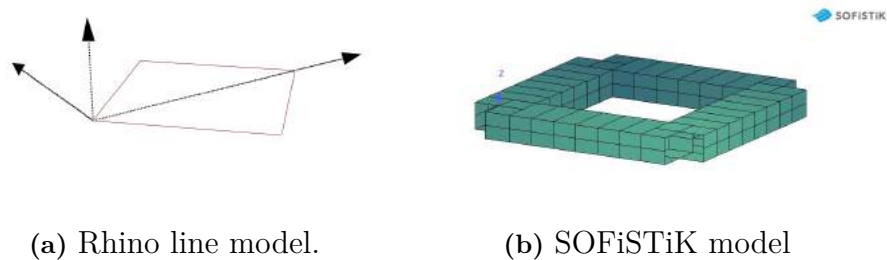


Figure 8.4: Parametric beam models

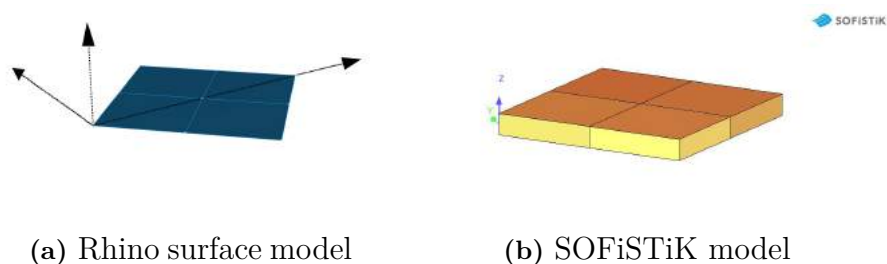


Figure 8.5: Parametric uniform QUAD models

8.1.3 Comparison and preliminary evaluation of parametric FE models

A preliminary evaluation of the different modelling approaches was conducted. The models were analysed in SOFiSTiK and compared with regard to tension/compression, bending and torsion, see Section 8.2. The comparisons were made by adjusting the parametric model and importing the results into Grasshopper for visual evaluation of deflections and stresses. The results were also compared in the SOFiSTiK environment. In this section the initial findings are only discussed, the results from detailed study which followed this study is presented in Section 8.2. The QUAD model was assumed to be the most accurate model since this is the only model which takes into account the materials for the node zones. This model was therefore used to compare and evaluate the two other models.

8.1.3.1 Comparison between detailed QUAD and beam models

A similar correspondence between beam and QUAD models could be seen here as was observed in Chapter 7. The deflections were mostly corresponding with some differences in the case of bending, however the correspondence was assumed to be accurate enough. The internal stresses and forces were also within range in the unidirectional zones, with local differences in the node zones, this is however expected due to the differences in structural models and material formulations in these zones.

8.1.3.2 Comparison between detailed QUAD and uniform QUAD models

It was attempted to find a stiffness of the uniform QUAD which would simulate the stiffness of the QUAD model. This was done by adapting the thickness of the QUAD elements, as well as adapting the stiffness of the elements in the local x and y directions[47]. In symmetric cases, see Figure 8.2a, the thickness of the element and the stiffness factors could be defined parametrically in Grasshopper as functions of the mesh area and density. With the adapted stiffness a correspondence could be seen between the deflections of the QUAD and uniform QUAD models, however in the case of stresses of forces it was not possible to directly relate the results of the uniform QUAD model to the detailed QUAD model. In the asymmetric case, see Figure 8.2b, a way to adjust the stiffness parametrically could not be found. This modelling approach was thus abandoned.

8.2 Comparison and evaluation of QUAD and beam models

A parametric study was conducted to compare the QUAD and beam models. Three load cases were defined, see Figures 8.6 to 8.8, and Table 8.2. The study was conducted for several parametric setups, in this Chapter the results are presented for the parametric setup shown in Table 8.1. The results for other parametric setups followed the same trends.

Table 8.1: Parameters used in comparison between QUAD and beam models

Model	Length [m]		
	L_1	L_2	θ
Symmetric	75	75	45°

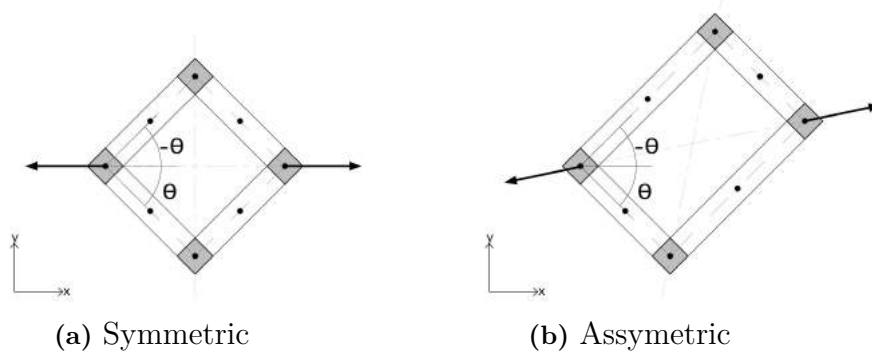


Figure 8.6: Load case 8.2.1

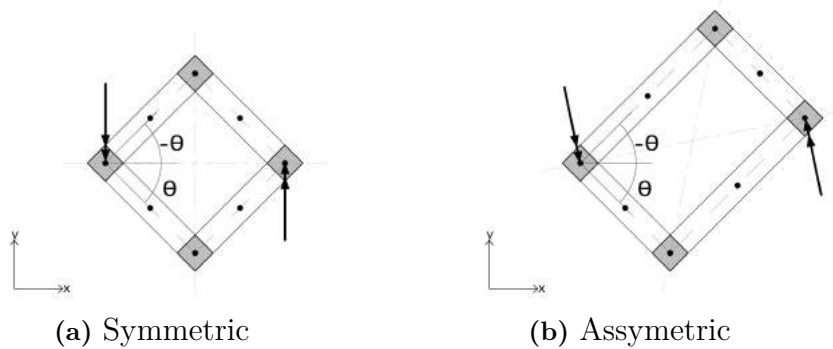


Figure 8.7: Load case 8.2.2

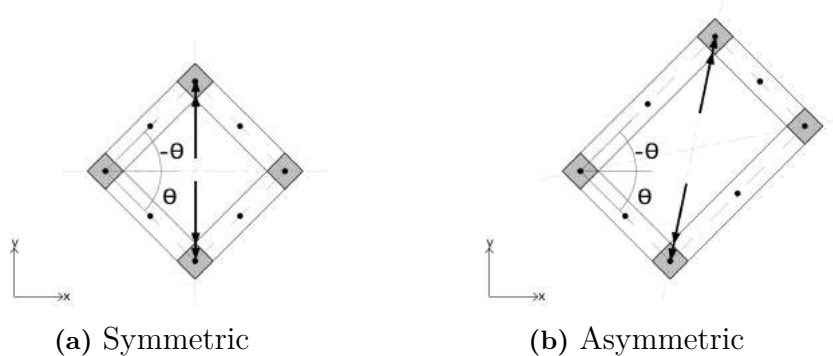


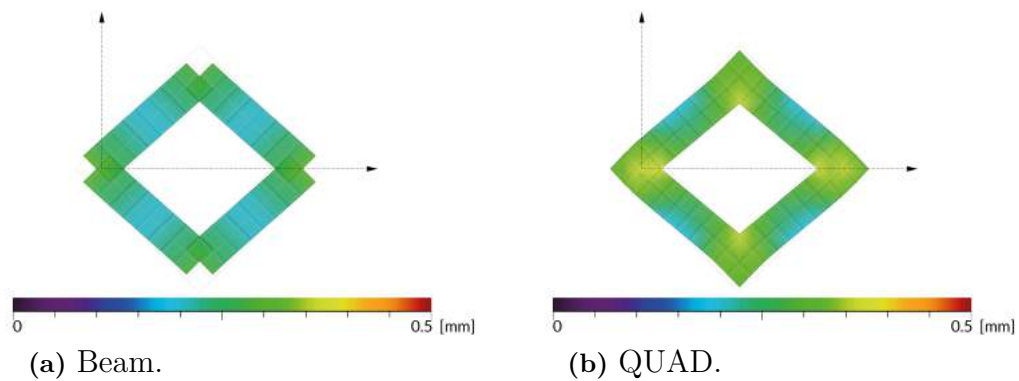
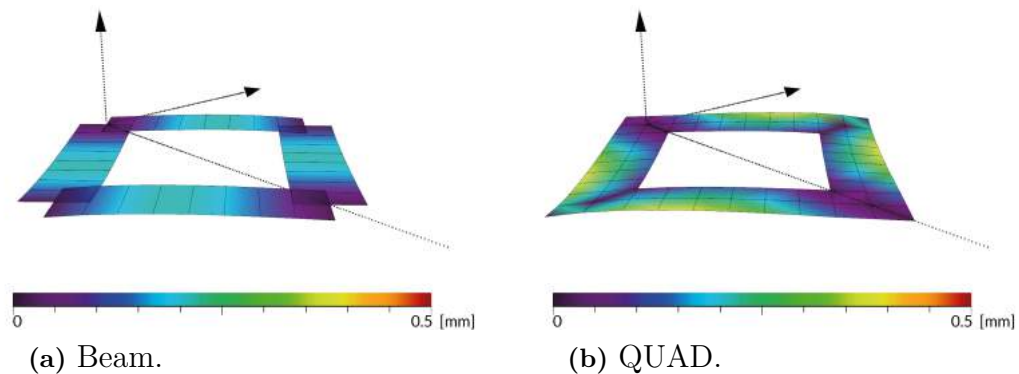
Figure 8.8: Load case 8.2.3

Table 8.2: Load cases used for comparison between QUAD and beam models for a mesh topology segment.

Load case	Force [kN]	Moment [kNm]
Name	P_x	M_y
Load case 8.2.1	9.4	
Load case 8.2.2		0.1
Load case 8.2.3		0.1

Table 8.3: Comparison of maximum and minimum displacements [mm] for Load case 8.2.1 to Load case 8.2.3.

Load case	Displacements [mm]				Comparison [%]	
	QUAD		BEAM		Min	Max
	Min	Max	Min	Max		
Load case 8.2.1	0.180	0.364	0.204	0.296	113%	81%
Load case 8.2.2	0.057	3.952	0.056	2.895	98%	73%
Load case 8.2.3		0.222		0.128		58%

**Figure 8.9:** Comparison between displacements for Load case 8.2.1.**Figure 8.10:** Comparison between displacements for Load case 8.2.3.

8.2.1 Comparison of displacements

A comparison between the minimum and maximum displacements for the parametric setup in Table 8.1 and the load case in Table 8.2 was done. The results from this comparison can be seen in Table 8.3. At first glance the differences appear large, however when visualised graphically in Grasshopper the displacements correspond well between the two models, see Figures 8.9 and 8.10. It can also be considered more important to compare the displacements on the points shown in Figure 8.2, especially in the uni-directional zones and along the centre line of the beams. It can also be seen in the QUAD models that the curvatures κ_x and κ_{xy} has some influence. However overall the displacements were assumed to be corresponding sufficiently well between the two models.

8.2.2 Comparison of stresses

The minimum and maximum stresses were compared between the two models and are presented in Table 8.4. Here it can be seen again that there seems to be significant differences between the two models, however when examining the overall stress visually in Grasshopper it can be seen that the differences are mainly due to local stress concentrations in the node zones, see Figures 8.11 to 8.13. Overall there was a good correspondence between the stresses, with slightly larger differences in shear stresses, see Figure 8.12.

Table 8.4: Normal and shear stresses, σ_x and τ_{xy} , in QUAD and beam models.

Load case	Position	σ_x [MPa]		τ_{xy} [MPa]	
		Min	Max	Min	Max
Load case 8.2.1 - QUAD	Center	-142.15	151.15	-75.68	75.68
	Top	0.00	0.00	0.00	0.00
	Bottom	0.00	0.00	0.00	0.00
Load case 8.2.1 - Beam	Center	-170.83	204.17	-25.00	25.00
	Top	0.00	0.00	0.00	0.00
	Bottom	0.00	0.00	0.00	0.00
Load case 8.2.2 - QUAD	Center	0.00	0.00	0.00	0.00
	Top	-72.55	245.08	-83.38	83.38
	Bottom	-245.08	72.55	-83.38	83.38
Load case 8.2.2 - Beam	Center	0.00	0.00	0.00	0.00
	Top	99.99	100.01	-67.73	67.73
	Bottom	-100.01	-99.99	-67.73	67.73
Load case 8.2.3 - QUAD	Center	0.00	0.00	0.00	0.00
	Top	-197.03	197.03	-185.96	4.32
	Bottom	-197.03	197.03	-4.32	185.96
Load case 8.2.3 - Beam	Center	0.00	0.00	0.00	0.00
	Top	-220.08	220.08	-3.33	3.33
	Bottom	-220.08	220.08	-3.33	3.33

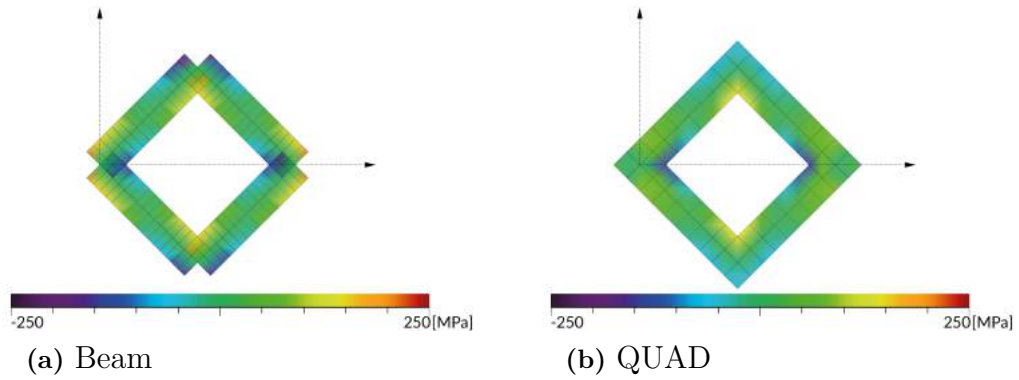


Figure 8.11: Comparison of normal stress σ_x in centre plane for Load case 8.2.1.

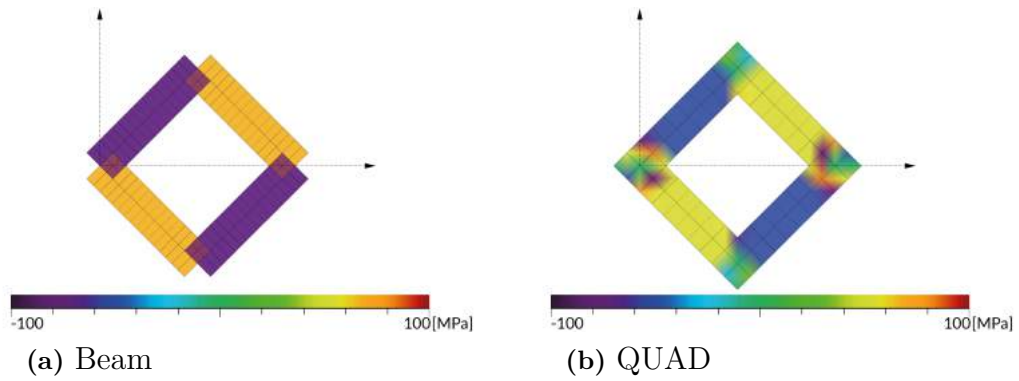


Figure 8.12: Comparison of shear stress τ_{xy} in centre plane for Load case 8.2.1.

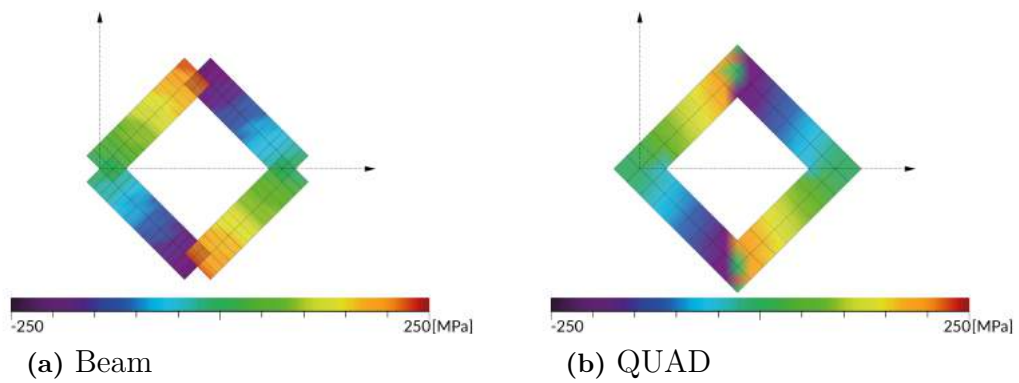
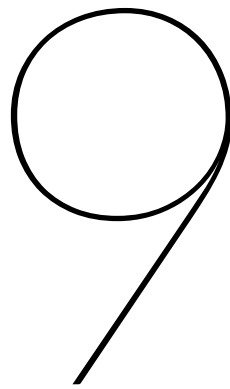


Figure 8.13: Comparison of normal stress σ_x in top plane for Load case 8.2.3.



VERIFICATION OF THE PROPOSED
PARAMETRIC DESIGN AND ANALYSIS
APPROACH

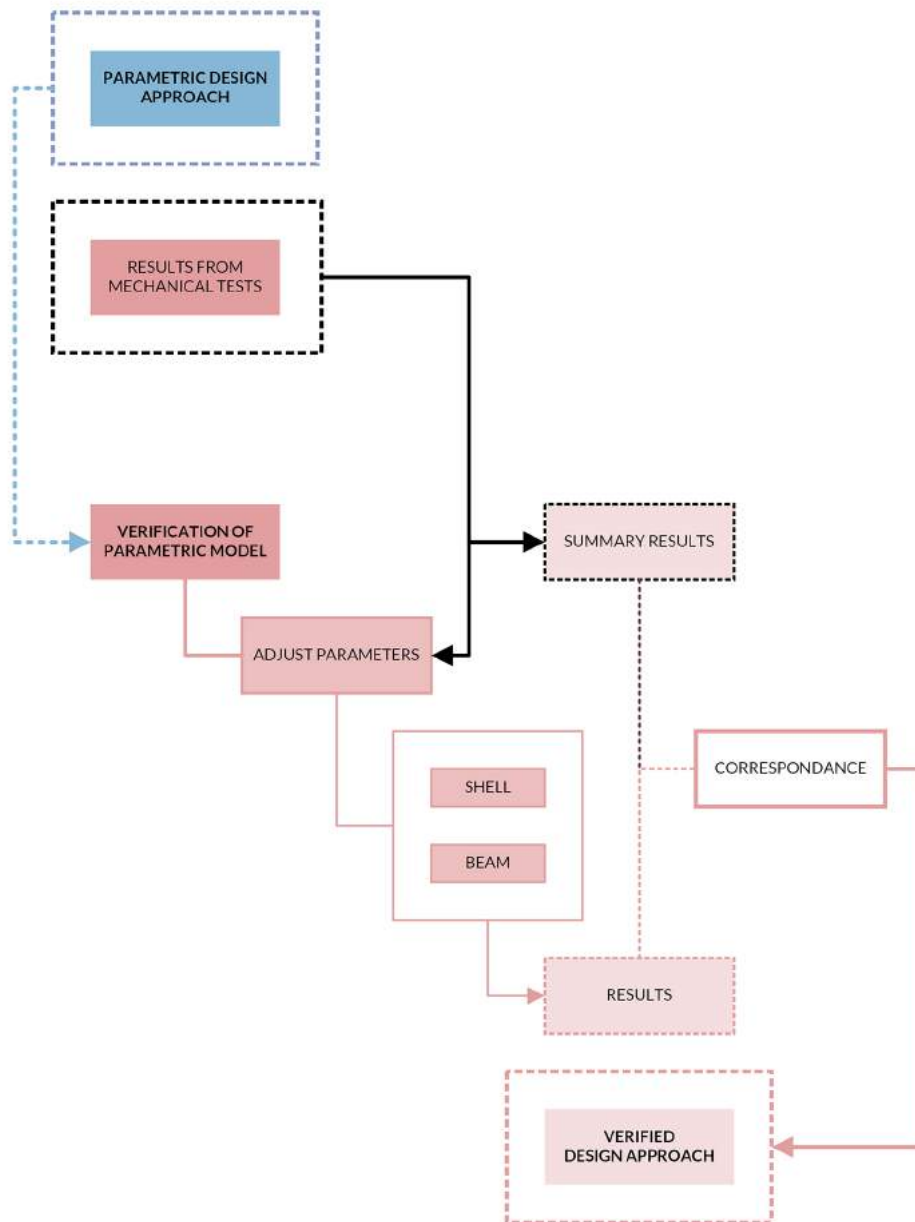


Figure 9.1: Flowchart describing the methodology used for the case studies presented in Chapter 9 - Verification of the proposed parametric design and analysis approach.

9.1 Verification and calibration approaches

Up until this point many assumptions have been made, and two models have been developed on the basis on these assumptions. The two models have a good correspondence, however the accuracy of the assumptions have not yet been determined, and without mechanical tests it cannot be said whether the simplifications made with regard to the nodes and discontinuity zones are accurate.

Further the material formulations considerations for material safety factors must be made. The EN Eurocodes are used as standards for design of buildings, where characteristic values and partial coefficients as well as methods for dimensioning can be found. However for FRP materials such a European Standard does not yet exist. A pre-normative document has been published by the European Commission's Joint Research Centre which summarises the current requirements which must be considered for the use of FRP materials in building construction. Here it is stated that characteristic values should be determined by laboratory tests in accordance with EN 1990 [6].

Verification and calibration of material should thus be carried out through mechanical tests, a principal methodology for this can be seen in Figure 9.1. Mechanical tests and FE analysis should be carried out using the same configurations, and the FE model should be adapted such that its results correspond sufficiently well with the results from the physical tests. Unfortunately it has not been possible to conduct mechanical tests within the time frame of this study, however this may be an opportunity for future work.

10

APPLICATION OF THE PROPOSED
PARAMETRIC DESIGN AND ANALYSIS
APPROACH

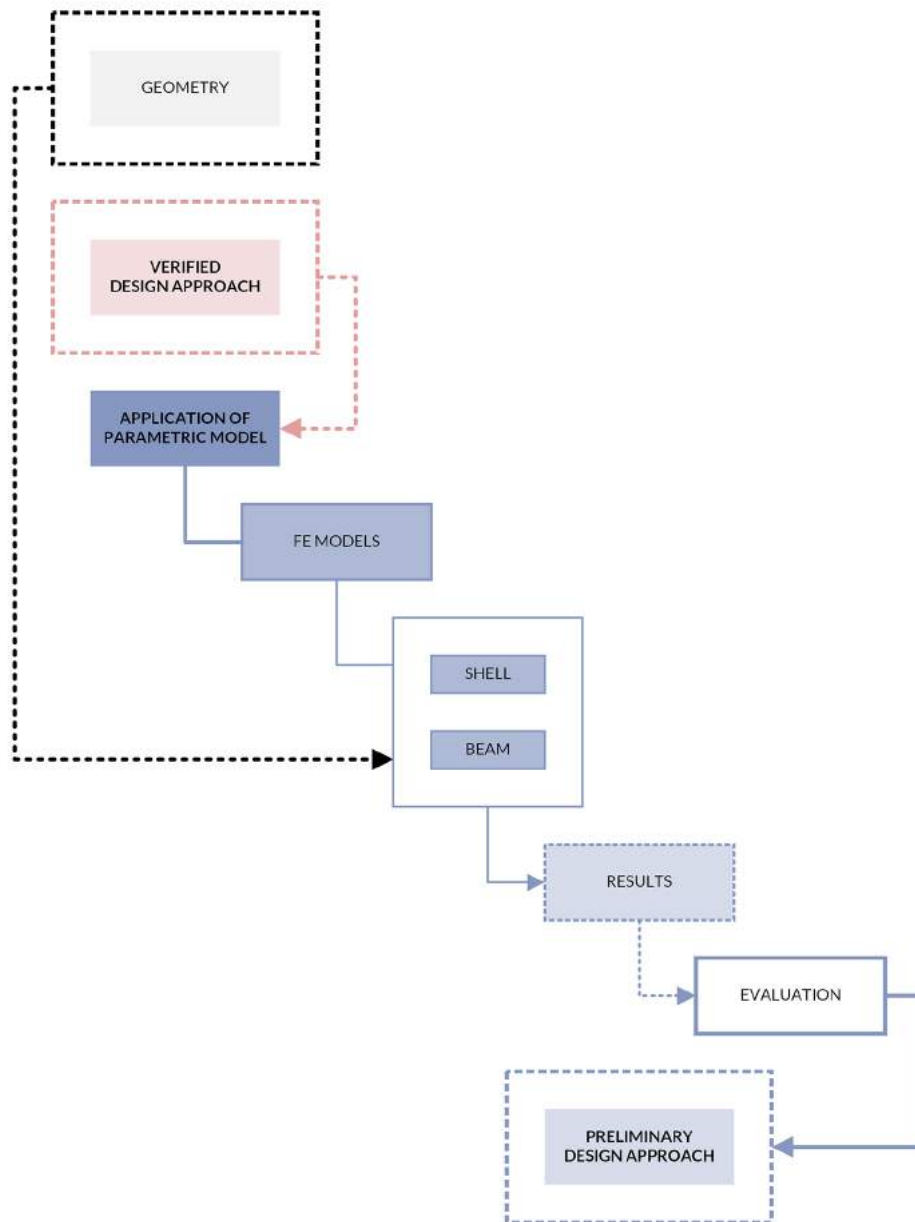


Figure 10.1: Flowchart describing the methodology used for the case studies presented in Chapter 10 - Development of a parametric design and analysis approach.

10.1 Evaluation of FE models for full scale FRP module

The parametric analysis method which was developed and presented in Chapter 8 was applied to a full scale FRP module and evaluated as shown in Figure 10.1. Even though the method has not been verified, see Chapter 9, it is still motivated to apply the method to evaluate if the method is applicable to large scale models, and if the assumptions made up until now also hold for the full scale modules.

10.1.1 Parametric FE model in Grasshopper

A parametric model was developed in Grasshopper and Rhino for the FRP module for QUAD and beam elements, see Figures 10.2 to 10.4.

The material definitions used in the QUAD model have been determined by the FRP module geometry. Here the uni-directional zones have been assigned the CFRP 100 material, see Table 7.1, and the materials in the node zones have been determined based on the topology mesh angle.

In the beam models the same material and cross section have been assigned to all beams in the models, where the shear area factor (see Section 7.4.1) has been determined by the average length of all beams.

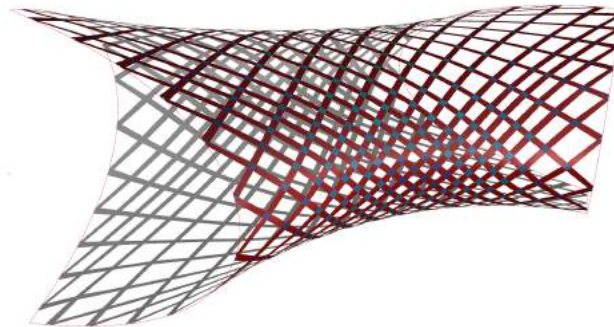


Figure 10.2: Surface model in Rhino which has been generated in Grasshopper for analysis of QUAD elements in SOFiSTiK. Attributes with structural information has been written to the geometric objects, and the colours indicate which material has been applied for the different zones. Here red indicates that it is a uni-directional zone. The materials in the node zones have been determined based on the mesh angle.

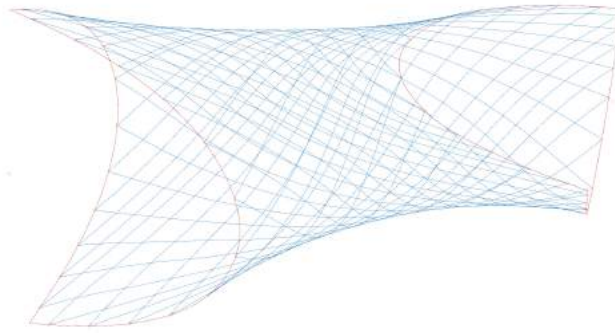


Figure 10.3: Line model in Rhino which has been generated in Grasshopper for analysis of beam elements in SOFiSTiK. Here all beams have been assigned the same materials and cross section.

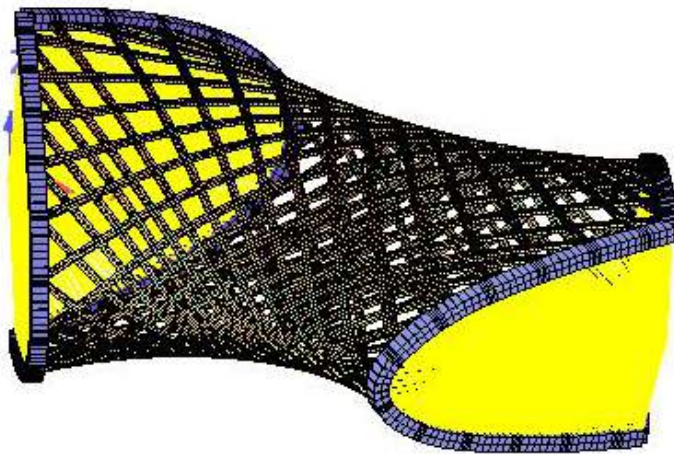


Figure 10.4: SOFiSTiK QUAD model for the FRP module.

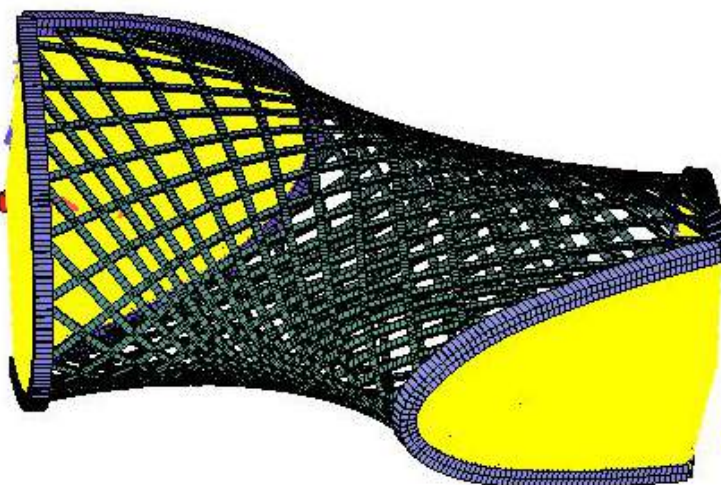
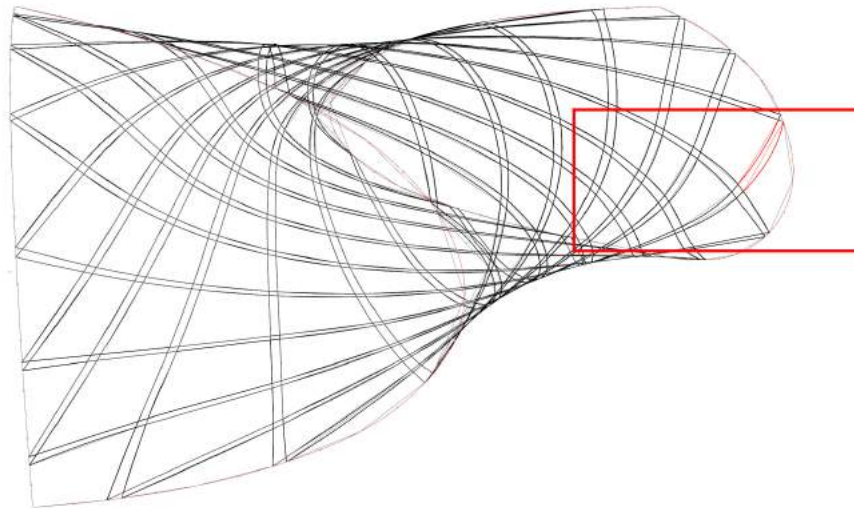


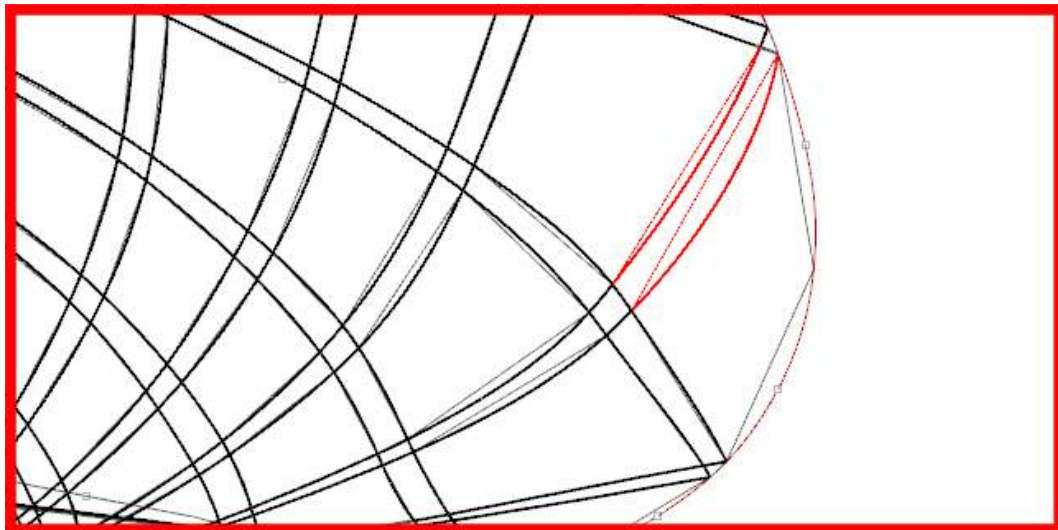
Figure 10.5: SOFiSTiK beam model for the FRP module.

10.1.2 Evaluation of non-planarity of mesh segment

In Chapter 8 the mesh segment was assumed to be planar, however this is not the case in the actual FRP module. A small study was conducted to evaluate the curvature of the FRP module, see Figure 10.6. The mesh was drawn using curved lines as well as straight lines and the two models were overlayed for comparison. It can be seen here that the assumption that the lines defining the mesh are straight, is mostly accurate. In some zones there is a large difference, however this large difference only occurs in modules with very low mesh densities. A mesh defined by straight lines was therefore used in analysis to simplify the model.



(a)



(b)

Figure 10.6: The assumption that the mesh is planar was evaluated by comparing the actual mesh with curved lines to a simplified mesh defined by straight lines. It can be seen here that the two meshes are similar, except in zones with low density and high curvature as in the zone marked in the image.

10.1.3 Evaluation of number of element numbers and mesh dependency

In Chapter 7 a mesh convergence study was conducted for simple QUAD model, and an establish mesh size was used in the case studies presented in Chapters 7 and 8. In the case of the FRP modules there is a larger complexity, especially at the element boundaries. A small convergence study was therefore conducted for the parametric FRP module models.

For the QUAD model of the FRP module the mesh was generated using SOFiSTiK's automatic meshing, where it is possible to adjust the coarseness of the mesh. The mesh was refined and the model analysed step-wise, and here it was seen that the full FRP modules required a finer mesh along the module boundary, in order to reach convergence. The mesh size in remaining areas did however not affect convergence, and the mesh size determined in Chapter 7 was sufficient here. This indicates that the QUAD model is very mesh dependent in the case of the FRP modules and must be adjusted according to the geometry.

The same was done for the beam models, where the models were analysed for an increasing number of subdivisions of the beam elements, and here no significant difference in the results could be observed. This indicates that beams are independent of element subdivision, however it should be noted here that the model was analysed using the same materials and beam cross sections for all elements.

10.1.4 Evaluation of computational times

The meshing and computation times for each model were compared and evaluated, the results can be seen in Table 10.1. Here it can be observed that the QUAD models require significantly longer meshing and computation times compared to the beam models, especially in the case where the mesh density is higher.

Table 10.1: Comparison of number of elements for QUAD and beam model with varying mesh densities

Density	Element number [-]		Meshing time [s]		Calculation time [s]	
	QUAD	Beam	QUAD	Beam	QUAD	Beam
Low	9046	864	9	3	25	17
Medium	17365	3456	44	6	56	25
High	34243	7776	170	9	147	42

10.2 Comparison between QUAD and beam models

The FRP module was analysed, using all three mesh densities, for three different load cases, see Figures 10.7 to 10.9. The module was fixed on one end by coupling the module boundary to a fixed node, see the yellow marking in Figures 10.7 to 10.9. The load was then applied to a node which was coupled to the other boundary edge. The resulting displacements and internal stresses of the QUAD and beam models were compared. The displacements were compared by importing the SOFiSTiK results into Grasshopper. The stresses however were only compared in SOFiSTiK due to the fact that the Grasshopper tools which were used to import the stresses were not optimised for such a large number of elements. No attempt was made to further develop this tool at this point.

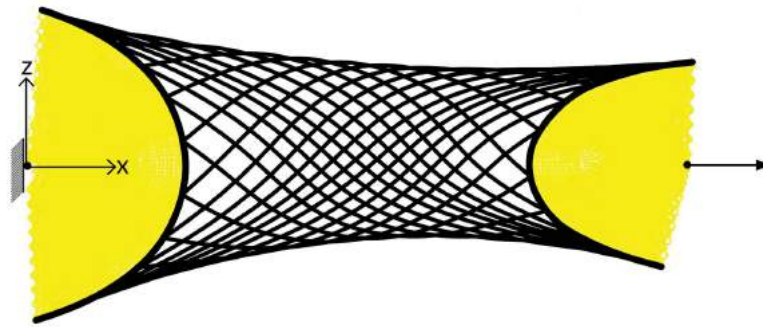


Figure 10.7: Load case 10.2.1. The FRP module was loaded with a normal force of 12 kN.

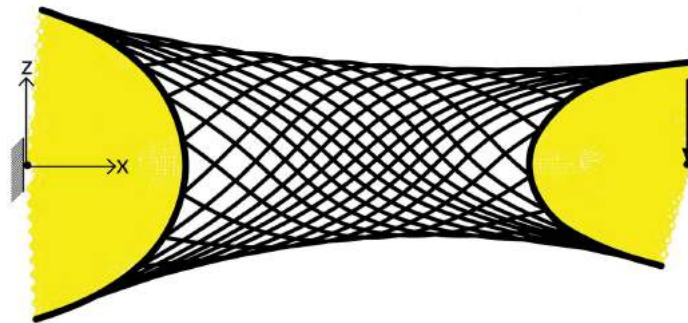


Figure 10.8: Load case 10.2.2. The FRP module was loaded with a force of 1.2 kN.

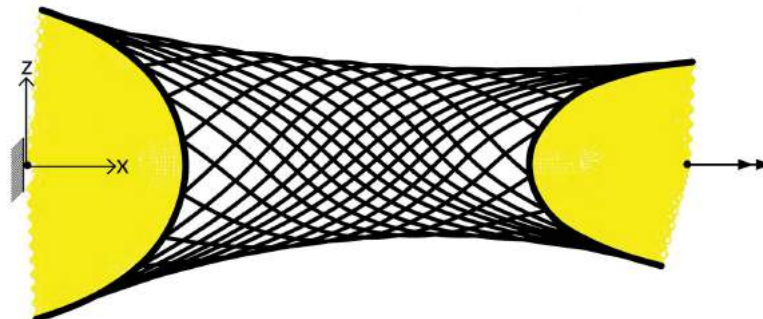


Figure 10.9: Load case 10.2.3. The FRP module was loaded with a moment of 12 kNm.

10.2.1 Comparison of stresses

The stresses were compared in SOFiSTiK's interface for graphical representation of results, Wingraf where it could be that there was a difference in stresses in the two models, mainly at the module boundaries. The QUAD model showed very large stress concentrations at the module boundaries compared to the beam models. It was of interest to evaluate and compare the stress in the elements not directly connected to the boundaries also. In these non-boundary zones the stresses had a better correspondence between the QUAD and beam models. It could be seen that there were stress peaks in the QUAD models in the transition between the uni-directional and node zones, which is expected. In the uni-directional areas the stresses has a good correspondence, as was also seen in Chapters 7 and 8. In Table 10.2 the von Mises stress for each load case are shown for the QUAD and beam models, both for the cases where the module boundaries was considered, and the cases where it was not.

Table 10.2: Maximum von Mises Stress in FRP module for each load case, both with and without consideration to module boundary.

Load case	With boundary [MPa]		Without boundary [MPa]	
	Quad	Beam	Quad	Beam
Load case 10.2.1	60.1	22.1	27.7	18
Load case 10.2.2	17.7	11.1	11.2	11.1
Load case 10.2.3	85.5	39.1	28	21

10.2.2 Comparison of displacements

The maximum displacements for each load case can be seen in Table 10.3. In **Load case 10.2.1** and **Load case 10.2.2** a similar correspondence can be seen as was previously observed in Chapter 8, however in **Load case 10.2.1** there is a much larger difference. The results were imported into Grasshopper and can be seen in Figures 10.10 to 10.12. Here it can be seen again that the overall displacements are similar for tension/compression and bending, however in the case of torsion there is a large overall difference as well as large local differences. Similar results could be seen for the two other mesh densities.

Table 10.3: Comparison of maximum and minimum displacements for **Load case 10.2.1** to **Load case 10.2.3**.

Load case	Displacements [mm]				Comparison [%]	
	QUAD		BEAM		Comparison	
	Min	Max	Min	Max	Min	Max
Load case 10.2.1		0.429		0.376		88%
Load case 10.2.2		1.334		1.166		87%
Load case 10.2.3		0.837		0.252		30%

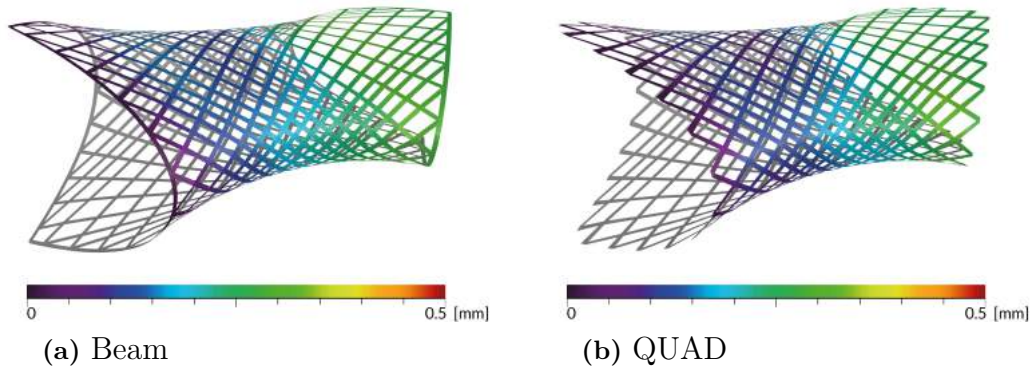


Figure 10.10: Comparison between displacements for load case 10.2.1.

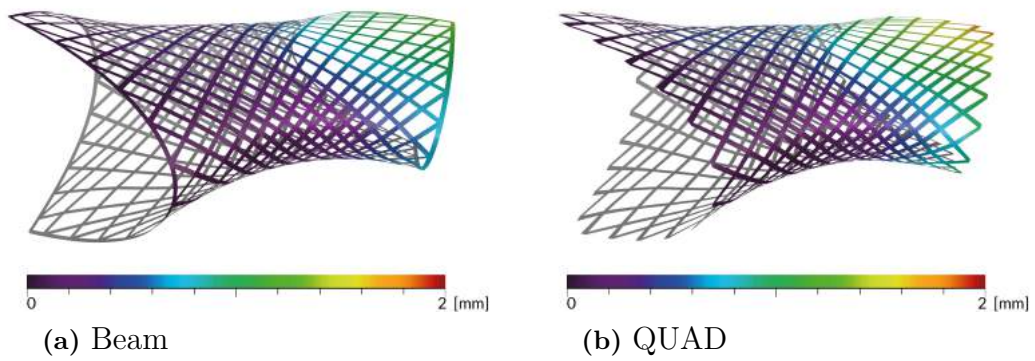


Figure 10.11: Comparison between displacements for load case 10.2.2.

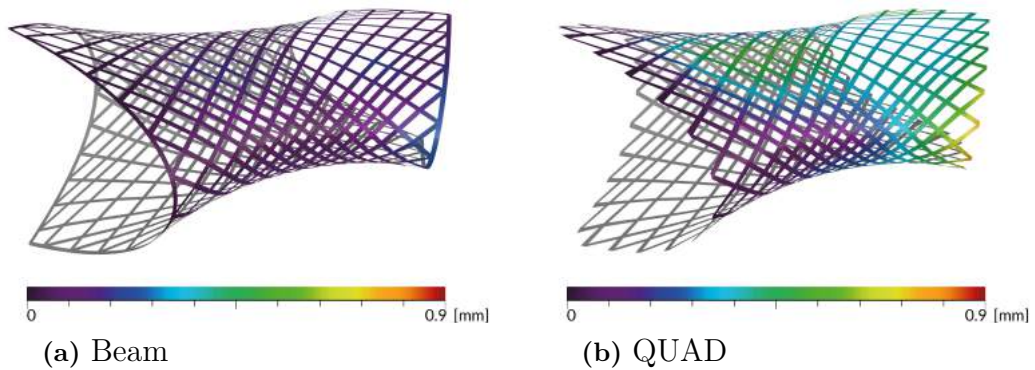


Figure 10.12: Comparison between displacements for load case 10.2.3.

11

DISCUSSION

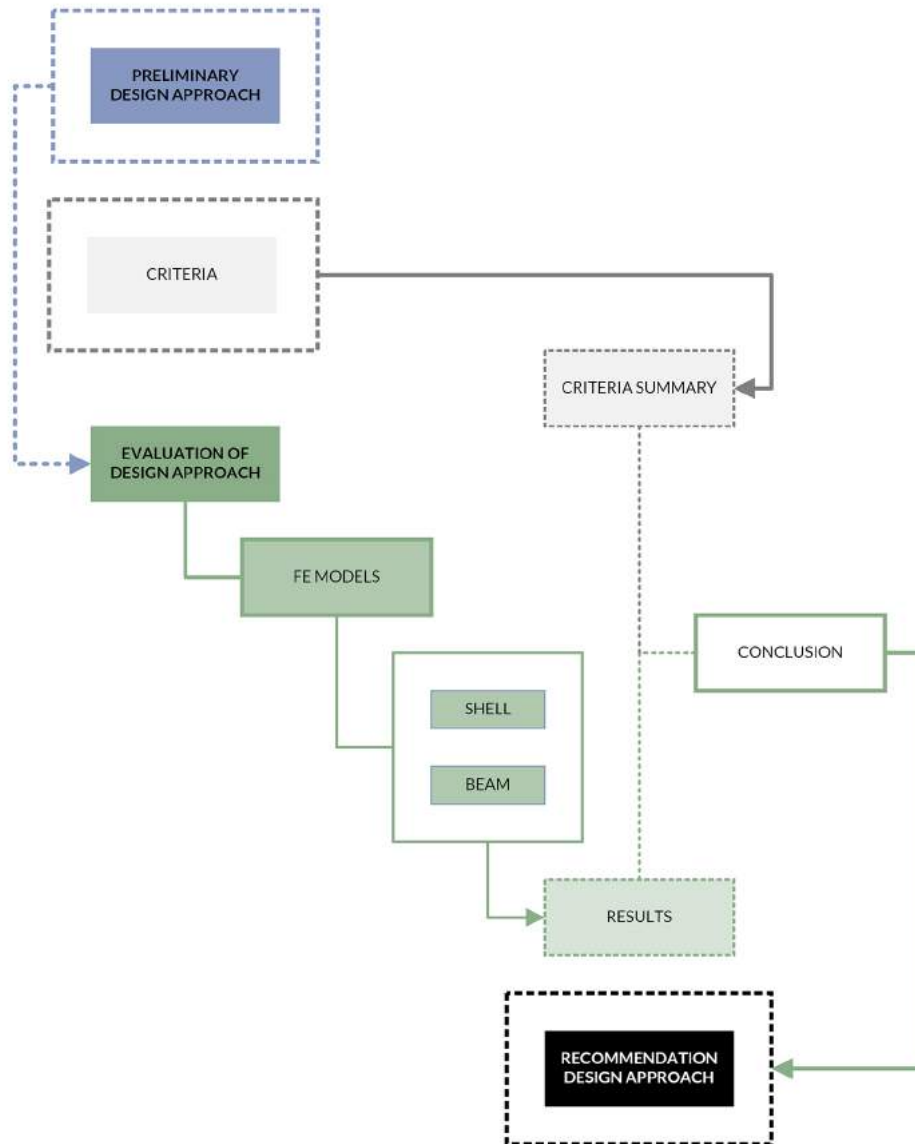


Figure 11.1: Flowchart describing the method for evaluation and comparison of FE models.

11.1 Establishment of design and analysis approach

This study was conducted in order to establish a new design and analysis approach for FRP modules in architectural and civil engineering contexts. The underlying basis for this study has been the research conducted at the University of Stuttgart. In this chapter the basis, scope and limitations, methodology, assumptions and results are discussed in relation to the previous research and the structural engineering context.

11.1.1 Importance of interdisciplinary cooperation

The building industry is far behind other industries when it comes to use of FRP as a structural material. The material has many properties which are interesting in architectural and structural engineering contexts. The ability to engineer the FRP material to exhibit certain structural behaviours can for instance enable the architect to be more expressive in design and achieve shapes and forms which may be difficult to achieve using other materials. This fact has also driven the structural engineer to fully utilise her knowledge in mechanics and structural design in this study, as well as attempt to adopt new strategies and tools.

The research conducted at the University of Stuttgart is a very good example of when interdisciplinary collaboration has led to interesting and important architectural and structural design developments. The method developed at the University of Stuttgart has however not been applicable in this study, which indicates that there is still a need for research and development in this field.

Even though the aim has been derived from a combined architectural and structural background, the main content is technical and has adopted a strategy which may be considered a traditional civil engineering method - a structural analysis approach has been developed based on architectural intent, with little or no freedom in expression in form of the structure, and there has been no interdisciplinary collaboration.

Equally important as it is to develop new strategies for analysis, is it to have a good collaboration between architects and engineers, so that the full potential of the material can be utilised both aesthetically and structurally.

11.1.2 The need for simplification in analysis

Building standards and design codes are essential in the civil engineering context, and as such it is logical that the tools used for building design are well adapted to take these regulations into account. Unfortunately this imposed many limitations in the presented work. Materials which are not defined in these standards and codes, are also not included in SOFiSTiK. Therefore it is difficult to implement FRP materials in analysis in SOFiSTiK. Analysis could very well be carried out in other FE analysis software, however this may not be recommended as there are several more aspects to consider here, other than material definitions. For instance safety factors and load combinations defined in the building codes are very easy to implement in softwares such as SOFiSTiK, which are developed specifically for the building industry.

In this study it was required to use SOFiSTiK. Therefore many aspects of the mechanical behaviour of FRP materials had to be omitted in analysis, such as mechanical coupling or

11. DISCUSSION

inter-laminar stress distributions. Within this context it may be more suited to perform detailed analysis using other analysis methods, based on results from a simplified, but safe-sided, analysis performed in SOFiSTiK. Thus it may very well be motivated to exclude discontinuities and singularities in analysis for preliminary design, if the analysis is safe-sided.

11.1.3 Evaluation of theory and references

Several literature references have been used throughout the work, which have been the basis for assumptions, but also used to evaluate assumptions made in this study.

The major theoretical basis here has been Classical Laminate Theory. In the literature references related to FRP mechanics it is clear that CLT is common practice in analysis of FRP materials. It can be said that it is motivated to use CLT for analysis of FRP composites. In most theory only plate theory is discussed as CLT is derived on the basis of plate theory, little reference or previous research was found for the application of beam theory and FRP materials.

In structural analysis in SOFiSTiK the manuals provided by SOFiSTiK has been used to find information about the theories used in analysis. Some guess work had to be done here, especially in the case of analysis of orthotropic materials. To evaluate the analysis in SOFiSTiK theoretical studies were conducted in MATLAB for evaluation and comparison of the SOFiSTiK analysis.

11.1.4 Evaluation of methodology

The work has been carried out in a logical and step wise manner, as was indicated in Chapter 3, following the logic *input - method - output*. In each step some input has been given or some assumption has been made, this has been followed by structured studies in which the input or assumption has been evaluated. From this some output data has been generated, which in turn has served as input in the next step. In this study where there have been many uncertainties, assumptions and a large numbers of structural models to evaluate, this working method has been very well motivated.

The work has been defined by investigation followed by evaluation and verification. In each step the results have been evaluated and in the cases where results could not be verified, assumptions have been disregarded, or models and methods omitted from the work.

11.2 Evaluation of assumptions and results

The assumptions made here have been made on basis on several literature references, derivations as well as findings in this study. The assumptions have been founded on mechanical principles, with clearly stated simplifications or limitations, and have been evaluated through theoretical studies and analytical and numerical analysis. In Chapter 2.1 a number of hypothesis were also made, these are discussed and evaluated here in relation to the results of this study.

11.2.1 Transverse isotropy

It has been assumed that the material can be simplified in analysis such that a transversely isotropic material formulation could be used. This was evaluated through literature studies, where it was found that the mechanical behaviour of a FRP laminate can be engineered by controlling the components of the \mathbf{A} , \mathbf{B} and \mathbf{D} matrices in the laminate constitutive equation. This can be done by adjusting thickness, lamina orientations and layup sequences of the laminate. Certain laminates will be designed such that these are fully orthotropic laminates, which means they will be transversely isotropic.

The laminates in this study are not designed in such a way that it can be said that they are transversely isotropic by design, however based on the literature studies it was hypothesised that even these laminates it can be said to be transversely isotropic due to the thickness of the laminates. This assumption was also motivated by literature, and verified through theoretical case studies.

A limitation to this assumption is that it neglects the influence of the plate thickness on the overall stiffness. Depending on geometry and theory used in analysis this plate thickness will have an influence. It was seen in the case studies that it may not be entirely motivated to neglect these effects, and this should be further evaluated in future research.

11.2.2 Uni-axial load transfer

It was assumed that the load transfer in the modules is mainly uni-axial and that beam elements can be used in analysis. It was seen in the small models that this was mainly correct, however when applying the method to the actual FRP module significant differences could be seen in the case of torsion and shear. This indicates that there may be multi-axial load transfer in the node zones and significant out-of-plane effects which may not be properly simulated using beam elements. The main limitation of beam elements is the inability to account for plate curvatures. In the case of FRP materials these effects should perhaps not be discounted due to material specific properties for certain layups with for instance large variations in the Major and Minor Poisson's ratios which may very well be above 0.5.

11.2.3 Calibration and verification

It was assumed that the FE method and models could be verified and calibrated against mechanical tests. It has not been possible to verify this assumption since mechanical tests could not be performed within the time frame of the study. In the case studies

11. DISCUSSION

it was observed that mechanical tests for verification and calibration are necessary in order to evaluate the simplifications made. The influence of the node zones in the QUAD models indicate that the simplifications made with regard to the discontinuity and node zones may not be fully motivated. Mechanical test should therefore be performed and the FE models should be adapted accordingly. However in Chapter 9 potential adaptations of the FE models were pointed out with indications on how the parametric models, materials and cross sections can be adapted in a verification and calibration situations. It should therefore be said that the parametric design and analysis method developed here is adaptable and that it is likely that it can be verified and calibrated against mechanical tests.

11.2.4 Applicability of results

It was assumed that results from a simplified global analysis of this FRP module can be used in a detailed design situation. In all evaluated models the correspondence between theory and analysis, as well as the correspondence between QUAD and beams models, can be said to be sufficient, with the exception of shear and torsional deformations and stresses where significant deviations could be seen between the QUAD and beam models.

Overall, and especially in the uni-directional zones, the correspondence was good where the deflections and stress results in the beam analyses were generally larger. This indicated that both methods can be used for analysis of the FRP module in this study, provided that mechanical tests can be performed with necessary adaptations to the parametric models.

11.2.5 Evaluation of tools

Three tools which were used to create structural objects in Grasshopper for analysis in SOFiSTiK were developed in this study. The development of these tools was motivated by the fact that the SOFiSTiK interface with Rhinoceros is not parametric, and there was thus a need for a tool to automate the creation of the structural models in Rhino. The tools were written using C# and implemented in Grasshopper, and could be used to create the structural elements in an easy and direct manner.

Other tools which could be used to evaluate results from structural analysis in SOFiSTiK were also developed, and these were verified by comparing the imported results in Grasshopper with results which could be seen in SOFiSTiK. These tools proved very valuable in comparison of the many models which were analysed, since it made it simple to make direct and qualitative comparison of structural analysis results in a 3D modelling environment. This made it possible to for instance measure deformations directly in the 3D software. The interface in SOFiSTiK which can be used to evaluate results visually does not have the same adaptability or interactivity. Thus in a parametric study where direct comparison of many models were necessary these tools proved to be essential.

11.2.6 Evaluation of parametric FE models

The parametric models were developed in Grasshopper and Rhinoceros with the additional use of C# and third party plugins. The models have been verified against the MATLAB

functions which were used in this study. The author of this thesis was part of the development of these functions as part of a student group project, at Chalmers University of Technology, where these functions were verified in theoretical studies. These functions were therefore considered to be accurate for verification of this study as well, and thus it can be said that the parametric models are also verified.

The parametric models have been applied to a large variety of parametric setups and analyses, this indicated that these fulfil the purpose of this study, in which an adaptable parametric model is required which can be applied to multiple geometries.

11.2.7 Evaluation of parametric design and analysis approach

The parametric design and analysis approach was developed on the basis on many limitations, simplifications and assumptions which have been discussed in this Chapter. The results of the structural analysis has mainly corresponded with the assumptions made, this however only indicates if the assumptions made, and analysis method are equally accurate or equally inaccurate. Verification against mechanical tests still remains. However some results of the analysis give indications of the accuracy or inaccuracy of the parametric analysis approach.

The method has been developed in a civil engineering context, thus it has required several simplifications in order for successful implementation in the context of this study. In the publications related to the research at the University of Stuttgart which were studied here it is stated that the lack of knowledge and suitable analysis tools for FRP composites in the building industry often lead to over-simplified structural analysis models. Here an in-depth study was made to gain sufficient knowledge, however it may be said that the method here has been over-simplified, with regard to geometric and structural complexity.

Some of the results of this study indicates inaccuracies in the assumptions made and the modelling and analysis approach. For instance, the large differences of deflections in the QUAD and beam models, when comparing FRP modules subjected to torsion, indicate that the curvature of the mesh topology should perhaps be taken into account, and that QUAD elements may be more suitable for analysis due to this aspect.

Stress concentrations due to geometric discontinuities and change of stiffness can be better simulated using QUAD elements, however detailed analysis of inter-laminar stress is nevertheless still required. With this in mind it may then be said that results acquired from a simplified analysis using beam elements may be taken as preliminary values for detailed design using analysis tools much more suited for analysis of laminated FRP composites. This can be said especially due to the fact that SOFiSTiK is not suited for this type of analysis, and also due to the fact that QUAD elements are inefficient in analysis due to mesh size dependency as well as long meshing and computational times.

The aim of this study was to develop a simplified, reliable and sufficiently accurate an safe-sided approach for design and analysis of the FRP module studied, and as such it may be said that the method established here fulfils this purpose, however this remains to be verified through mechanical tests.

12

CONCLUSION AND RECOMMENDATIONS

12.1 Concluding remarks

In this study a straight forward to use, simple and reliable parametric design and analysis method has been developed for a specific type of FRP module. Based on the findings and results a number of conclusions can be made for this approach with regard to the aim and scope of this study. It should however be noted that these conclusions are valid for the studied type of FRP module, and only if the design and analysis can be verified and calibrated against mechanical tests.

Global and detailed analysis context

The established design and analysis approach has proven to be applicable in a civil engineering context using SOFiSTiK as an analysis tool.

The QUAD and beam models had very different performance, and it can be said that the QUAD models are not recommended for analysis of large scale models due to long meshing and computation times.

Safe sided approach

It cannot be said whether the results are safe-sided until the method has been verified and calibrated against mechanical tests. The beam models, however, typically showed larger displacements and stresses, and depending on analysis context considerations should be made for this fact.

Applicability of results

The FE model was compared against theoretical case studies, and an overall correspondence could be seen for both the QUAD and beam models. It could therefore be said that the results can be used in a detailed design situation.

Parametric design approach

The parametric tools and models proved stable and reliable. It was also seen that it could be applied to a variety of configurations with satisfactory results.

Calibration

Verification and calibration could not be performed, however it is likely that the parametric design and analysis method can be verified and calibrated due to reliability and adaptability in application, as well as results indicating the both the QUAD and beam material and cross section parameters can be adjusted in analysis to achieve correspondence with desired mechanical behaviours.

12.1.1 Recommendation of parametric design and analysis approach

Assuming that mechanical tests and calibration can be performed it can be said that it may be more suitable to use beam theory rather than plate theory in analysis of the studied FRP module for preliminary design. This is motivated by the fact that the beam models proved to be more efficient than the QUAD models with regard to computational times, as well as due to the similarities between the two modelling approaches.

12.2 Suggestions for future research

In this study some potential limitations and aspects which may be reconsidered has been pointed out. These are listed below and may offer opportunities for continued research within the field of computational mechanics and parametric design for architecture and civil engineering contexts.

Mechanical tests for verification and calibrations

Mechanical tests should be conducted for the studied FRP module, to verify the accuracy of the parametric models. The parametric analysis and design method should be adjusted to correspond to the mechanical tests, and characteristic values for design should be established.

Reconsideration and adaptations of discontinuity and node zones

When the parametric model was applied to the actual FRP module geometry some differences could be observed in the QUAD and beam models, mainly in the case of torsion. This may indicate that there is multi-axial load transfer, and thus the discontinuity and node zones may have to be re-evaluated to account for this.

Extend method to other geometries and topologies

The method has been applied to one type of topology and geometry, however the method may for instance also be adapted for triangulated mesh topologies where the load transfer is mainly uni-axial.

Engineered materials for structural and architectural optimisation

One topic studied here was the in- and out-of-plane mechanical coupling which is a material property in FRP which can be design. Thus the material can be engineered to deform, or carry load in a certain way. This can be interesting in architectural and structural applications where form-finding or expressive shapes may be of interest.

Fatigue and failure and instability phenomena

No consideration for fatigue or failure, nor instability, was taken into account in this study, however it may be of interest to study this in the case of this FRP module. Due to distinctive unidirectional zones buckling tendencies may be especially important to study.

Structural analysis and dedicated manufacturing

In this study a specific FRP module was studied, and the structural analysis was dictated by the assumed laminate layup in the node zones. In many applications where FRP composites are used dedicated structural analyses and manufacturing methods have been developed for specific purposed. This may be of interest in architectural and civil engineering contexts where standardisation is of high importance. Development of dedicated design and manufacturing methods may enable more use of FRP composites in these contexts.

BIBLIOGRAPHY

- [1] M. Legault, "Architectural composites: Rising to new challenges," 2018.
[Online] Available: <https://www.compositesworld.com/articles/architectural-composites-rising-to-new-challenges>, Accessed on May 05, 2018.
- [2] F. Waimer, R. La Magna, S. Reichert, T. Schwinn, A. Menges, and J. Knippers, "Integrated design methods for the simulation of fibre-based structures," 09 2013. Proceedings of the Conference: Design Modelling Symposium, 2013. [Online]. Available: https://www.researchgate.net/publication/292745702_Integrated_design_methods_for_the_simulation_of_fibre-based_structures, Accessed on: May 5, 2018.
- [3] J. Hale, "Boeing 787 from the ground up." Aero, pp. 17-24, 2006 [Online]. Available: http://www.boeing.com/commercial/aeromagazine/articles/qtr_4_06/index.html Accessed on: May 05, 2018.
- [4] Wikimedia contributor Spaceaero2, "All nippon airways boeing 787-8 (ja801a) land at okayama airport, 2011." [Electronic image]. Available: https://commons.wikimedia.org/wiki/File:All_Nippon_Airways_Boeing_787-8_Dreamliner_JA801A_OKJ.jpg, Accessed on: May 05, 2018.
- [5] Creative Commons , "Attribution-ShareAlike 3.0 Unported (CC BY-SA 3.0)". [Online]. Available: <https://creativecommons.org/licenses/by-sa/3.0/deed.en>, Accessed on June 8, 2018.
- [6] L. Ascione, J.-F. Caron, P. Godonou, K. van Ijsele, J. Knippers, T. Mottram, M. Oppe, M. Gantier, S. Sorensen, J. Taby, and L. Tromp, "Prospect for new guidance in the design of frp," 2016. Publications Office of the European Union, Luxembourg, EUR 27666 EN-2016. [Online]. Available: <http://publications.jrc.ec.europa.eu/repository/handle/JRC99714>, Accessed on: May 16, 2018.
- [7] E. Joint Research Centre (JRC), "Cen/tc250 produces the en eurocodes," 2018. [Online] Available: <http://eurocodes.jrc.ec.europa.eu/showpage.php?id=23>, Accessed on May 05, 2018.
- [8] San Francisco Museum of Modern Art, SFMOMA, "Architecture," 2018. [Electronic image] Available: <https://www.sfmoma.org/about/our-expansion-2016/architecture/>, Accessed on June 08, 2018.
- [9] San Francisco Museum of Modern Art, SFMOMA, "San francisco museum of

- modern art, architectural fact sheet,” 2018. [Electronic document] Available: <https://www.sfmoma.org/about/our-expansion-2016/architecture/>, Accessed on June 08, 2018.
- [10] D. Prado, M., J. M., Solly, A. Menges, and J. Knippers, “Elytra filament pavilion: Robotic filament winding for structural composite building systems, in fabricate rethinking design and construction,” 2017. Proceedings of the Fabricate Conference, 2017. pp. 224-233. [Online]. Available: <https://www.ucl.ac.uk/bartlett/architecture/events/2017/apr/fabricate-2017-international-peer-reviewed-conference-and-publication>, Accessed on: May 5, 2018.
- [11] ICD/ITKE, “Research pavillion process photo, 2014.” [Electronic image]. Available: <http://www.itke.uni-stuttgart.de/archives/portfolio-type/icd-itke-research-pavilion-2013-14>, Accessed on: May 05, 2018.
- [12] ICD/ITKE, “Research pavilion process photo, 2014.” [Electronic image]. Available: <http://www.itke.uni-stuttgart.de/archives/portfolio-type/icd-itke-research-pavilion-2013-14>, Accessed on: May 05, 2018.
- [13] ICD/ITKE, “Research pavilion process photo, 2015.” [Electronic image]. Available: <http://www.itke.uni-stuttgart.de/archives/portfolio-type/icditke-research-pavilion-2014-15>, Accessed on: May 05, 2018.
- [14] ICD/ITKE, “Research pavilion process photo, 2015.” [Electronic image]. Available: <http://www.itke.uni-stuttgart.de/archives/portfolio-type/icditke-research-pavilion-2014-15>, Accessed on: May 05, 2018.
- [15] S. Reichert, T. Schwinn, R. L. Magna, F. Waimer, J. Knippers, and A. Menges, “Fibrous structures: An integrative approach to design computation, simulation and fabrication for lightweight, glass and carbon fibre composite structures in architecture based on biomimetic design principles,” *Computer-Aided Design*, vol. 52, pp. 27 – 39, 2014. [Online]. Available: <http://www.sciencedirect.com/science/article/pii/S0010448514000293> . Accessed on May 05, 2018.
- [16] ICD/ITKE, “Development process, research pavilion 2014.” [Electronic image]. Available: <https://www.itke.uni-stuttgart.de/archives/portfolio-type/icd-itke-research-pavilion-2013-14>, Accessed on: June 08, 2018.
- [17] SSIGRAFIL®Continuous Carbon Fiber Tow, Meitingen, Germany. SGL Technologies GmbH, 2018. [Online]. Available: https://www.sglgroup.com/cms/international/infokorb/Downloadcenter/index.html?__locale=en, Accessed on: May 16, 2018.
- [18] SIGRAPREG®Pre-impregnated Materials made from Carbon, Glass and Aramid Fibers, Meitingen, Germany. SGL Technologies GmbH, 2018. [Online]. Available: https://www.sglgroup.com/cms/international/infokorb/Downloadcenter/index.html?__locale=en, Accessed on: May 16, 2018.
- [19] B. D. Agarwal, L. J. Broutman, and K. Chanddrashekhara, *Analysis and Performance of Fibre Composites*. Hoboken, New Jersey, USA: John Wiley & Sons, Inc., 2006. Third Edition.

- [20] I. Krucinska and T. Stypka, "Direct measurement of the axial poisson's ratio of single carbon fibres," *Composites Science and Technology*, vol. 41, no. 1, pp. 1 – 12, 1991. [Online]. Available: <http://www.sciencedirect.com/science/article/pii/026635389190049U>, Accessed on: May 16, 2018.
- [21] H. Lundh, *Grundläggande hållfasthetslära*. Stockholm, Sweden: KTH, Hållfasthetslära, 2013.
- [22] W. Jabi, *Parametric Design for Architecture*. London, England: Laurence King publ, 2013.
- [23] J. Frazer, "Parametric computation: History and future," *Architectural Design*, vol. 86, no. 2, pp. 18–23, 2016. [Online]. Available: <https://onlinelibrary.wiley.com/doi/pdf/10.1002/ad.2019>, Accessed on: May 31, 2018.
- [24] Rhinoceros 3D, "Rhino 5, version 5 sr12 64-bit," 2017. [Software]. Available: <https://www.rhino3d.com/>, Accessed on May 05, 2018.
- [25] Grasshopper, "Grasshopper, version 0.9.0076," 2017. [Software]. Available: <http://www.grasshopper3d.com/>, Accessed on May 05, 2018.
- [26] SOFiSTiK AG, "Sofistik rhinoceros interface." [Online] Available: <https://www.sofistik.eu/solutions/structural-fea/rhinoceros-interface/>, Accessed on May 31, 2018.
- [27] A. Heumann, "Human + tree frog," 2018. [Software]. Available: <http://www.food4rhino.com/app/human>, Accessed on: May 05, 2018.
- [28] G. Piacentino, "Weaverbird - topological mesh editor." [Software]. Available: <http://www.giuliopiacentino.com/weaverbird/>, Accessed on: May 05, 2018.
- [29] J. Schumacher, "TT toolbox 1.9," 2017. [Software]. Available: <http://www.food4rhino.com/app/tt-toolbox>, Accessed on: May 05, 2018.
- [30] N. Miller, "Lunchbox 2017.8.1," 2017. [Software]. Available: <http://www.food4rhino.com/app/lunchbox>, Accessed on: May 05, 2018.
- [31] H. Närhi, "Color a mesh," 2018. [Software]. Available: <http://www.food4rhino.com/app/color-mesh>, Accessed on: May 05, 2018.
- [32] Microsoft, "C# programming guide," 2017. [Electronic]. Available: <https://docs.microsoft.com/en-us/dotnet/csharp/tour-of-csharp/index>, Accessed on: May 31, 2018.
- [33] Microsoft, "Visual studio 2015," 2015. [Software]. Available: <https://www.visualstudio.com/>, Accessed on: May 31, 2018.
- [34] McNeel, "Grasshopper assembly for v5," 2017. [Electronic resource]. Available: <https://marketplace.visualstudio.com/items?itemName=McNeel.GrasshopperAssemblyforv5>, Accessed on: May 31, 2018.
- [35] SOFiSTiK AG, "Sofistik 2016, version 16.13 -33_64 servicepack: 2016 - 13," 2017. [Software]. Available: <https://www.sofistik.com/>, Accessed on May 05, 2018.
- [36] SOFiSTiK AG, "Cadinp - text based input," 2017. [Online]. Available: https://www.sofistik.eu/no_cache/solutions/structural-fea/cadinp/.

- [37] SOFiSTiK AG, “Wingraf, version 18.13-33,” 2018. [Online]. Available: <https://www.sofistik.de/documentation/2018/en/tutorials/listoftutorials/general-workflows/wingraf.html>, Accessed on June 06, 2018.
- [38] Mathworks, “Matlab r2014a,” 2017. [Software]. Available: <https://www.mathworks.com>, Accessed on May 05, 2018.
- [39] H. Närhi and M. Stadler, “Computer assignment 1 - stress analysis of thermomechanically loaded laminate,” 2016. Project in TME240 Composite Mechanics, Unpublished.
- [40] C. York and P. Weaver, “Balanced and symmetric laminates: new perspectives on an old design rule, in 51st aiaa/asme/asce/ahs/asc structures, structural dynamics, and materials conference,” 2010. [Online]. Available: <https://arc.aiaa.org/doi/abs/10.2514/6.2010-2775>, Accessed on: May 16, 2018.
- [41] E. Valot and P. Vannucci, “Some exact solutions for fully orthotropic laminates,” *Composite Structures*, vol. 69, no. 2, pp. 157 – 166, 2005. [Online] Available: <http://www.sciencedirect.com/science/article/pii/S0263822304002144>, Accessed on: May 16, 2018.
- [42] C. York, “Stacking sequences for extensionally isotropic, fully isotropic and quasi-homogeneous orthotropic laminates,” Apr 2008. Proceedings of the Conference: 49th AIAA/ASME/ASCE/AHS/ASC Structures, Structural Dynamics and Materials Conference, Schaumburg, IL, USA. [Online]. Available: <http://eprints.gla.ac.uk/4526/>, Accessed on: May 15, 2018.
- [43] AQUA, Materials and Cross Sections, AQUA Manual 2016:14. SOFiSTiK AG, Oberschleissheim, Germany, 2016.
- [44] T. C. T. Ting and T. Chen, “Poisson’s ratio for anisotropic elastic materials can have no bounds,” *The Quarterly Journal of Mechanics and Applied Mathematics*, vol. 58, no. 1, pp. 73–82, 2005. Accessed on: May 16, 2018.
- [45] AQB, Design of Cross Sections, AQUA Manual 2016:14. SOFiSTiK AG, Oberschleissheim, Germany, 2016.
- [46] K.-J. Schneider and K. Berner, *Bautabellen für Ingenieure, mit berechnungshinweisen und Beispielen*. Köln, Germany: Bundesanzeiger Verlag GmbH, 2016. 22nd Edition.
- [47] ASE, General Static Analysis of Finite Element Structures, ASE Manual 2016:12. SOFiSTiK AG, Oberschleissheim, Germany, 2016.

List of Figures

1.1	Nearly half of the air frame of the Boeing 787 consists of carbon fibre reinforced plastics and other composites [3]. From [4]. Reproduced with permission, CC-BY-SA 3.0 [5].	2
1.2	Examples of existing structures in Europe where FRP composites have been used as structural materials [6].	3
1.4	ICD/ITKE Research pavilions photos and development process.	4
1.6	Principal geometry, topology and layout of uni-directional fibre bundles of the proposed FRP module.	6
1.7	Discontinuity of the node zones.	7
1.8	Principal geometry and fibre layout of different types of nodes.	7
3.1	Flowchart describing the method and report outline.	17
3.2	Flowchart describing the method and report outline.	19
4.2	Definition of topology for FRP module.	25
4.3	Terminology for the FRP module topology.	26
4.4	FRP module mesh density.	26
4.6	Local reference coordinate systems for the uni-directional elements (left) and the node zones (right). The orientation of the coordinate axes has been chosen based on the conventions used Classical Laminate Theory, see Chapter 5 - <i>Theoretical background</i>	27
5.1	Principal cross sections of uni-directional fibre composites.	34
5.2	Principal representation of a uni-directional fibre composite.	35
5.3	Specially and generally orthotropic laminae.	38
5.4	Description of a FRP laminate and terminology	40
5.5	A laminate with orientation code $[0\backslash 90\backslash +45\backslash -45\backslash +45\backslash -45\backslash 90\backslash 0]$. Adapted from Figure A3-1 [19, pg. 543].	41
5.6	Strain and strain variation in a principal FRP laminate.	41
5.7	Deformation of a laminate.	42
5.8	FRP laminate which is coupled with regard to in-plane extension and shear.	45
5.9	FRP laminate which is coupled with regard to in-plane extension and out-of-plane bending	45
5.10	A symmetric laminate.	46
5.11	A balanced laminate.	47
6.1	Flowchart describing the methodology used for the case studies presented in Chapter 6 - Material parameters for structural analysis.	52
6.2	Symmetric and balanced laminates studied in MATLAB.	54
6.3	Engineering constants for FRP laminae as a function of the volume fraction, V_f	55
6.4	The calculated ratio $\bar{Q}_{16,rel}$, for $\pm 30^\circ$ and $\pm 45^\circ$ lamina orientations. . . .	56
6.5	The calculated ratio $\bar{Q}_{\pm\theta,rel}$, for $\pm 30^\circ$ and $\pm 45^\circ$ lamina orientations. . . .	57
6.6	Components of the extensional stiffness matrix, \mathbf{A} , for a thin symmetric laminates with varying ply orientations.	59

LIST OF FIGURES

6.7	Components of the extensional stiffness matrix, \mathbf{A} , for a symmetric laminate with lamina orientations $\pm 30^\circ$ for an increasing number of plies.	59
6.9	Components of the coupling stiffness matrix, \mathbf{B} , for a thin balanced laminates with varying ply orientations.	60
6.10	Components of the coupling stiffness matrix, \mathbf{B} , for a balanced laminate with lamina orientations $\pm 30^\circ$ for an increasing number of plies.	60
6.12	Equivalent orthotropic elastic moduli derived for a 10 mm thick symmetric laminate with varying lamina orientations.	65
6.13	Equivalent orthotropic Poisson's ratio derived for a 10 mm thick symmetric laminate with varying lamina orientations.	65
6.14	Strains for different laminates with 10 millimeter thickness subjected to a load N_1	67
7.1	Flowchart describing the methodology used for the case studies presented in Chapter 7 - Material parameters for FE analysis.	70
7.2	Definition of parametric model used for QUAD models.	71
7.3	Parametric FE QUAD model in SOFiSTiK.	71
7.4	Definition of parametric model used for beam models.	72
7.5	Parametric FE beam model in SOFiSTiK.	72
7.6	The error "447" will occur during analysis in SOFiSTiK if the relation in Equation 7.1 is not fulfilled.	73
7.7	Diagrams showing the relation between the Poisson's ratios calculated for fully orthotropic laminates in Chapter 6 and the adaptations required for analysis in SOFiSTiK.	74
7.10	Mesh convergence study in SOFiSTiK for a rectangular plate.	76
7.11	Load cases used in QUAD case studies.	77
7.14	Displacement plots for axial strains, for CFRP 130.	80
7.15	Displacement plots for plate curvatures, for CFRP 130.	80
7.16	Displacement plots for shear strain and curvature, for CFRP 130.	80
7.17	Stress plot, showing small stress variations, for plate subjected to shear bending.	81
7.18	Stresses in bottom plane of QUAD element for the material CFRP 130.	82
7.19	Stresses in bottom plane of QUAD element for the material CFRP 130.	82
7.20	Stresses in bottom plane of QUAD element for the material CFRP 130.	82
7.21	Stresses in centre plane of QUAD element for the material CFRP 130.	83
7.22	Stresses in centre plane of QUAD element for the material CFRP 130.	83
7.23	Stresses in centre plane of QUAD element for the material CFRP 130.	83
7.24	Stresses in top plane of QUAD element for the material CFRP 130.	84
7.25	Stresses in top plane of QUAD element for the material CFRP 130.	84
7.26	Stresses in top plane of QUAD element for the material CFRP 130.	84
7.27	Loads applied in Load case 7.4.1 to Load case 7.4.4	88
7.28	Comparison of maximum displacements in the x direction for QUAD and beam elements, with cross section dimensions 20×10 mm and 100mm lengths for Load case 7.4.1	89
7.29	Comparison of maximum displacements in the y direction for QUAD and beam elements, with cross section dimensions 20×10 mm and 100mm lengths for Load case 7.4.4	89

7.30	Comparison of maximum displacements in the z direction for QUAD and beam elements, with cross section dimensions 20×10 mm and 100mm lengths for Load case 7.4.3	90
7.31	Comparison of maximum displacements in y direction QUAD and beam elements with adapted shear deformation areas for Load case 7.4.4 . .	90
7.32	Comparison of maximum displacements in the x direction for QUAD and beam elements, with cross section dimensions 20×10 mm and 200mm lengths for Load case 7.4.1	91
7.33	Comparison of maximum displacements in the y direction for QUAD and beam elements, with cross section dimensions 20×10 mm and 200mm lengths for Load case 7.4.4	91
7.34	Comparison of maximum displacements in the z direction for QUAD and beam elements, with cross section dimensions 20×10 mm and 200mm lengths for Load case 7.4.3	92
7.35	Comparison of displacements for Load case 7.4.1	92
7.36	Comparison of displacements for Load case 7.4.2	92
7.37	Comparison of displacements for Load case 7.4.3	92
7.38	Comparison of displacements for Load case 7.4.4	92
8.1	Flowchart describing the methodology used for the case studies presented in Chapter 8 - Development of a parametric design and analysis approach.	98
8.2	Principal illustration of the parametric model developed for a mesh segment.	99
8.6	Load case 8.2.1	102
8.7	Load case 8.2.2	102
8.8	Load case 8.2.3	102
9.1	Flowchart describing the methodology used for the case studies presented in Chapter 9 - Verification of the proposed parametric design and analysis approach.	108
10.1	Flowchart describing the methodology used for the case studies presented in Chapter 10 - Development of a parametric design and analysis approach.	112
10.2	Surface model in Rhino which has been generated in Grasshopper for analysis of QUAD elements in SOFiSTiK.	113
10.3	Line model in Rhino which has been generated in Grasshopper for analysis of beam elements in SOFiSTiK.	114
10.6	The assumption that the mesh is planar was evaluated by comparing the actual mesh with curved lines to a simplified mesh defined by straight lines.	115
11.1	Flowchart describing the method for evaluation and comparison of FE models.	122
A.1	Grasshopper components which are connected by wires.	A3
B.2	An overview of the Grasshopper routines used for evaluation of results from the case studies conducted in this study.	B3

LIST OF FIGURES

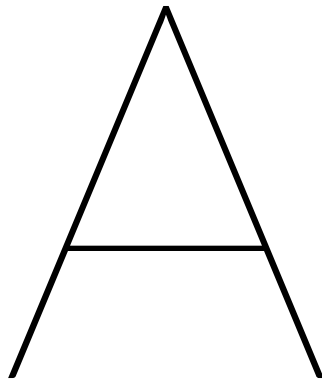
B.1	Parametric Grasshopper definition. The three types of models which were created for this study can be seen here, as well as the part where results from SOFiSTiK was imported. Note that the wires which connect the components have been hidden to give a clear overview of the Grasshopper definition.	B4
B.3	MakeSPT Grasshopper component.	B5
B.4	MakeSLN Grasshopper component.	B6
B.5	MakeSAR Grasshopper component.	B7

List of Tables

4.1	Cross section parameters.	28
4.2	Material properties of fibres	28
4.3	Material properties of matrix.	28
6.1	The calculated values for $\bar{Q}_{16,rel}$, which compares the \bar{Q}_{16} term of the \bar{Q} matrix for all lamina orientations and volume fractions, to the overall maximum \bar{Q}_{16}	56
6.2	The calculated values for $\bar{Q}_{\pm\theta,rel}$, which compares the \bar{Q}_{16} and \bar{Q}_{11} terms of the \bar{Q} matrix for each lamina orientation and fibre volume fraction. . .	57
6.3	Thin laminates with lamina orientations $\pm 0^\circ \leq \theta \leq \pm 45^\circ$	58
6.4	Thick laminates with lamina orientations $\pm 30^\circ$ and $\pm 45^\circ$	58
6.5	Thin and thick symmetric and balanced laminate layups. These laminates were studied for lamina orientations $\pm 30^\circ$ and $\pm 45^\circ$	61
6.6	Strains for a 10 mm thick symmetric laminate ($\epsilon_1, \epsilon_2, \gamma_{12}$) compared to the strains ($\epsilon'_1, \epsilon'_2, \gamma'_{12}$) for a 1 mm thick symmetric laminate subjected to a uniform load N_1 and N'_1 respectively.	63
6.7	Curvatures for a 10 mm thick balanced laminate ($\kappa_1, \kappa_2, \kappa_{12}$) compared to the curvatures ($\kappa'_1, \kappa'_2, \kappa'_{12}$) for a 10 mm thick symmetric laminate subjected to a uniform load N_{12} and N'_{12} respectively.	63
6.8	Derived engineering constants for a 10 mm thick symmetric laminate with varying lamina orientations.	64
6.9	Thin and thick fully orthotropic laminates studied with equivalent orthotropic material parameters derived for lamina orientations $\pm 0^\circ$ to $\pm 45^\circ$	66
7.1	SOFiSTiK material parameters for QUAD elements.	75
7.2	Applied strains and curvatures in loadcases 7.3.1 to 7.3.6	78
7.3	Resulting strains and stresses in MATLAB and SOFiSTiK for Load case 7.3.1	85
7.4	Resulting strains and stresses in MATLAB and SOFiSTiK for Load case 7.3.2	85
7.5	Resulting strains and stresses in MATLAB and SOFiSTiK for Load case 7.3.3	86
7.6	Resulting curvatures and stress in MATLAB and SOFiSTiK for Load case 7.3.4	86
7.7	Resulting curvatures and stress in MATLAB and SOFiSTiK for Load case 7.3.5	87
7.8	Resulting curvatures and stress in MATLAB and SOFiSTiK for Load case 7.3.6	87
7.9	Beam dimensions used in FE material case studies.	88
7.10	Loads applied in Load case 7.4.1 to Load case 7.4.4	88
7.11	Normal and shear stresses, σ_x and τ_{xy} , in QUAD and beam models for Load case 7.4.1 to Load case 7.4.4	95
8.1	Parameters used in comparison between QUAD and beam models	102
8.2	Load cases used for comparison between QUAD and beam models for a mesh topology segment.	103

LIST OF TABLES

8.3	Comparison of maximum and minimum displacements [mm] for Load case 8.2.1 to Load case 8.2.3.	103
8.4	Normal and shear stresses, σ_x and τ_{xy} , in QUAD and beam models. . . .	104
10.1	Comparison of number of elements for QUAD and beam model with varying mesh densities	116
10.2	Maximum von Mises Stress in FRP module for each load case, both with and without consideration to module boundary.	118
10.3	Comparison of maximum and minimum displacements for Load case 10.2.1 to Load case 10.2.3.	118
A.1	Laminate variations of FRP module	A1



EXPLANATIONS AND DEFINITIONS

APPENDIX A - CONTENTS

A.1	Additional descriptions of FRP module	A1
A.1.1	Laminate layup in node zones	A1
A.2	Explanations of 3D modelling and programming terms	A2
A.2.1	3D modelling terminology	A2
A.2.2	Grasshopper terminology	A3
A.2.3	Programming terminology	A4
A.3	Additional theory	A5
A.3.1	Stiffness and compliance matrices for FRP composites	A5
A.3.2	Transformation matrices	A7
Appendix A	- References	A8

A.1 Additional descriptions of FRP module

In this section additional descriptions of the FRP module is presented.

A.1.1 Laminate layup in node zones

The laminate layup of the node zones in the FRP module is assumed to be either symmetric or balanced (angle-ply), with a total thickness of 10 or 15 mm. The thickness of the individual laminae are assumed to be approximately 0.1 or 0.3 mm. Thus a total of eight variations of laminates can be constructed, see Table A.1. The layups are either balanced or symmetric with alternating lamina orientations, meaning the layup sequence pattern will be $[\theta \backslash -\theta \backslash \theta \backslash -\theta \backslash \dots]$. For symmetric laminates this layup sequence can be denoted as $[\pm\theta \backslash -\theta]_s$, and for balanced the layup sequence can be denoted as $[\pm\theta]$

Table A.1: Laminate variations of FRP module

Laminate type	Thickness [mm]		Count [-]
	Laminate	Lamina	Layers
Symmetric	10	≈ 0.1	101
Symmetric	10	≈ 0.3	33
Symmetric	15	≈ 0.1	151
Symmetric	15	≈ 0.3	51
Balanced	10	≈ 0.1	100
Balanced	10	≈ 0.3	32
Balanced	15	≈ 0.1	150
Balanced	15	≈ 0.3	50

A.2 Explanations of 3D modelling and programming terms

Terms related to 3D modelling and programming, which have been used throughout the report are described in this appendix. Some aspects which could be important to consider in relation to parametric modelling and analysis are also mentioned here.

A.2.1 3D modelling terminology

In this section some terms which are commonly used in 3D modelling, especially in the Rhino and Grasshopper environments, will be briefly explained.

NURBs

Non-Uniform Rational B-Spline, NURBs, are mathematical representations of 2D or 3D geometry, which are defined by a degree, control points and knots [48]. These geometries are very accurate and can be used to describe complex and free form geometries using only little information. Benefits of NURBs geometries are that they are easy to define, easy to change and that they have high accuracy. Downsides of NURBs geometries could be that the format is not very compact, meaning it uses a lot of storage space when storing data [49]. This can become an issue when a mesh geometry has been converted to a NURBs geometry, or for instance when the NURBs geometry is defined by a large number of control points.

Polygon mesh

Polygon meshes is a collection of 2D and 3D surfaces [49]. These surfaces are called mesh facets, and in Rhino these have either three or four edges. The corner points of these facets are called vertices. To represent a smooth and complex geometry many facets and vertices would therefore be required.

One benefit of converting a NURBs surface into a mesh is that a mesh format is more compact than a NURBs surface, meaning it can store much more data in an efficient manner. However since NURBs geometries are mathematically defined these are much better suited for representing smooth or complex geometries, since a mesh geometry would require a large amount of polygon faces to represent a smooth complex surface.

In cases where it is important to have smooth surfaces which are easily editable NURBs geometries are much better suited, however in cases where geometric tolerances and geometric complexity is of less importance meshes may be much more suited with regard to computational performance.

Geometric tolerances

In Rhino geometric tolerances can be set to define how much accuracy is required, or how much error is allowed [50]. Even though Rhino is NURBs modelling software it is still not 100% correct, and thus tolerances must be considered.

In this study geometric tolerances have been an important aspect, since it is necessary to ensure that structural lines, points and areas are properly intersecting. Since the structural analysis is conducted using FE analysis, which is a numerical approximation, it is very important to ensure that the geometric tolerance set in Rhino is set to the same geometric tolerance used when defining the topology mesh.

In a parametric model directions and orientations are often described by relating one geometry to an other, and sometimes new geometry is defined by Boolean intersections. Here it can be preferred to use meshes since these are more memory efficient. And in the case of Boolean intersections it is also important to set the tolerances correctly since these operations are always approximated in Rhino. [50]

A.2.2 Grasshopper terminology

Grasshopper is a graphical programming interface for Rhino [51]. Below is a brief description of terms which are commonly used in this contexts.

Component

The Grasshopper components can be described like building blocks [52]. Each component typically takes some input, performs an action and generates an output. The inputs and outputs of a component can be connected to other components by using wires, see Figure A.1.

Canvas

The components are places on the Grasshopper Canvas, which is the graphical visualisation of the Grasshopper program.

A Grasshopper definition

A network of components is called a Grasshopper definition [53]. This is basically the solution, or task, which is carried out by the specific network of components. Sometimes this is also called Grasshopper routine, solution or script.

Baking

The geometry which has been defined in Grasshopper can be viewed in Rhino, however this is only a preview. [53] To edit the geometry in Rhino the geometry must be baked. The baking generates a copy of the Grasshopper geometry inside Rhino, where it can be edited or exported to other software. Once the geometry has been baked it is fix, and it cannot be adjusted parametrically anymore in Grasshopper.

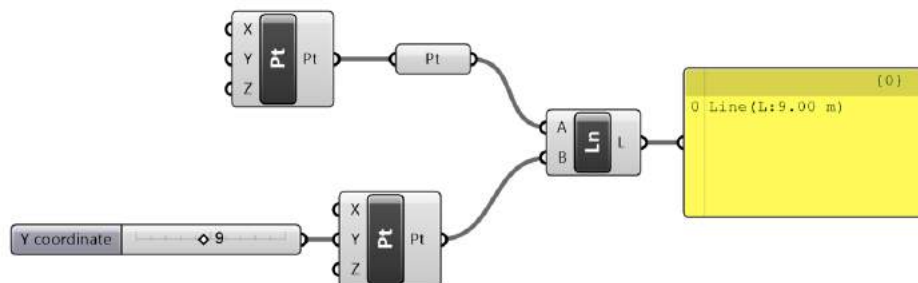


Figure A.1: Grasshopper components which are connected by wires.

A.2.3 Programming terminology

A traditional computer program can be viewed as a series of operations which are carried out in sequence, in an input-processing-output order [54]. In Object Oriented Programming, OOP, this is no longer the case. Here the order of operations can be allowed to vary, and the actions of the user of the program may be unpredictable and the program must therefore be written to take this into account. Some terms related to OOP which have been used in this study are mentioned and briefly described here.

Objects and classes

Sometimes the terms object and class are used to describe the same thing. [55] A class is typically a description of a type, and an object is an instance of a type. To make it clear how this is used in programming one can use a blueprint analogy, where the class is the blueprint and the object is what the blueprint describes.

In this report the word object has been used to refer to geometrical objects in Rhino such as curves, surfaces or points. These are in fact instances of objects which contain a geometry and attribute part [56].

Attributes and properties

In this study the term attribute has been used to refer to properties which are assigned to an object. In this study this was done by defining Object User Data, which contains information that is linked to an object [57].

A.3 Additional theory

Some additional theory related to Classical Lamination Theory is presented in this section.

A.3.1 Stiffness and compliance matrices for FRP composites

Hooke's generalised law in three dimensions can be written on the extended matrix form as in Equation A.1, where \mathbf{E}_{ijkl} is a fourth order tensor with 81 constants, describing the stiffness of the material, however due to symmetry this can be reduced to 21 independent components.

$$\begin{bmatrix} \sigma_{11} \\ \sigma_{22} \\ \sigma_{33} \\ \tau_{23} \\ \tau_{31} \\ \tau_{12} \\ \tau_{32} \\ \tau_{13} \\ \tau_{21} \end{bmatrix} = \begin{bmatrix} E_{1111} & E_{1122} & E_{1133} & E_{1123} & E_{1131} & E_{1112} & E_{1132} & E_{1113} & E_{1121} \\ E_{2211} & E_{2222} & E_{2233} & E_{2223} & E_{2231} & E_{2212} & E_{2232} & E_{2213} & E_{2221} \\ E_{3311} & E_{3322} & E_{3333} & E_{3323} & E_{3331} & E_{3312} & E_{3332} & E_{3313} & E_{3321} \\ E_{2311} & E_{2322} & E_{2333} & E_{2323} & E_{2331} & E_{2312} & E_{2332} & E_{2313} & E_{2321} \\ E_{3111} & E_{3122} & E_{3133} & E_{3123} & E_{3131} & E_{3112} & E_{3132} & E_{3113} & E_{3121} \\ E_{1211} & E_{1222} & E_{1233} & E_{1223} & E_{1231} & E_{1212} & E_{1232} & E_{1213} & E_{1221} \\ E_{3211} & E_{3222} & E_{3233} & E_{3223} & E_{3231} & E_{3212} & E_{3232} & E_{3213} & E_{3221} \\ E_{1311} & E_{1322} & E_{1333} & E_{1323} & E_{1331} & E_{1312} & E_{1332} & E_{1313} & E_{1321} \\ E_{2111} & E_{2122} & E_{2133} & E_{2123} & E_{2131} & E_{2112} & E_{2132} & E_{2113} & E_{2121} \end{bmatrix} \begin{bmatrix} \epsilon_{11} \\ \epsilon_{22} \\ \epsilon_{33} \\ \epsilon_{23} \\ \epsilon_{31} \\ \epsilon_{12} \\ \epsilon_{32} \\ \epsilon_{13} \\ \epsilon_{21} \end{bmatrix} \quad (\text{A.1})$$

In the case of orthotropic materials this can further be reduced to nine independent constants, see Equation A.2.

$$\begin{bmatrix} E_{1111} & E_{1122} & E_{1133} & 0 & 0 & 0 \\ E_{1122} & E_{2222} & E_{2233} & 0 & 0 & 0 \\ E_{1133} & E_{2233} & E_{3333} & 0 & 0 & 0 \\ 0 & 0 & 0 & E_{2323} & 0 & 0 \\ 0 & 0 & 0 & 0 & E_{1313} & 0 \\ 0 & 0 & 0 & 0 & 0 & E_{1212} \end{bmatrix} \quad (\text{A.2})$$

By introducing new notation the stress-strain relation for an orthotropic material can now be written as in Equation A.3.

$$\begin{bmatrix} \sigma_1 \\ \sigma_2 \\ \sigma_3 \\ \tau_{23} \\ \tau_{13} \\ \tau_{12} \end{bmatrix} = \begin{bmatrix} C_{11} & C_{12} & C_{12} & 0 & 0 & 0 \\ C_{12} & C_{11} & C_{12} & 0 & 0 & 0 \\ C_{12} & C_{12} & \frac{C_{11}-C_{12}}{2} & 0 & 0 & 0 \\ 0 & 0 & 0 & \frac{C_{11}-C_{12}}{2} & 0 & 0 \\ 0 & 0 & 0 & 0 & \frac{C_{11}-C_{12}}{2} & 0 \\ 0 & 0 & 0 & 0 & 0 & \frac{C_{11}-C_{12}}{2} \end{bmatrix} \begin{bmatrix} \varepsilon_1 \\ \varepsilon_2 \\ \varepsilon_3 \\ \gamma_{23} \\ \gamma_{12} \\ \gamma_{12} \end{bmatrix} \quad (\text{A.3})$$

A. EXPLANATIONS AND DEFINITIONS

For specially orthotropic materials the out-of-plane stress components, σ_1 , τ_{23} and τ_{13} , are assumed to be zero. The stress-strain relation can thus be expressed, in terms of the longitudinal and transverse material axes, as in Equations A.4 to A.5. The \mathbf{Q} matrix is the stiffness matrix of the specially orthotropic material. The inverse of the matrix \mathbf{Q} , \mathbf{S} , is called the compliance matrix.

$$\begin{bmatrix} \sigma_L \\ \sigma_T \\ \tau_{LT} \end{bmatrix} = \begin{bmatrix} Q_{11} & Q_{12} & 0 \\ Q_{21} & Q_{22} & 0 \\ 0 & 0 & Q_{66} \end{bmatrix} \begin{bmatrix} \varepsilon_L \\ \varepsilon_T \\ \gamma_{LT} \end{bmatrix} \quad (\text{A.4})$$

$$\begin{bmatrix} \varepsilon_L \\ \varepsilon_T \\ \gamma_{LT} \end{bmatrix} = \begin{bmatrix} S_{11} & S_{12} & 0 \\ S_{21} & S_{22} & 0 \\ 0 & 0 & S_{66} \end{bmatrix} \begin{bmatrix} \sigma_L \\ \sigma_T \\ \tau_{LT} \end{bmatrix} \quad (\text{A.5})$$

Now the components of \mathbf{S} can be expressed in terms of the engineering constants, E_T , E_L , G_{LT} , ν_{LT} and ν_{TL} , see Equations A.6 to A.12

$$\varepsilon_L = S_{11}\sigma_L + S_{12}\sigma_T \quad (\text{A.6})$$

$$\varepsilon_T = S_{12}\sigma_L + S_{22}\sigma_T \quad (\text{A.7})$$

$$\gamma_{LT} = S_{66}\tau_{LT} \quad (\text{A.8})$$

$$S_{11} = \frac{1}{E_L} \quad (\text{A.9})$$

$$S_{22} = \frac{1}{E_T} \quad (\text{A.10})$$

$$S_{12} = -\frac{\nu_{LT}}{E_L} = -\frac{\nu_{TL}}{E_T} \quad (\text{A.11})$$

$$S_{66} = \frac{1}{G_{LT}} \quad (\text{A.12})$$

Since there exists a one-to-one relation between the \mathbf{Q} and \mathbf{S} matrices the components of the stiffness matrix can be expressed directly in terms of the engineering constants for specially orthotropic laminae.

A.3.2 Transformation matrices

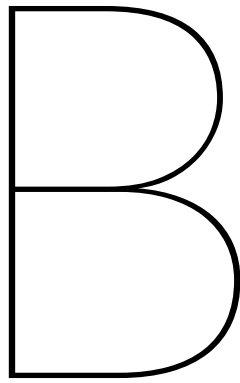
The stiffness matrix of a generally orthotropic laminae can be expressed in relation to a reference coordinate system by applying a transformation using the matrices \mathbf{T}_1 and \mathbf{T}_2 which are shown in Equations A.13 and A.14.

$$\mathbf{T}_1 = \begin{bmatrix} \cos^2(\theta) & \sin^2(\theta) & 2 \sin(\theta) \cos(\theta) \\ \cos^2(\theta) & \cos^2(\theta) & -2 \sin(\theta) \cos(\theta) \\ -\sin(\theta) \cos(\theta) & \sin(\theta) \cos(\theta) & \cos^2(\theta) - \sin^2(\theta) \end{bmatrix} \quad (\text{A.13})$$

$$\mathbf{T}_2 = \begin{bmatrix} \cos^2(\theta) & \sin^2(\theta) & \sin(\theta) \cos(\theta) \\ \cos^2(\theta) & \cos^2(\theta) & -\sin(\theta) \cos(\theta) \\ -2 \sin(\theta) \cos(\theta) & 2 \sin(\theta) \cos(\theta) & \cos^2(\theta) - \sin^2(\theta) \end{bmatrix} \quad (\text{A.14})$$

APPENDIX A - REFERENCES

- [48] Robert McNeel & Associates®, “What are nurbs?,” 2018. [Online]. Available: <https://www.rhino3d.com/nurbs>, Accessed on June 10, 2018.
- [49] Robert McNeel & Associates®, “The meshtonurb command,” 2018. [Online]. Available: <https://wiki.mcneel.com/rhino/meshtonurb>, Accessed on June 10, 2018.
- [50] Robert McNeel & Associates®, “Understanding tolerances,” 2018. [Online]. Available: <https://wiki.mcneel.com/rhino/faqtolerances>, Accessed on June 11, 2018.
- [51] Grasshopper, “Grasshopper, version 0.9.0076,” 2017. [Software]. Available: <http://www.grasshopper3d.com/>, Accessed on May 05, 2018.
- [52] TOI-Pedia, “Grasshopper,” 2018. [Online]. Available: <http://wiki.bk.tudelft.nl/toi-pedia/Grasshopper>, Accessed on June 12, 2018.
- [53] TOI-Pedia, “Getting started with grasshopper,” 2018. [Online]. Available: http://wiki.bk.tudelft.nl/toi-pedia/Getting_Started_with_Grasshopper, Accessed on June 11, 2018.
- [54] R. A. Mata-Toledo and P. Gupta, “Object-oriented programming,” 2014. [Online]. Available: <https://www.accessscience.com/content/object-oriented-programming/757337>, Accessed on June 11, 2018.
- [55] Microsoft, “Object-oriented programming (C#),” 2017. [Electronic]. Available: <https://docs.microsoft.com/en-us/dotnet/csharp/programming-guide/concepts/object-oriented-programming>, Accessed on: May 31, 2018.
- [56] D. Rutten, “7 geometry,” 2018. [Online]. Available: <http://developer.rhino3d.com/guides/rhinoscript/primer-101/7-geometry/#72-objects-in-rhino>, Accessed on June 11, 2018.
- [57] S. Baer, “Object user data,” 2018. [Online]. Available: <http://developer.rhino3d.com/guides/rhinocommon/plugin-user-data/#object-user-data>, Accessed on June 11, 2018.



PROGRAMS AND PARAMETRIC TOOLS

APPENDIX B - CONTENTS

B.1	MATLAB functions and programs	B1
B.1.1	Description of MATLAB functions	B1
B.1.2	Description of MATLAB programs	B2
B.2	Grasshopper definitions	B3
B.2.1	PlotStrainCurvature	B3
B.2.2	PlotDisplacements	B3
B.2.3	PlotStresses	B3
B.3	Grasshopper components	B5
B.3.1	MakeSPT	B5
B.3.2	MakeSLN	B6
B.3.3	MakeSAR	B7

B.1 MATLAB functions and programs

The MATLAB functions and programs which were used in development of the parametric design and analysis approach are presented and briefly described here.

B.1.1 Description of MATLAB functions

These MATLAB functions, which are listed below, were use to calculate engineering, constants and constitutive equations for FRP composites, as well as in analysis of FRP laminates to evaluate strains and curvature as well as forces and stresses.

ABDMatrix.m

This function calculates the A , B and D matrices for a laminate based on the layup and Q matrix.

calcAlpha.m

This function calculates the thermal expansion coefficients of the laminate.

calcEps0.m

This function calculated the mid-plane strains and curvatures in a laminate subjected to loading.

calcMax.m

This function finds the maximum stress in a laminate and output in which lamina this stress occurs.

calcQ.m

This function calculates the Q from the composite engineering constants, for specially orthotropic laminae.

calcStressStrain.m

This function calculates through the thickness strains and stresses for a laminate given the Q , layup, mid-plane strains and curvature, and if a temperature is proved it will also take into account thermal effects.

compositePlot.m

Plots the layup of the laminate.

compProperties.m

Calculates E_T , E_L , G_{LT} , ν_{LT} , ν_{TL} , α_L and α_T for a laminate given the mechanical properties of the constitutive materials and their volume fractions.

plotStressStrain.m

Plots the strains and stresses though the thickness for a laminate.

Qbar.m

Calculates the transformed stiffness matrix for a generally orthotropic lamina given its orientations relative a reference coordinate system.

T1.m

Calculates the T_1 matrix for a lamina given its orientations relative a reference coordinate system.

T2.m

Calculates the T_2 matrix for a lamina given its orientations relative a reference coordinate system.

thickness.m

Calculates the coordinates for bottom and top positions for each lamina in a laminate.

B.1.2 Description of MATLAB programs

A number of programs were written in MATLAB to evaluate the assumptions made, and to verify the SOFiSTiK materials which had been defined.

EvalLamina.m

This program was used to calculate engineering constants and stiffness matrices for FRP laminae with varying fibre volume fractions and lamina orientations.

MechanicalCoupling.m

This program was used to evaluate mechanical coupling in thin and thick laminates with varying lamina orientations. This was done by calculating the A , B and D laminates for laminates with varying lamina orientations and number of laminates.

EvalLaminate.m

The mechanical responses was evaluated for thin and thick laminates with this program. This was done by applying a load to the laminate and then calculating the strain and curvature response.

In this program engineering constants were also calculated for the laminates, assuming that these are fully orthotropic, by neglecting any non-zero A_{16} and A_{26} components in the A matrix. The engineering constants were then exported as lists in text files.

OrthotropicLaminate.m

This program was used to evaluate the mechanical response in Fully Orthotropic Laminates. The engineering constants, which were used to calculate the Q matrix of a fictional lamina, were read from text files. From this a laminate was constructed from uni-directional layers of the fictional laminae.

The strain and curvature response in these laminates was evaluated by applying a load and calculating the resulting strains and curvatures.

EquivalentLaminate.m

This program was written to evaluate orthotropic laminates. A strain or curvature was applied to the laminate, and resulting strains and curvatures were calculated using static condensation. The stresses caused by the applied strains were also calculated.

The results from this program was used to verify the materials defined in SOFiSTiK.

B.2 Grasshopper definitions

A number of parametric tools were developed in this study to simplify comparison of results and the creation of the parametric models. These tools were created as Grasshopper routines. In Figure B.1 an overview of the Grasshopper routine created for this study. The Results sections, see Figure B.2 of this Grasshopper routine contains three tools which were developed for evaluation of results from the case studies. These three tools are briefly described in this section.

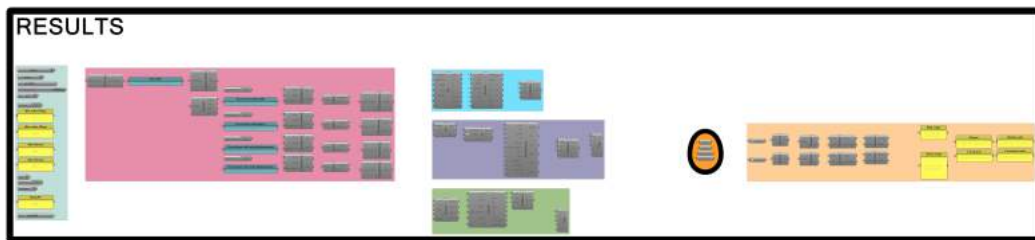


Figure B.2: An overview of the Grasshopper routines used for evaluation of results from the case studies conducted in this study.

B.2.1 PlotStrainCurvature

This tool was created to calculate and display strains and curvatures of a FE mesh. The results can be visualised as a deformed mesh, and the strains and curvatures are also calculated and given as numerical values.

B.2.2 PlotDisplacements

This tool was created to display displacements of a FE mesh. The displaced mesh can be visualised both as a deformed mesh, as well as a mesh with a colour gradient. The colour of the mesh is determined by the displacement of each node.

B.2.3 PlotStresses

This tool was created to display stress results on a FE mesh. The stresses can be visualised as a colour gradient on either the non-deformed or deformed mesh.

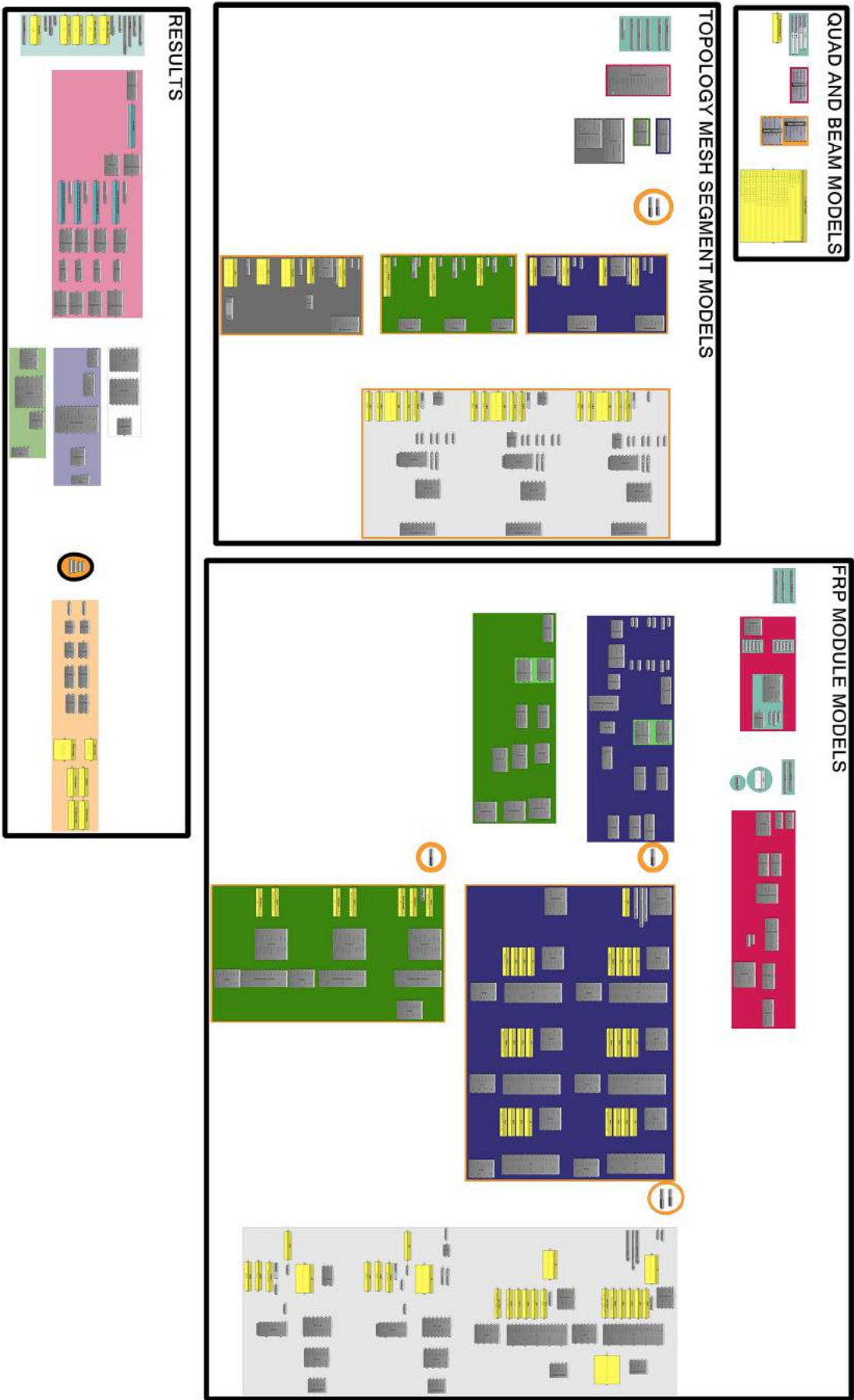


Figure B.1: Parametric Grasshopper definition. The three types of models which were created for this study can be seen here, as well as the part where results from SOFiSTiK was imported. Note that the wires which connect the components have been hidden to give a clear overview of the Grasshopper definition.

B.3 Grasshopper components

A number of Grasshopper components were developed in this study to automate and simplify the creation of FE models for SOFiSTiK. These components are briefly described below.

B.3.1 MakeSPT



Figure B.3: MakeSPT Grasshopper component.

This component creates structural information for point objects in Grasshopper/Rhino for export to SOFiSTiK. The inputs and outputs of the component can be seen in Figure B.5.

B.3.2 MakeSLN

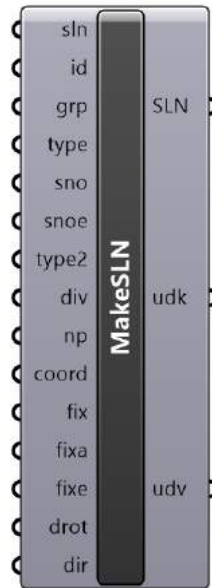


Figure B.4: MakeSLN Grasshopper component.

This component creates structural information for line and curve objects in Grasshopper/Rhino for export to SOFiSTiK. The inputs and outputs of the component can be seen in Figure B.5.

B.3.3 MakeSAR

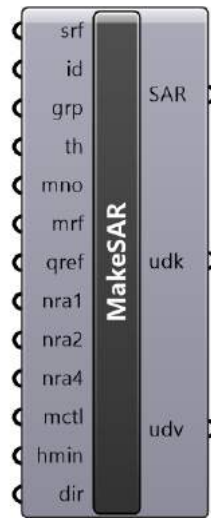


Figure B.5: MakeSAR Grasshopper component.

This component creates structural information for surface objects in Grasshopper/Rhino for export to SOFiSTiK. The inputs and outputs of the component can be seen in Figure B.5.

